



Fin Schmidt

Real-time vibration monitoring system for the pellet centrifuge at ASDEX Upgrade with empirically derived limit values

IPP 2024-12
April 2024



STUDIENGANG MASCHINENBAU

B A C H E L O R A R B E I T

Name

Fin Schmidt

Thema

**Real-time vibration monitoring system for the
pellet centrifuge at ASDEX Upgrade with
empirically derived limit values**

Bachelorarbeit

zur Erlangung des akademischen Grades eines
Bachelor of Engineering (B.Eng.)



MAX-PLANCK-INSTITUT
FÜR PLASMAPHYSIK



Ausgabetermin:	2023.12.12
Abgabetermin:	2024.03.15
Autor:	Fin Schmidt
Hochschule:	Hochschule für angewandte Wissenschaften Coburg Friedrich-Streib-Straße 2 96450 Coburg
Studiengang:	Maschinenbau
Durchgeführt bei:	Max-Planck-Institut für Plasmaphysik
Firmenbetreuer:	Bernhard Ploeckl
Erstprüfer:	Prof. Dr. Martin Prechtl

Statutory Declaration

I, Fin Schmidt, hereby confirm that I have written this thesis independently and have not used any resources other than those stated. The passages in the thesis that are taken from other works (including Internet sources) in terms of wording or meaning have been identified by stating the source.

85748 Garching, 2024.03.15

(Place, Date)

(Signature)

Abstract

The ASDEX Upgrade centrifuge pellet launcher, utilized to reliably control the particle flux and ELM frequency, is now in operation for more than 30 years. The units age as well as its unique design necessitate a real-time vibration monitoring system, to reliably detect, warn and prevent damage or malfunctions. Due to space restrictions, two sensors were affixed close to the lower ball bearing. This configuration allows for an efficient monitoring of both the overall structure and at least one of the two bearings, providing some insight into the stability of the rotor. In the absence of literature and established standards for vibration control specific to this structure and application, the key to find vibrational limits is to derive them empirically. Setting a baseline for limit values considers the current operational values as optimal and establishes more precise limits based on the observed behavior of the unit during different operational states. Advanced tools, such as envelope analysis, are employed to monitor specific machine components, especially the ball bearings. Beyond enhancing the safety of pellet injection at ASDEX Upgrade, the current state of the system includes a scheme to safely shutting down the centrifuge before reaching threatening vibration magnitudes.

Contents

1	Introduction	1
2	Max-Planck-Institut für Plasmaphysik	3
2.1	Institut für Plasmaphysik as a part of the Max Planck Society	3
2.2	Research at the Institut für Plasmaphysik	3
2.3	Tokamak Scenario Development and the Pellet Group	4
3	Fundamentals of vibration measurement and analysis	7
3.1	Oscillation	7
3.1.1	Classification of oscillations according to their temporal change.....	7
3.1.2	Classification of oscillations according to their mechanism of origin	8
3.2	Resonance in mechanical systems.....	9
3.3	Fundamental frequency and harmonics.....	9
3.4	Side bands and Modulation	10
3.5	Damping in mechanical systems	11
3.6	Fast Fourier Transform.....	11
3.7	Filters for signal processing	12
3.8	Piezoelectric acceleration sensor.....	12
4	Theory of vibration monitoring and analysis on the AUG centrifuge	14
4.1	Why vibration monitoring on the AUG centrifuge?	14
4.2	Measuring vibration	14
4.2.1	Measurement method: Machine category	14
4.2.2	Measurement method: Analytic process	17
4.2.3	Sensor selection.....	18
4.2.4	Measurement location: Optimal points and mounting method	20
4.3	System in use.....	23
4.4	Analysis tools	24
4.4.1	Time domain analysis.....	24
4.4.2	Frequency domain analysis	26
5	Analyzing vibration measurements on the AUG centrifuge	28
5.1	Existing vibration data and deductions	28
5.2	Software tools for vibration analysis.....	29

5.3	Vibration velocity root mean square (vRMS)	31
5.4	Diagnostics Characteristic Value (DKW)	32
5.5	Frequency spectrum (velocity)	33
5.6	Frequency spectrum (acceleration)	35
5.7	Envelope spectrum (acceleration)	37
6	Empirically deriving limit values	39
6.1	Elimination of disruptive effects	39
6.1.1	Temperature	39
6.1.2	Electromagnetic Fields	40
6.1.3	Triboelectric effects.....	41
6.1.4	Stochastic vibrations	41
6.2	Calculating Warn- and Alarm-Limits	42
6.2.1	Limit values for the vibration velocity's RMS.....	44
6.2.2	Limit values for the DKW.....	44
6.2.3	Limit bands for the velocity's frequency spectrum.....	45
6.2.4	Limit bands for the acceleration's frequency spectrum	45
6.2.5	Limit bands for the envelope spectrum	46
6.2.6	Limit values for the centrifuge's speed	46
7	Shutdown scheme for the AUG centrifuge	47
7.1	Overview of the real-time vibration monitoring system	47
7.2	System processes: Logic trees.....	48
7.2.1	Speed monitoring	48
7.2.2	Vibration monitoring.....	49
7.2.3	Boundary condition monitoring	50
8	Summary	52
A	Appendix A: Finite Element Method	59
B	Appendix B: Limit value tables	62

List of Abbreviations

(v)RMS	(Vibration velocity) root mean square
AI	Analog input
AL	Alarm- Limit
AUG	ASDEX Upgrade
BP	Band-Pass
BPF0	Ball Pass Frequency Outer Race
BPFI	Ball Pass Frequency
BSF	Ball Spin Frequency
CAD	Computer-aided design
CMS	Condition monitoring system
DFT	Discrete Fourier Transform
DKW	Diagnostics Characteristic Value
ELMs	Edge Localized Modes
EURATOM	European Atomic Energy Community
FFT	Fast Fourier Transform
FTF	Fundamental Train (Cage) Frequency
HFS	High field side
HMI	Human Machine Interface
HP	High-Pass
IAEA	International Atomic Energy Agency
IPP	Institute for Plasma Physics
KIT	Karlsruhe Institute of Technology
LFS	Low field side
LP	Low-Pass
MIL	Military Specification
MPG	Max Planck Society
PLC	Programmable logic controller
TMP	Turbomolecular pump
VIB	Vibration sensor
WL	Warn-Limit

1 Introduction

The inescapable, ever-increasing demand for more and more energy is one of, if not the most important challenge we face as a species today [1]. Coupled with the fact that our traditional sources of energy, such as oil and gas, have a negative impact on both the health of the planet and our own, the search for new sources of energy is more important than ever [2]. Throughout the evolutionary history of our planet, every single organism has drawn, directly or indirectly, energy from a consistent source. The sun, located nearly 150 million kilometers from us, has been our planet's supplier of fusion energy for over 4.5 billion years [3]. With solar panels being installed all over the world and wind turbines utilizing the heat differential created by the sun, we have found ways to use its energy more efficiently than ever before. The only problem is that both renewable energy sources depend on things we cannot actively control, such as the Earth's rotation.

To avoid these complications, scientists have been working to bring fusion energy directly to us. Since the late 1950s, a global cooperation called the International Atomic Energy Agency (IAEA) has been the driving force behind international fusion research. Unlike coal-fired and nuclear power plants, fusion reactors are much safer, produce much less radioactive waste and cannot end in a meltdown [4]. They work as baseload plants because they are not dependent on wind or sunlight. In the future, these could serve as a green alternative to coal burning and nuclear fission. To do so, however, they must operate as reliably and continuously as these processes. [5]

To increase reliability, engineers often turn to vibration analysis. Humans have always had the ability to evaluate systems based on vibration. Even in the Stone Age, people were able to use vibration analysis, albeit in a very primitive way, to judge whether a tool was still intact or broken. At that time, of course, people did not use electrical or mechanical sensors, but simply their own ears. With the onset of the Industrial Revolution, this diagnosis was extended from tools to machines. The foundation of vibration mathematics was laid by Galileo Galilei and further developed by many well-known and respected scientists such as Robert Hooke, Isaac Newton and Daniel Bernoulli. However, it was not until the early 20th century (around 1930) that people began to interpret vibrations and use them to improve a system. At that time, the behavior of houses during earthquakes was observed. Around 1940, the first vibration analysis was performed on a machine or machine parts. Such measurements were primarily performed on aircrafts which were being developed in both the civil and military sectors at the time. The increasing complexity and variety of instrumentation on board these machines required more accurate vibration monitoring. In the years that followed, the measurement methods evolved rapidly. Important milestones were the invention and commercialization of piezoelectric accelerometers (1943) and the development of the FFT algorithm by J.W. Cooley and J.W. Tukey (1965). [6], [7]

Today, the term vibration analysis encompasses an enormous amount of software and hardware, as well as nearly 100 years of research. Starting with listening devices, analog filters and mechanical frequency meters (which are still in use today), measurement technology has evolved into an electric-digital measurement chain. The tasks and complexity have also changed and increased over time. While in the beginning it was mainly possible to analyze the resonance of machines, today there is an enormous variety of analysis methods. These include areas such as bearing diagnostics, rotor path measurement and balancing. Vibration analysis is applied before the components of a machine are used, after they are assembled and while the machine is running. A shaft is balanced before assembly, checked for misalignment after mounting, and often monitored for faults throughout its life. [6], [8]

Much has changed in the 21st century, especially in the latter area of (automated) long-term monitoring. The two most important aspects, for the economic sector, are cost and effort. On the one hand, it is important to know long before the machine fails completely when its condition changes. On the other hand, finding out what exactly caused the change will help to get it under control as quickly as possible. The use of sensors, digital filters and advanced software can significantly increase machine uptime and reduce unplanned downtime. Vibration monitoring can be of great importance not only in terms of sustainability, which is becoming increasingly important in such issues, but also in terms of enabling stable infrastructure, such as power supply. [8], [9]

By combining the history of both fusion reactors and vibration analysis, an indispensable component of the future sustainable energy source can be operated more reliably. To ensure that fuel is continuously fed into the plasma, a centrifuge must be constantly ready to transport new pellets of hydrogen. Since the centrifuge pellet launcher in ASDEX Upgrade's (AUG) Torus Hall has been in use for more than 30 years and is unique in its composition, the *Pellet Team* says it needs to be treated *like a raw egg*. A further step in this direction is the installation of a vibration monitoring system with empirically derived limit values and a shutdown scheme if these are exceeded. To delay the need for a new centrifuge, the monitoring system should both give an early alarm and shut down the centrifuge before a total failure occurs. This required extensive research into machine vibrations, possible disturbances and the derivation of limit values. [10], [11]

2 Max-Planck-Institut für Plasmaphysik

2.1 Institut für Plasmaphysik as a part of the Max Planck Society

The Max Planck Society (MPG) has existed in its present form since 1948. The former Kaiser Wilhelm Society, founded in 1911, was restructured into the MPG after the Second World War by the then director Werner Heisenberg. Twelve years later, the Institute for Plasma Physics (IPP) was founded by Heisenberg himself and the Society. Initially still financially managed by the Helmholtz Association, the IPP with its approximately 1100 employees was incorporated into the MPG in January 2021, not only legally but also financially as before. [12]

2.2 Research at the Institut für Plasmaphysik

„The research conducted at Max-Planck-Institut für Plasmaphysik (IPP) in Garching and Greifswald is concerned with investigating the physical basis of a fusion power plant. Like the sun, such a plant is to generate energy from fusion of atomic nuclei.“ [13]

Germany entered fusion research in 1956, at that time as a small working group led by Werner Heisenberg. The Wendelstein 1-A stellarator facility went into operation in 1960, mainly thanks to the financial support of the European Atomic Energy Community (EURATOM), with which the IPP still cooperates today. Ten years later, IPP's second fusion project, the ASDEX tokamak, was launched. Since 1991, research on the ASDEX Upgrade fusion reactor has been conducted in Garching, the IPP site with the largest number of employees. In the new institute building in Greifswald, which was completed around 2000, plasmas have been successfully generated in the Wendelstein 7-X stellarator since December 10, 2015. The main difference between a stellarator and a tokamak is the shape of the coils. While the tokamak uses planar coils (Figure 1a), the stellarator uses twisted coils (Figure 1b) [14]. The reason for this is to generate a twisted magnetic field cage, which is required for operation. In present day tokamaks, this requires a longitudinal current in the plasma generated by a generator, which limits the system to pulsed operation. The stellarator, with its special coils, avoids this problem and is suitable for continuous operation. [12], [15]

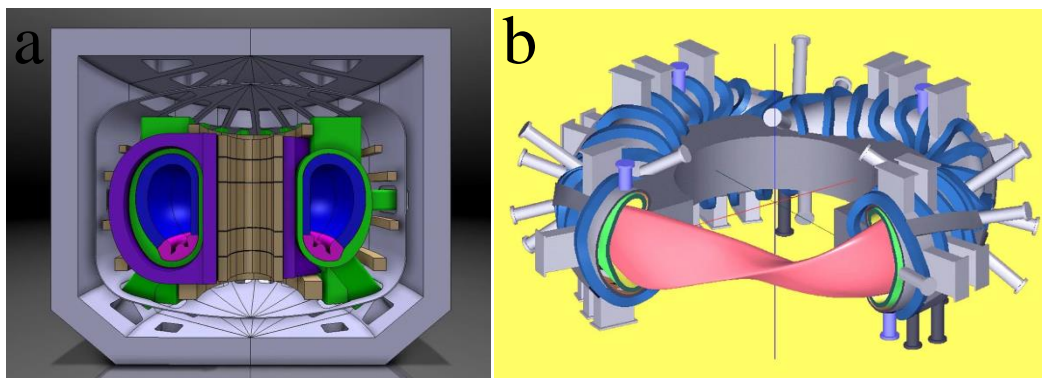


Figure 1: (a) Tokamak ASDEX Upgrade at the IPP in Garching. The ring-shaped coils are shown in purple; (b) Wendelstein 7-X stellarator at the IPP in Greifswald. The twisted coils are shown in blue. [14]

The Institute's two sites are divided into ten scientific areas (plus junior research groups). At each site, research is carried out both in theory and practice by physicists, engineers, and technicians. In Garching, the scientists work not only on problems and tasks related to their own machine, but also on topics relevant to JT-60SA, ITER and DEMO. [15], [16]

The fact that fusion research is becoming increasingly relevant in today's world is confirmed by the current position paper on fusion research and the associated investments planned by the German government. The funding of 370 million euros announced by the Federal Government is to be made available to the IPP and other institutions involved in fusion research, such as the Karlsruhe Institute of Technology (KIT), until 2028. In particular, the areas of magnetic and laser fusion are to be strongly promoted through investments and synergies. [17], [18]

2.3 Tokamak Scenario Development and the Pellet Group

„The Tokamak Scenario Development Division (E1) operates the tokamak ASDEX Upgrade which concentrates on treating the physical principles for a fusion power plant. Prominent is the preparation of the ITER large-scale experiment and the European demonstration power plant DEMO.“ [19]

The pellet group is an important part of this division. To produce pellets, hydrogen (D_2 and H_2) must be cooled to a few Kelvins using a cryostat and extruded as an ice rod. A lever is then used to move the ice strand towards the chopper (Figure 2). The chopper is responsible for cutting a certain amount of ice into a pellet. The pellet falls into a specially designed stop cylinder inside the centrifuge. Here, it is completely slowed down before being accelerated radially by the centrifuge arm. Through an opening in the centrifuge housing, the frozen hydrogen is transported through a looping track at a speed of $v > 240$ m/s and shot from the magnetic high field side (HFS) of ASDEX Upgrade (Figure 3). [20], [21]

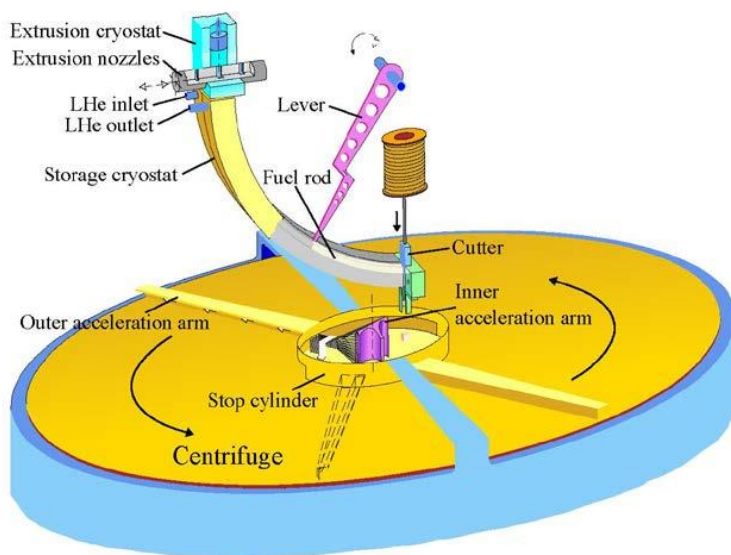


Figure 2: Schematic representation of the pellet centrifuge at ASDEX Upgrade. On top of the centrifuge sits a cryostat, used for producing ice rods for pellet production. [16]

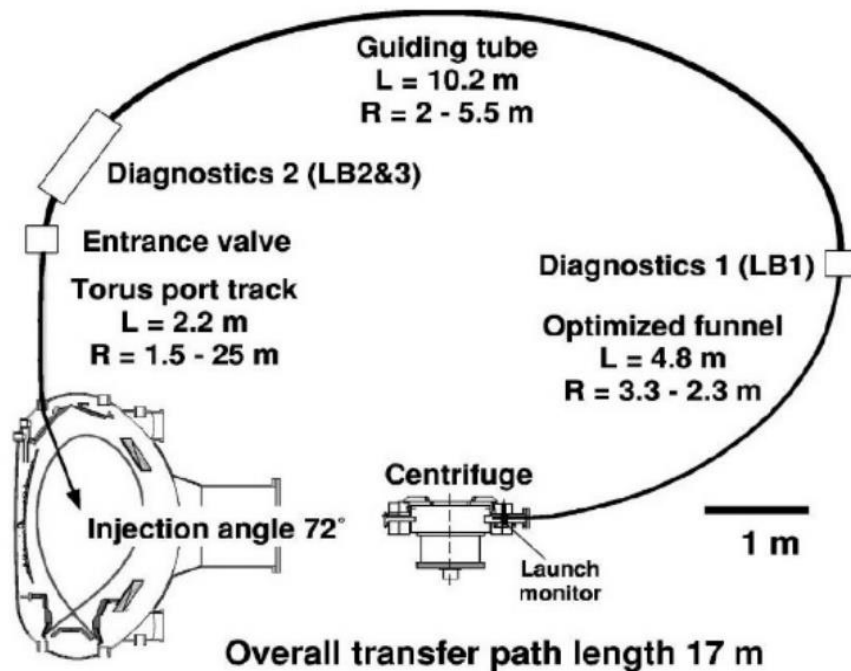


Figure 3: Schematic representation of the pellet injection system. Introduced in October 2002 to be able to inject pellets from the high field side of the magnetic field. The looping-shaped guiding tube results from the need to overcome space restrictions in the Torus Hall. [22]

The two main tasks of the pellets at the IPP in Garching are refueling the plasma core and the control of Edge Localized Modes (ELMs). ELMs are plasma instabilities that occur in certain operating states of the tokamak and have a mostly negative effect on operation. In both cases, hydrogen is frozen and injected as described above. Prior to the loop track implemented at ASDEX Upgrade, the pellets were injected from the magnetic low field side (LFS). After several tests, it was found that feeding from the HFS produced significantly better results for fuel replenishment. This can be attributed to the fact that the pellets on this side experience more extensive transport into the interior of the plasma, leading to increased fuel delivery to the plasma core. According to [23], there are indications that pellets fired from the HFS are more likely to deliberately trigger ELMs than pellets arriving on the LFS. [19], [24]

In addition to the cryostat and the AUG centrifuge in the Torus Hall, the Pellet Group laboratory has a centrifuge and cryostat test rig. Another system that the group had been working on for some time after its expansion is the so-called blower gun. This system, which is also suitable for both applications mentioned above, has been disregarded for further technology development. One of the reasons for this is the much shorter scattering time of the pellets entering the plasma (Figure 4). The blower gun's average scattering time was 8.76 ms. Despite the 7 m longer flight path, the centrifuge's time scatter was only 0.22 ms. This parameter is particularly important for ELM control. That is why the centrifuge acceleration technology is still state-of-the-art. [23], [25]

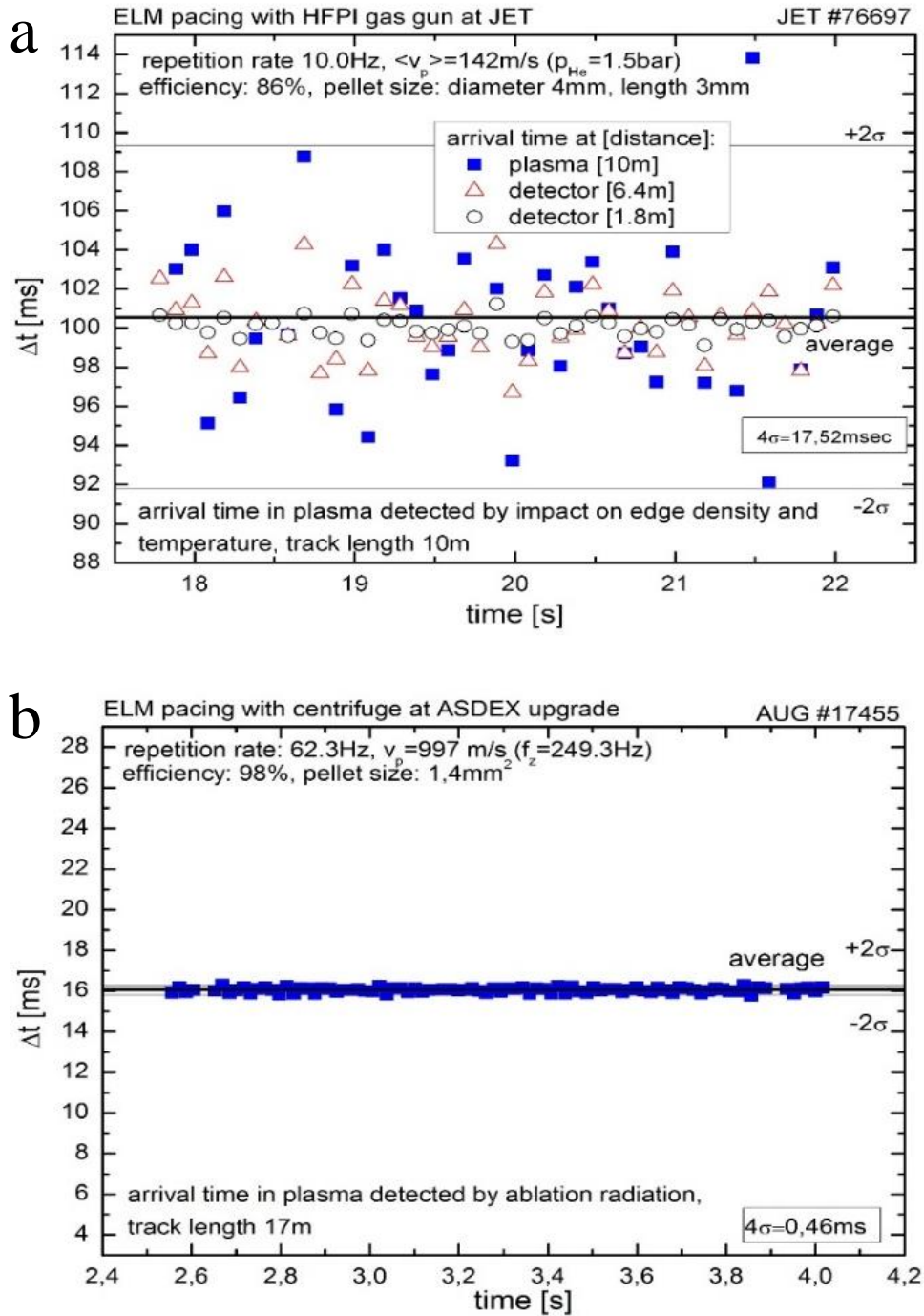


Figure 4: (a) Shown in blue is the time jitter of pellets injected into the Joint European Torus (JET) plasma by a blower gun; (b) The time jitter of pellets injected by the centrifuge into the plasma of ASDEX Upgrade. [25]

3 Fundamentals of vibration measurement and analysis

3.1 Oscillation

In its most basic form, vibration, or oscillation in general, is a state variable x that changes with time.

$$x = x(t) \tag{1}$$

Where x represents various parameters such as pressure, temperature, or other relevant factors. In the technical context, vibrations are considered side effects resulting from imperfections. [26]

3.1.1 Classification of oscillations according to their temporal change

Oscillations can occur with different behavior and in different forms. According to DIN ISO 1311-1, these can be divided into distinct categories according to their temporal characteristics (Figure 5).

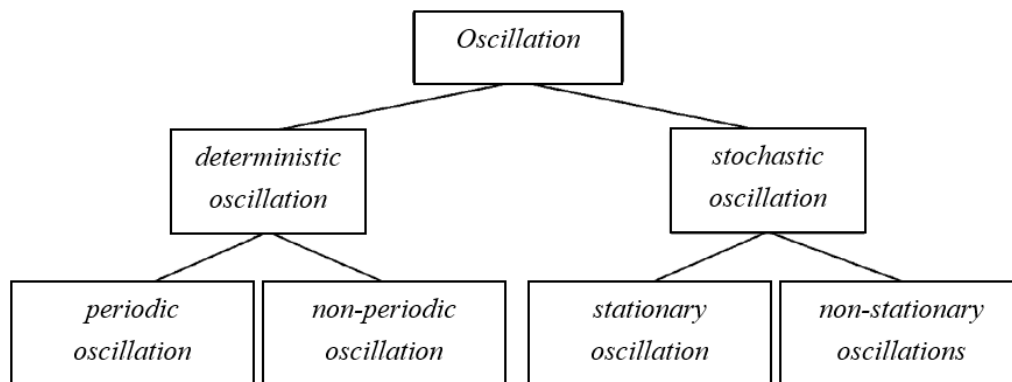


Figure 5: Classification of vibrations according to their temporal evolution. [27]

Unlike stochastic oscillations, deterministic oscillations can be described by a mathematical function. If this function is known, e.g. through modeling, the oscillatory behavior can be predicted. A special case is periodic oscillations (2), where the time pattern repeats after a certain period T .

$$x(t) = x(t + T) \tag{2}$$

The behavior of (2) does not apply to *non-periodic deterministic oscillations*. *Stochastic oscillations*, also known as random oscillations, cannot be predicted. An example is the surface structure of a road. As soon as a vehicle starts moving on it, stochastic vibration patterns are generated by unevenness, cracks, or similar imperfections. If both the condition of the road surface and the speed of the vehicle do not change, *stationary stochastic vibrations* can be assumed. If the road surface changes significantly or the vehicle speed changes during the specified measurement period, unpredictable *transient stochastic vibrations* are measured. Each periodic and stochastic type can be further subdivided into special cases. This information is

presented in both [26] and [27], but will not be further elaborated here due to its scope and relatively low relevance to the topic.

However, one of these subdivisions can be used to easily explain many basic concepts related to oscillations. *Harmonic oscillations* are characterized by the fact that they can be described by a *sine* or *cosine* function. An example of this is shown in (3).

$$x(t) = \hat{x} \cos(\omega t + \varphi_0) \quad (3)$$

Where the amplitude \hat{x} represents the peak value of the harmonic oscillation. The angular frequency ω relates the frequency f to the circumference of the unit circle 2π (4). As is known, frequency is given in Hertz (Hz) or s^{-1} and calculated according to (5) by the period duration.

$$\omega = 2\pi f \quad (4)$$

$$T = \frac{1}{f} \quad (5)$$

The angular frequency is required for the representation of oscillations in the frequently used pointer diagram (Figure 6). In this plot, the length of the pointer represents the amplitude of the oscillation, and the position of the pointer is determined by the phase angle $\varphi(t)$. The temporal evolution of $\varphi(t)$ is determined by the argument $\omega t + \varphi_0$ in equation (3). The phase angle φ_0 indicates the angle at $t = 0$. The rotational speed of the pointer is equivalent to the angular frequency. The same information can also be represented in a different way by a complex phasor diagram. [26], [27]

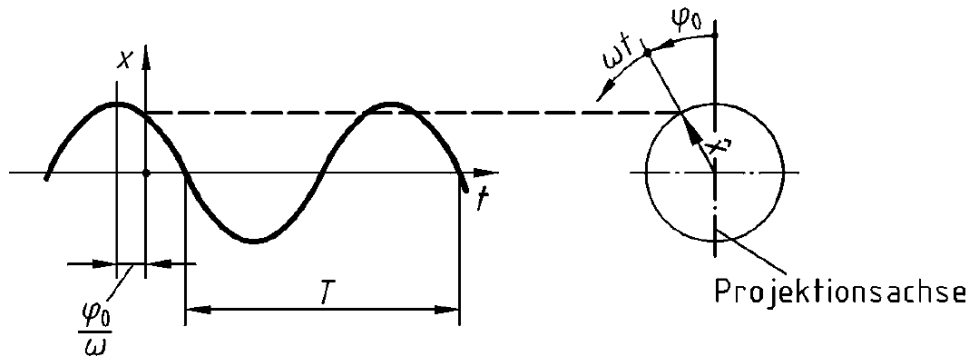


Figure 6: Temporal evolution of a harmonic oscillation (left) and phasor diagram (right). Both plots can be used to describe and evaluate vibration signals. [27]

3.1.2 Classification of oscillations according to their mechanism of origin

In addition to the time-dependent classification, the oscillations are also categorized according to their generation mechanism. This is divided into *autonomous* and *heteronomous oscillations* (Figure 7). *Autonomous free oscillations* are solely dependent on their initial state, i.e. no further energy flows into the system. The oscillation decays solely due to the natural damping of the system. *Autonomous self-excited oscillations*, on the other hand, are dependent on their initial state and additional energy input. This energy can be transferred to the system in the form of

unsteady flow or friction, for example. When one system is excited by another, e.g. a foundation by a machine standing on it, it is called a *heteronomous forced oscillation*. A condition that distinguishes this type of vibration from *self-excited oscillation* is that the excitation forces (of the machine) must occur even without the oscillation of the system (foundation). This would not be true in the case of a flow hitting an airfoil. *Heteronomous parameter-excited oscillations* occur only when there is a temporal change in a parameter of the system. This parameter can be, for example, the change in stiffness of a component due to temperature fluctuations. [26], [27]

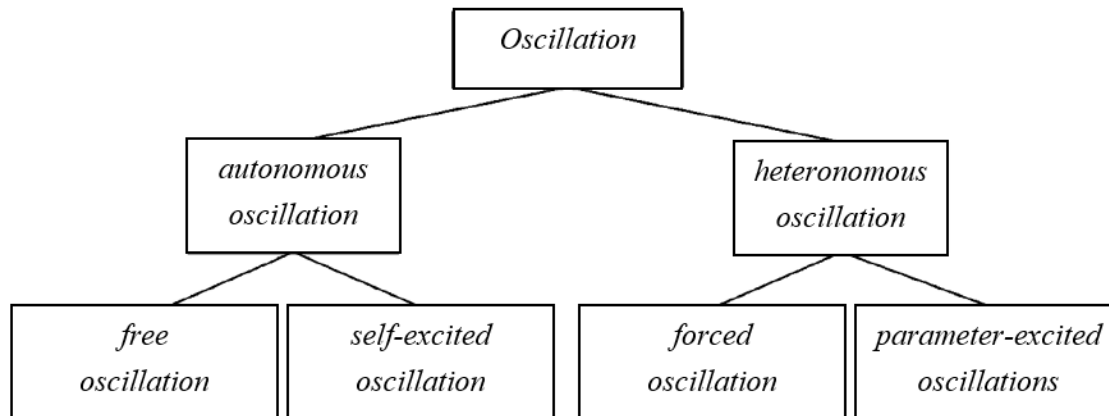


Figure 7: Classification of oscillations according to their mechanism of origin. [27]

3.2 Resonance in mechanical systems

A church bell vibrates at its natural circular frequency ω_0 after being excited (rung). A similar procedure can be performed on any component or machine. While the vibrations are measured by one or more sensors, the component is excited by a blow with an impact hammer. When the vibrations are analyzed in the form of a frequency spectrum or Bode diagram, the natural frequencies can be determined from the peaks that occur. [26], [28], [29]

When a system is vibrated by an exciter, the angular frequency Ω of the exciter and ω_0 of the systems may match. In this case, the amplitude builds up. In a theoretical model, without damping, the amplitude of the vibration would increase continuously. In reality, this is prevented by the material damping, which does not mean that damage cannot occur. In order to avoid bearing or shaft failure and other damage to a machine, these so-called resonance regions should be passed through quickly, thus preventing build-up. If the operating points and resonance ranges of the machine overlap, either the operational point or the machine's parameters (e.g. damping) should be altered. [26], [30]

3.3 Fundamental frequency and harmonics

When vibration is measured on machines with spinning rotors, the periodic component can be divided into the *fundamental frequency* and its *harmonics*. If the rotor of a machine rotates at 3,000 rpm, the fundamental frequency h_1 (also known as the first harmonic or speed harmonic)

is 50 Hz. From this, the second, third and all other n -fold harmonics h_n can be calculated according to (6). [31]

$$h_n = n * h_1 \quad (6)$$

Where $n \in \mathbb{N}$ must be true. All harmonics for which $n > 1$ and $n \notin \mathbb{N} \cap n \in \mathbb{Q}^+$ apply are defined as *interharmonics*. Harmonics with the property $n < 1 \cap n \in \mathbb{Q}^+$ are called *subharmonics*. [8]

3.4 Side bands and Modulation

In vibration analysis, side bands appear when a signal is modulated due to imperfections of the mechanical system. This modulation is often found in high frequency data, related to bearings and gears. The most common variation of this, is the so-called *amplitude modulation*. A carrier and modulating signal result in a new waveform, varying only in amplitude, not frequency (Figure 8). When looking at this signal in the frequency domain, lower (left) and upper (right) sidebands appear next to the carrier peak. Since a bearing fault causes such behavior, monitoring these sideband amplitudes is vital to early wear detection [8]. Not just a rising amplitude, but a change in general, can be a hint, that the fault is evolving. Apart from magnitude information, it is, for the same reason, important to keep an eye on how many side band peaks are present, and if that number changes with time. [32], [33]

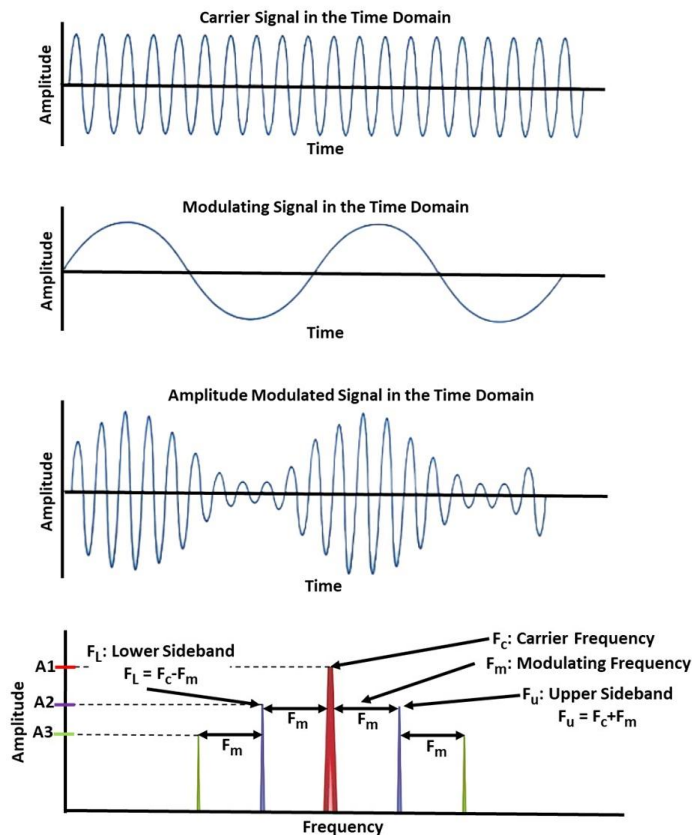


Figure 8: Two differently composed signals create a new, modulated waveform. This process of amplitude modulation leads to the formation of sidebands, which can appear on both sides of the carrier frequency. [33]

3.5 Damping in mechanical systems

Damping is defined as an energy dissipating property of moving or deforming components and assemblies. It can be divided into three different types of energy dissipation. Material damping, which is present in every real component, dissipates energy primarily through deformation of the component. Structural damping, which is the damping of an assembly of interconnected components, includes both material damping of the individual components and energy dissipation by friction between the components. Finally, radiation damping dissipates some of the vibration energy into the environment. [34]

The damping properties of a system can be deliberately parameterized in advance and adjusted afterwards. During the design phase, material damping can be influenced by selecting different materials and the associated dissipation factor [35]. In addition, the damping behavior can be influenced by increasing or decreasing the stiffness of an assembly. This method was applied to the centrifuge in the pellet laboratory. The stiffness of the system was increased by anchoring the centrifuge housing to the floor. As a result of the affected damping, differences in the vibration patterns of the machine were determined. The effectiveness of radiation damping can be influenced by the design of the foundation. The larger the contact area with the foundation, the more energy is dissipated into the ground. [36]

3.6 Fast Fourier Transform

Fourier Transform is a vital part of vibration analysis, as it allows us to deconstruct complex vibration signals into their frequency components. Thus, providing a more detailed picture of the system's dynamic behavior and enabling the identification of specific frequency related machinery faults. [8]

The algorithm that enables us to *efficiently* calculate the Discrete Fourier Transform (DFT) of vibration signals, is called Fast Fourier Transform (FFT). The DFT itself is the computation of a dense $n \times n$ matrix (7), thus requiring $O(n^2)$ operations, every time a signal must be transformed. While on a small scale this was still manageable, datasets with $n \gg 1$ proved to be a problem. [37]

$$\begin{bmatrix} \hat{f}_1 \\ \hat{f}_2 \\ \hat{f}_3 \\ \vdots \\ \hat{f}_n \end{bmatrix} = \begin{bmatrix} 1 & 1 & 1 & \dots & 1 \\ 1 & \omega_n & \omega_n^2 & \dots & \omega_n^{n-1} \\ 1 & \omega_n^2 & \omega_n^4 & \dots & \omega_n^{2(n-1)} \\ \vdots & \vdots & \vdots & \ddots & \vdots \\ 1 & \omega_n^{n-1} & \omega_n^{2(n-1)} & \dots & \omega_n^{(n-1)^2} \end{bmatrix} \begin{bmatrix} f_1 \\ f_2 \\ f_3 \\ \vdots \\ f_n \end{bmatrix} \quad (7)$$

The one-dimensional vector \hat{f} is the result of a multiplication including the (real) input vector f and the (imaginary) Fourier coefficient matrix F , where $\omega_n = e^{-2\pi i/n}$. As can be seen, the complex output \hat{f} contains both information about magnitude and phase of the signal. This is especially useful and convenient for vibration analysis, as both parameters play an important role in both monitoring and fault diagnostics. [37], [38]

The FFT algorithm, published in 1965 by Cooley and Tukey [39], was found to be an excellent way of capitalizing from the huge amount of symmetry there is in the DFT matrix. Thus, the FFT scales as $O(n \times \log(n))$. While being significantly faster, neither the quality nor the quantity of the solution changes. [37]

3.7 Filters for signal processing

The correct usage of (digital) filters plays a critical role in vibration analysis. High-Pass (HP) and Low-Pass (LP) filters can be used to eliminate antialiasing, low frequency noise as well as creating narrowband data. The Band-Pass (BP) filter, a combination of these two, could for example generate a frequency band that is limited to frequencies between 10 Hz and 200 Hz (Figure 9). This creates a window, in which component-specific frequencies can be examined in greater detail. [40]

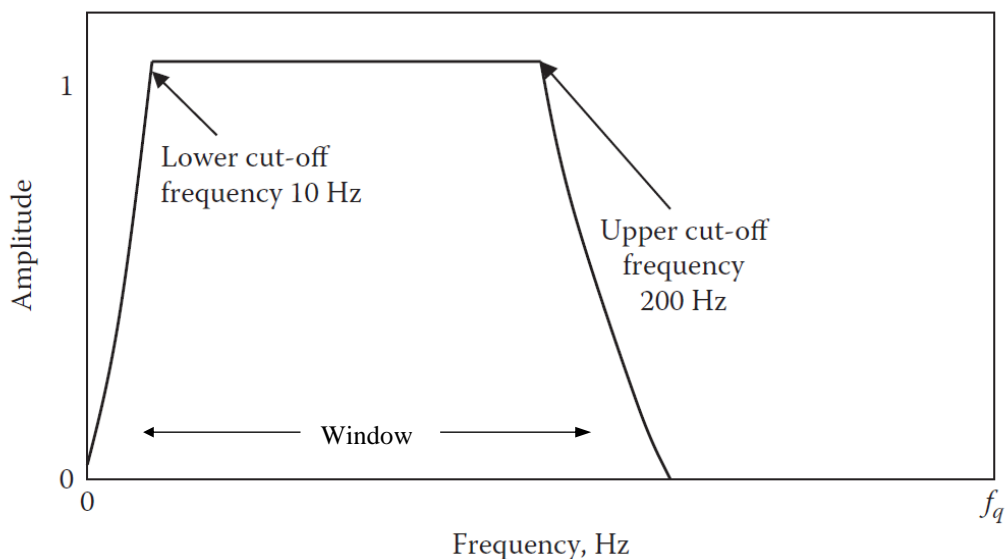


Figure 9: A typical band-pass filter characteristic. This filter allows frequencies between 10 Hz and 200 Hz to pass. No real filter has a rectangular shaped passband, leading to a small amount of unwanted frequencies to pass it. This is shown by the gradual descend of the passband. [40]

3.8 Piezoelectric acceleration sensor

Because of their excellent dynamic- and frequency ranges, piezoelectric acceleration sensors are the most widely used transducers for vibration analysis tasks. The fact that these types of sensors are easy to mount on almost any machine, combined with their outstanding durability, places them as the best choice for almost any long-term system. To be suitable for measurement, the mass of the sensor must be much smaller than that of the machine. Otherwise, the extra mass would change the dynamics of the system and reduce the quality of the analysis. The natural frequency of the transducers should not be close to that of any of the components it is monitoring. Since they are designed to have a very high natural frequency, this is usually not a problem. [8], [41]

Depending on the overall structure of the machine and its surroundings, an optimal mounting method can be selected. While a direct connection between sensor head and surface would always provide the best measurement quality, sometimes this configuration is not possible. For example, if the only surfaces close to a vibration source (shaft, bearing, gear, etc.) have a curvature, using adhesive to attach the sensor to one of these planes is the preferred method. Even though the coupling quality itself is lower, the superior signal information close to a vibratory source will easily make up for this. [42], [43]

In every piezoelectric acceleration sensor, a piezoelectric element (P) is attached to a seismic mass (M) which is fixed by a clamping element (S), forming a spring mass system (Figure 10). When an external force, in this case because of the vibration of the machine, is applied to the sensor head (B), the mass produces a changing force on the piezoelectric element. The element itself then produces an electrical charge proportional to that force. By using an implemented amplifier to convert the charge to a voltage signal, analysis modules can precisely derive the vibration magnitude and frequency. [8]

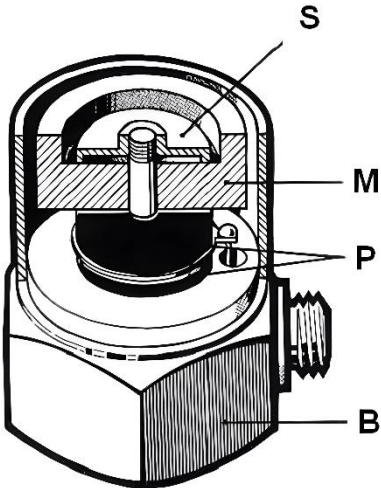


Figure 10: Compression-type accelerometer. B = Basis, P = Piezoelectric element, M = Seismic mass, S = Clamping element. [8]

4 Theory of vibration monitoring and analysis on the AUG centrifuge

4.1 Why vibration monitoring on the AUG centrifuge?

The ASDEX Upgrade pellet centrifuge launcher has now been in service for over 30 years. It is unique in its composition and only a handful of other centrifuges worldwide fulfil the same task. For some time now it has become obvious that the unit, as well as its parts are wearing out. Since there are no spare parts or active service contracts for the machine, it must be treated accordingly. The most recent sign that a real-time vibration monitoring system has become necessary, is the existence of bearing play ($+0.028^\circ / -0.0095^\circ$), measured by the *Pellet Group*.

4.2 Measuring vibration

4.2.1 Measurement method: Machine category

Machine vibrations can be measured either on non-rotating parts (housing, foundation, ...) or rotating parts (shaft, bearings, ...). The selection of one of these methods, primarily depends on the design and type of the machine, as well as the accessibility of its bearings and shaft(s). Over 30 years ago, when the centrifuge was designed, no measuring points were provided for shaft vibrations, so new ones would first have to be added. This requires the housing to be drilled out, which would lead to a breach in the vacuum. As the centrifuge must always operate in a vacuum due to its specific task of transporting frozen hydrogen, this option is not viable. Due to the given boundary conditions, only vibration monitoring on non-rotating parts, in this case the casing of the centrifuge, remains. The reason for still looking into ways to find out what needs to be measured, is to know whether vibration signals measured on the housing include useful information about the shaft's vibratory behavior or not. [44]

According to DIN ISO 20816, machines can be classified in four categories: 1. Reciprocating piston machines; 2. Rotating machines with rigid rotors; 3. Rotating machines with flexible rotors; 4. Rotating machines with quasi-rigid rotors. Depending on which category is the correct one, the standard gives information about whether it is necessary or not to measure on rotating parts of the machine. Type 1, 2 and 3 do not necessitate a sensor monitoring vibrations close to the shaft, as the signal transduced on non-rotating parts contains enough information about the rotor behavior. This is not the case for machines with flexible rotors (Type 4), here a sensor should be placed on (or close to) a rotating part, preferably the rotor. Since we know that the centrifuge is a rotating machine, only categories 2, 3 and 4 come into consideration. To find out whether a rotor is rigid or flexible, its first critical speed, which coincides with the first natural frequency of the system, must be calculated. If the machine operates below this frequency, it can be viewed as rigid, above it behaves flexible. [44]

There are several approaches to finding the first critical speed, one of which is the impact hammer test as explained in section 3.2. The area around the first peak is considered to be the first critical speed. Despite the simplicity of this experiment, it cannot be performed on the pellet launcher. The unit to be excited must consist only of the rotating parts, not the entire machine itself. Since there is no easy way to disassemble the centrifuge, it would not be possible to differentiate between the natural frequencies of the housing and the rotor. [45]

Another method is to use a CAD model of the rotor to calculate its first critical speed with an FEM tool. Fortunately, a 3D model of the entire centrifuge already exists. However, since the documentation, such as technical drawings, is incomplete and not always accurate, some assumptions, such as dimensions or material properties, had to be made when designing the individual parts. This analysis is only accurate if all rotating parts are taken into account. To simplify FEM modeling, done in *Ansys*, the masses and inertias of all rotating parts connected to the shaft were calculated in *CATIA*. Using this information, a *point mass* was applied to the shaft to simulate the missing parts, eliminating the need for complex contact modeling (Figure 11). The centrifuge shaft is supported by two bearings. The lower (floating) bearing was replaced by applying frictionless support to the contact surface. The effects of the upper (fixed) bearing were simulated using remote displacement, where all motion (except for z-rotation) was set to 0. To analyze at what rotational speed the centrifuge would pass its first critical speed, the model included five different steps, each with an individual shaft frequency (0 Hz, 60 Hz, 140 Hz, 180 Hz, 210 Hz).

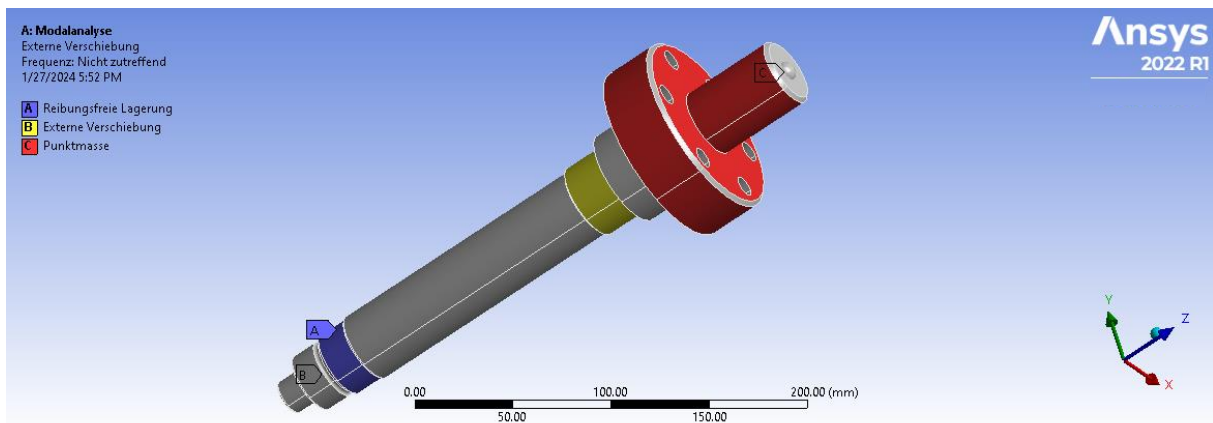


Figure 11: *Ansys* FEM model of the AUG centrifuge's shaft. The surfaces on which a point mass was applied, can be seen in red. The frictionless support for floating bearings, can be seen in blue. The fixed bearing simulation, here in form of a remote displacement, can be seen in yellow/green. Marker C, on top of the shaft, marks the heavy point of the applied point mass. This allows for a precise calculation of mass moment of inertia.

First, the model was computed looking only for the first mode (natural frequency). For this, the rotor behaved rigidly during all five steps, which means that the first critical speed of the system is > 210 Hz (Figure 12). Since adjacent modes influence each other, this simulation did not include any of these dependencies. To improve the accuracy of the results, the mode limit was set to 2, 10, and then 50 to ensure that overlapping effects were included in the FEM calculations. The effect of this step can be evaluated by comparing the first mode evolution in

the Campbell diagrams (Figure 12, Figure 13). The Campbell diagram is a graphical representation showing the relationship between rotor speed and natural frequencies of a rotating system. Clearly, mode overlap plays an important role in model validation. This and the Coriolis effect, which was activated in *Ansys* before starting the calculations, strongly influence the simulation result. When two modes were used for the computations, the critical speed shifted to 11471 rpm, for 10 and 50 modes (*Appendix A*) it was 11461 rpm (≈ 191 Hz), resulting in a rigid rotor behavior and thus a category 2 machine for both operating frequencies of the centrifuge (~ 60 Hz, 140 Hz). Since only nearby resonant regions influence each other, further calculations with > 50 modes were not necessary. The result correlates with other experiments carried out in the years 2010 - 2022. During run-ups and -downs of the centrifuge, a significant resonance region was found between 170 Hz and 200 Hz (Figure 26), providing one more reason why this range should be avoided at all costs. [44], [46]

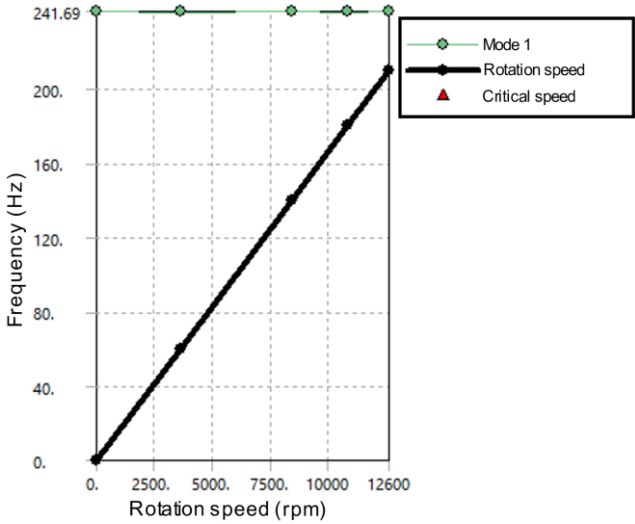


Figure 12: Campbell diagram of a simulation with six speed-steps and one mode. A mode displays the critical speed’s frequency. Both the x- and y-axis represent possible values for the shafts speed, only in different units. Although the legend includes the *critical speed*, there is no cross section and therefore no value for it.

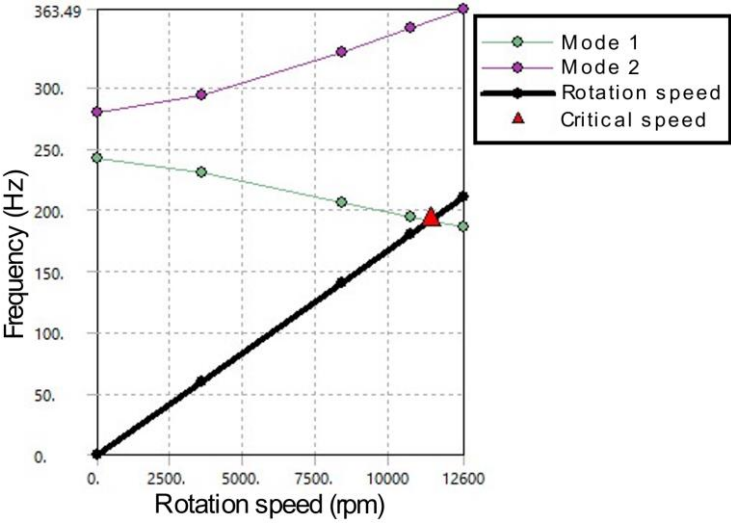


Figure 13: Campbell diagram of a simulation with six speed-steps and two modes. A mode displays the critical speed’s frequency. Both the x- and y-axis represent possible values for the shafts speed, only in different units.

4.2.2 Measurement method: Analytic process

Since the selection of a measurement method based solely on the machine category, which was not done using the real centrifuge but only a simplified model of it, is not considered to be the most accurate experiment, another method was investigated. An analytical procedure to determine the correct measurement method is to calculate the stiffness ratio α according to (8). [44]

$$\alpha = k_2^*/k_1^* \quad (8)$$

Where k_2^* is the amount of dynamic stiffness of the bearing pedestal, and k_1^* is that of the bearing in N/mm.

Depending on the size of the ratio, a decision can be made whether to measure on rotating or non-rotating parts (Figure 14). According to [44], when $\alpha \leq 1$, it is recommended to measure on the housing, which is a non-rotating component. Absolute shaft vibration, i.e. on a rotating component, should be measured when $0,2 \leq \alpha \leq 5$ is observed. Relative shaft vibration is usually measured when $\alpha \geq 2$. In the case of the centrifuge, it is not easy to calculate the rigidity. Apart from the already mentioned incomplete technical drawings, there is no information on the installed shoulder ball bearings. Hence, the stiffness of the bearing pedestal is not easy to determine due to its complexity. Ideally, assumptions about the stiffness ratio can be made from existing value tables. However, since the AUG centrifuge is not a machine covered by a standard, a statement could, if possible, only be made based on similarities to other machines. DIN ISO 20816 (partly still 10816) is divided into nine separate documents. For obvious reasons, the centrifuge does not fall within the scope of either wind turbines or piston engines. The documents for turbines and generators do not cover the centrifuge either. Although part three of the standard (Industrial Machinery) is very broad, no machine similar to the centrifuge is mentioned. Parts five and seven of the standard discuss, among other things, pumps. However, DIN ISO 10816-7 only contains instructions and data for pumps that work with liquids. Even if a first glance at part five of the standard suggests hope, as it deals with pumps driven by electric motors, it is not compatible with the centrifuge for two reasons. Firstly, the standard does not mention turbomolecular pumps (TMPs), and secondly, the document focuses on larger and much slower rotating machines ($60 \text{ min}^{-1} - 1000 \text{ min}^{-1}$). Since the pellet centrifuge is an electrically driven TMP with a maximum operating speed of 8400 min^{-1} , neither stiffness ratios, limit values nor the exact measurement method can be derived from standards. [42], [44], [47], [48], [49]

Since no solution was found using the analytical approach, the combination of FEM analysis results and the fact that shaft vibration measurement is simply not possible leaves only the method of *measuring on non-rotating parts*. Nevertheless, vibrations are expected to contain enough information about rotating parts so that a monitoring system carried out in this way still maintains a high level of quality.

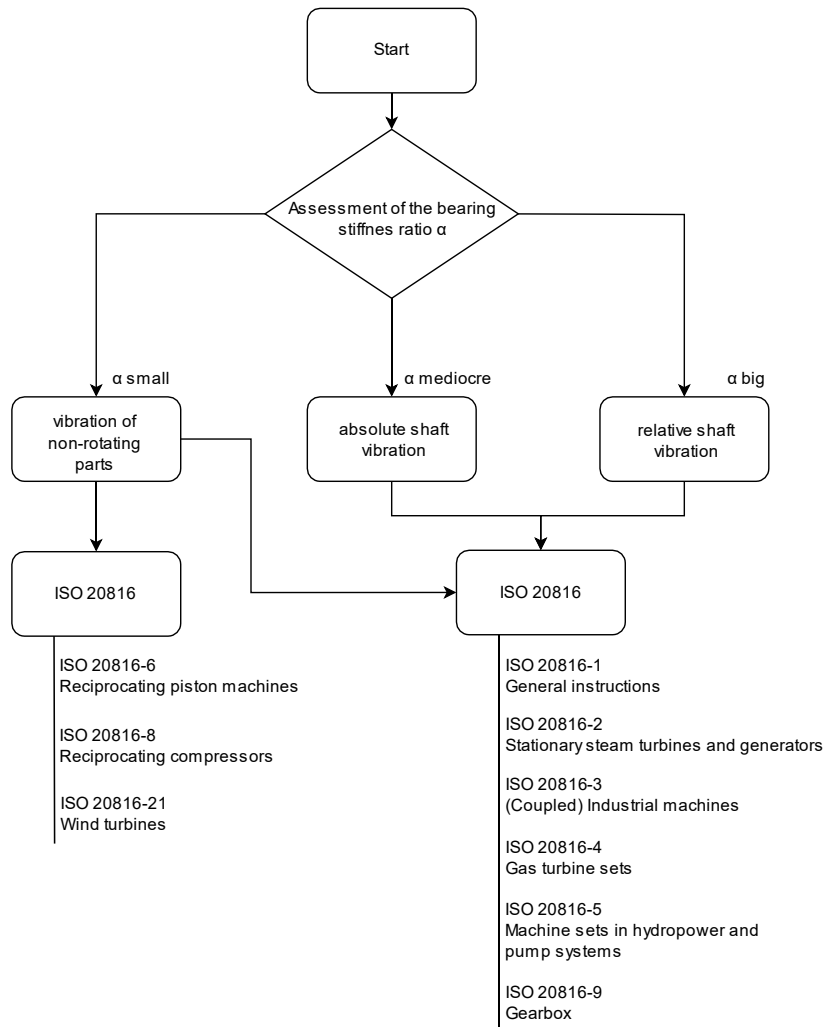


Figure 14: Flow chart for analytical selection of the appropriate standard for machine vibration assessment. Each stiffness ratio leads to a different subset of the DIN ISO 20816. [44]

4.2.3 Sensor selection

Sensor selection plays an important role in instrumentation, including vibration monitoring. Sensors for this application are basically divided into three categories: Acceleration sensors, velocity sensors and non-contact sensors. Before the best sensor can be selected, the measurement task must be clearly defined. For the centrifuge, vibration measurement on the housing was chosen for the reasons mentioned above. Eddy current proximity probes, which are non-contact sensors, are commonly used to measure shaft vibration and are therefore not suitable for monitoring the centrifuge. From Figure 15, it is easy to see why acceleration sensors are used in most cases rather than velocity sensors. The dynamic range is a parameter that describes the frequencies (x-axis) and vibration velocity amplitudes (y-axis) each sensor can reliably measure. The piezoelectric sensor's dynamic range clearly exceeds that of the electromechanical, especially in the frequency range. With an electromechanical sensor, monitoring the bearings of the centrifuge (high frequency range) could therefore be difficult. Since the piezoelectric accelerometer proved to be well suited for the measurement task, it was selected as sensor. [41]

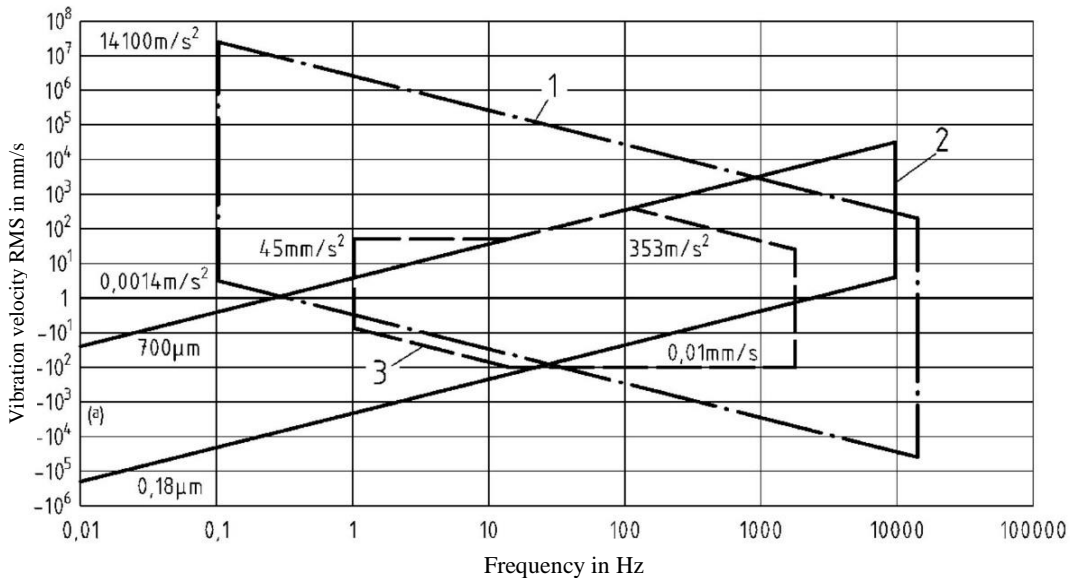


Figure 15: Dynamic ranges of vibration transducers typically used for machine condition monitoring as a function of frequency. Curve 1 represents the dynamic range of a piezoelectric acceleration sensor, curve 2 that of an eddy current displacement sensor, and finally curve 3 the range of an electromechanical velocity sensor. [41]

Piezoelectric sensors differ primarily in design. Depending on the application, special sensors can be selected, such as those suitable for high temperatures or shocks. Since the centrifuge is located in a part of the torus hall where no extreme conditions (relevant for piezoelectric sensors) occur, a standard design is used (Figure 16). Two models of the Siemens *VIB-SENSOR-03* with a frequency range of 0.2 Hz to 3 kHz were selected. The sensors have a sensitivity of approximately 500 mV/g, which translates to an output voltage of 500 mV at one $g \approx 9,81 \text{ m/s}^2$. The measuring range extends over 10 g, resulting in a maximum output voltage of 5000 mV. The sensors have a Military Specification (MIL) connector at the top. [41], [50], [51]

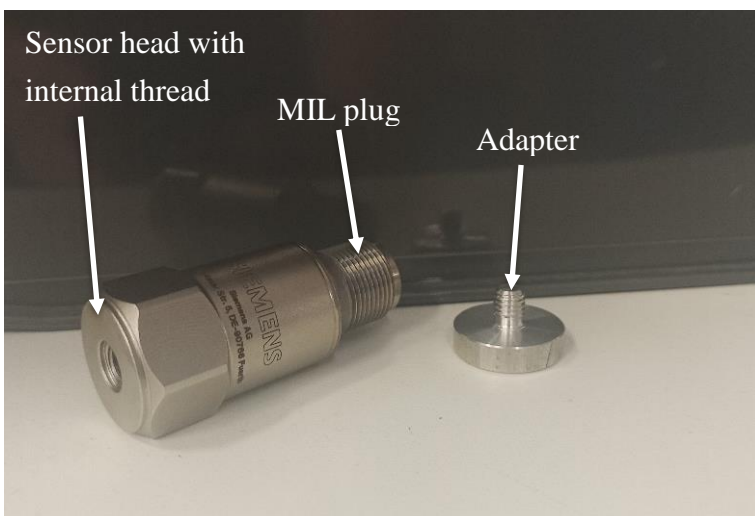


Figure 16: Siemens piezoelectric acceleration sensor. The adapter was screwed to the sensor head for installation and attached to the AUG centrifuge housing.

4.2.4 Measurement location: Optimal points and mounting method

One of the most important initial considerations is the selection of meaningful measurement points. While there often are predefined locations for new and especially serial machines, other systems require custom mounting solutions. For piezoelectric accelerometers in particular, there are a number of conditions that must be met. For example, the point on the machine should have a smooth and flat surface. If only curved surfaces are accessible, as it is for the centrifuge, a special mounting of the sensor, e.g. by using an adhesive can be applied [38]. When considering the system environment, temperatures, magnetic fields, and other external influences must be taken into account. The most important criterion, however, is the distance and, above all, the composition of the space between the vibration source and sensor. This should be as short and undamped as possible, which can be problematic for machines not designed for this measurement technology. Vibration sources are primarily the drive shaft, rotors and plain or roller bearings of a machine. [43], [50]

In the case of the pellet centrifuge, measuring points near the bearings are particularly suitable. The main reasons for this are the structure and the actual condition of the machine. The large housing, which also serves as protection against flying parts, severely limits the choice of monitoring locations. The wooden casing (Figure 17) and the relatively large distance between the bearings (Figure 18) make measurements around the rotor center impractical. The distance between a component and the nearest possible sensor eliminates the possibility of measuring near the upper bearing. Location 6, which is much closer to the lower bearing, measures 0.2 - 0.3 times the distance of location 4. Since both accessibility and distance favor the lowest (and already used) measurement location 6, it was reused in almost the same way.

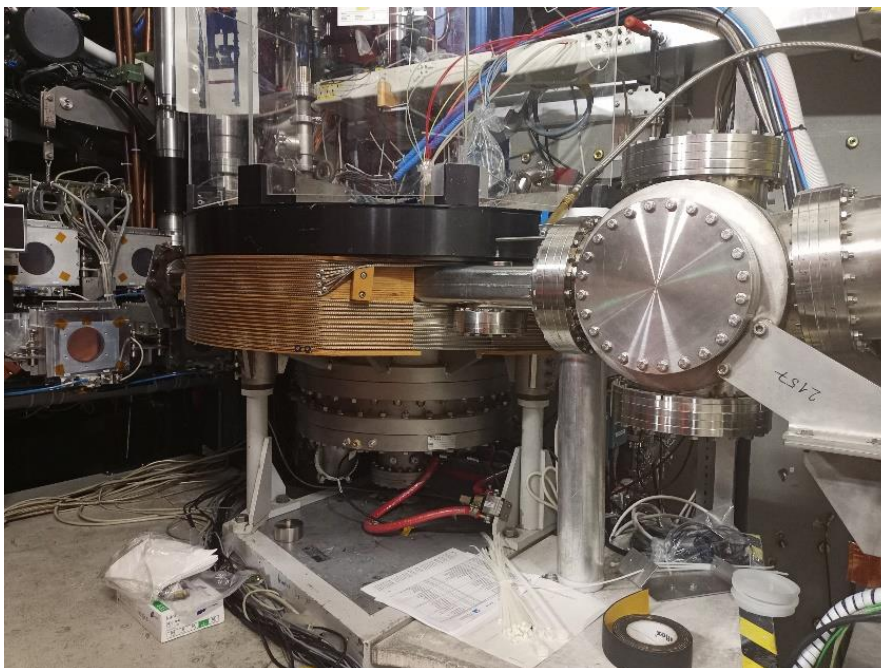


Figure 17: (a) General view of the AUG centrifuge, located in the Torus Hall, with clearly visible wooden casing. On top of the centrifuge is usually the cryostat for ice production. On the right, the start of the looping-shaped guiding tube can be seen. The centrifuge is mounted to the ground using three identical support beams.

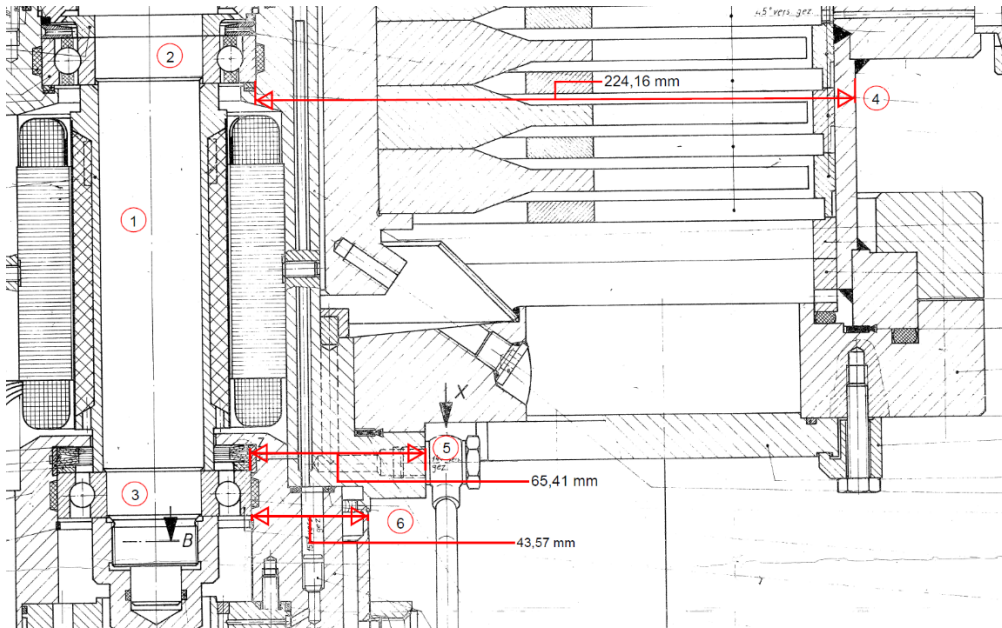


Figure 18: Detail of the overall technical drawing of the AUG centrifuge. The shaft (1) and the upper (2) and lower (3) bearings are shown. The distances of the possible measuring points (4, 5, 6) were determined by comparison with other, dimensioned distances on the drawing.

When using two sensors, as is the case here, there are two different ways to arrange them. The vibrations can either be recorded only horizontally or both horizontally and vertically. If the system under consideration is to be monitored continuously over a long period of time, it is sufficient to measure the vibrations in the radial direction. Machines with axial bearings are an exception. Since the centrifuge does not have any axial bearings (but shoulder ball bearings), two sensors are used in the radial direction. These are mounted at a 90° angle, but since there is limited space at the bottom of the centrifuge, only four specific points (Pos. 1-4) were selected to start out with (Figure 19). The 90° angle allows for precise vibration phase measurements, where one sensor uses the other sensors phase signal as a reference point. This can be used for analysis tools such as bode plots. [42], [52]

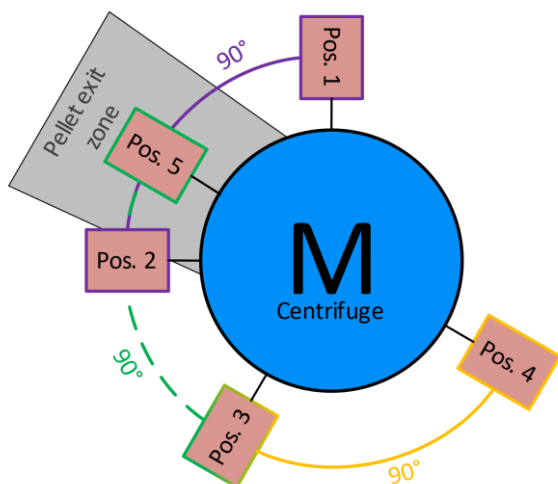


Figure 19: Possible sensor positions at the selection locations at the AUG centrifuge with a 90° angle between 1&2, 3&4 as well as 3&5. All locations are the same in the horizontal plane.

Picking the correct measurement point, depends on where the highest levels of vibration can be transduced. To ensure sure that both sensors measure the same signal when connected to a specific position, VIB1 was first affixed to Pos. 1 and VIB2 to Pos. 2, after that they were swapped. During a short run-up and -down, signals from both tests were compared and found to be consistent. After days of operation with this setup, VIB1 and 2 were connected to Pos. 3 and 4, respectively. By comparing the different RMS levels, it became clear, that the favorable measurement points are 2, and especially 3 (Figure 20). However, since a 90° angle between both sensors should be maintained, using these two positions together would not be possible. Therefore, VIB1 stayed connected to Pos. 3, and two VIB2 options were investigated. First, another adapter was affixed to the new Pos. 5. Unfortunately, even lower RMS amplitudes were transduced from this setup. Therefore, the second option, Pos. 4, turned out to be the optimal solution for a real-time monitoring system. This was found to be true for both 58 Hz and 140 Hz operation of the centrifuge.

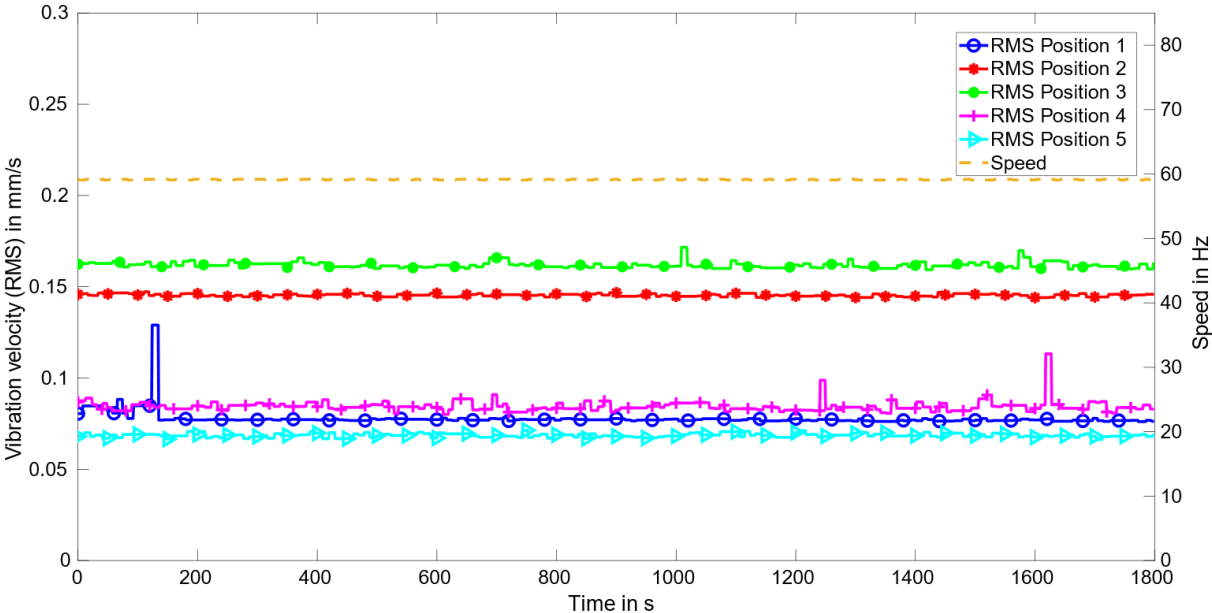


Figure 20: This graph shows the different RMS levels for each of the AUG centrifuge's sensor position (1-5). Position 1&2 were tested first, then 3&4, and at last 5. The peaks, especially the ones seen of location 1 and 4, can be attributed to external vibration sources, like labor close to the centrifuge (more precisely, those sensor positions). The speed was constant for each series of measurements (58 Hz).

For these experiments, sensors had to be affixed and later removed from a certain location several times. The best way to mount a sensor in terms of measurement results is to use a threaded pin or screw. One side of the pin is connected to the head of the sensor and the other side is screwed into a threaded hole in the housing. Since it is not possible to drill into the housing of the centrifuge due to the vacuum, another method had to be chosen. Two common methods are using magnets or gluing the sensor or an adapter to the housing. Because of the stainless-steel vacuum vessel of the centrifuge, the sensors had to be glued in place. Due to the good properties of epoxy resin adhesives, both probes were screwed together with an adapter piece and glued to the housing using a 2-component epoxy resin adhesive (*UHU Plus*

ENDFEST 300). The adapter piece is used for the need of an easy (dis)assembly of the sensor during repair work around the measuring point, as well as for later modification. [43]

4.3 System in use

In order to be able to evaluate the vibrations measured on the centrifuge, a measurement chain must be established between the sensors and the screen output, which filters and converts the measured state variables in a meaningful way. Today, a large number of condition monitoring systems (CMS) are available for this purpose.

Selected filters are used to process this data so that it can be converted to velocity by the first derivative and to displacement by the second derivative. Both velocity and acceleration signals can be converted to frequency-dependent data in the base unit using FFT. The *Siemens X-Tools* software is available for further analysis. The actual speed of the centrifuge is often of interest. Since neither the shaft nor the acceleration arm of the machine are accessible to measuring devices, the speed must be transferred to the module via a signal from the motor controller. For this purpose, the first analog input (AI1) is configured as shown in Figure 21. Since the input signal ranges from 0 V to 10 V, the lower half of the analog input (-10 V to 0 V) had to be compensated with speed values -12000 rpm to 0 rpm. The value of the input is permanently overwritten on SPEED2, an internal channel of the module, and can therefore be read and monitored in the trend graphs. [53]

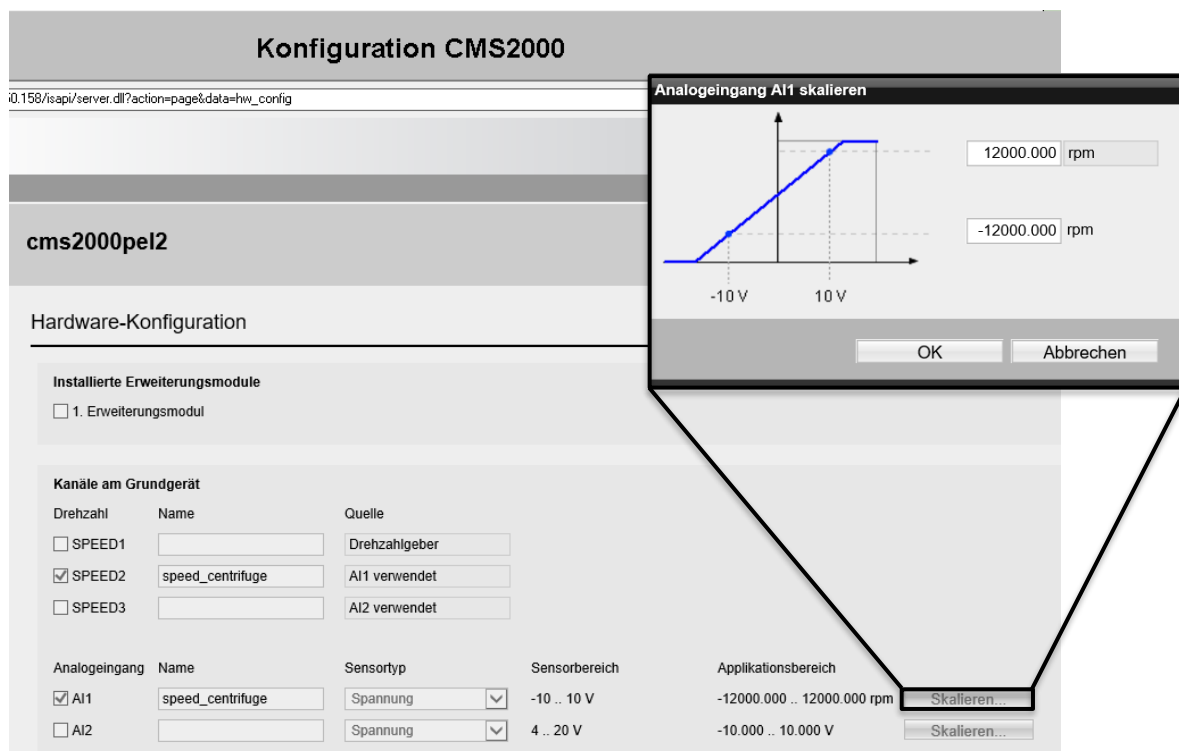


Figure 21: Hardware configuration of the *CMS2000*. The scaling function allows any value (e.g. rpm) to be plotted on a voltage scale from -10 V to 10 V.

The base module, as found in the Torus Hall, is powered by the 24V DC power supply (Figure 22). The values measured by the sensors are transmitted to the controller via two vibration inputs VIB1 and VIB2. As described above, the analog input is used to obtain the shafts rotational velocity. The module can be accessed in a browser window using the ethernet connection. The indicator lights on the front of the module reflect the current status of the system. [53]

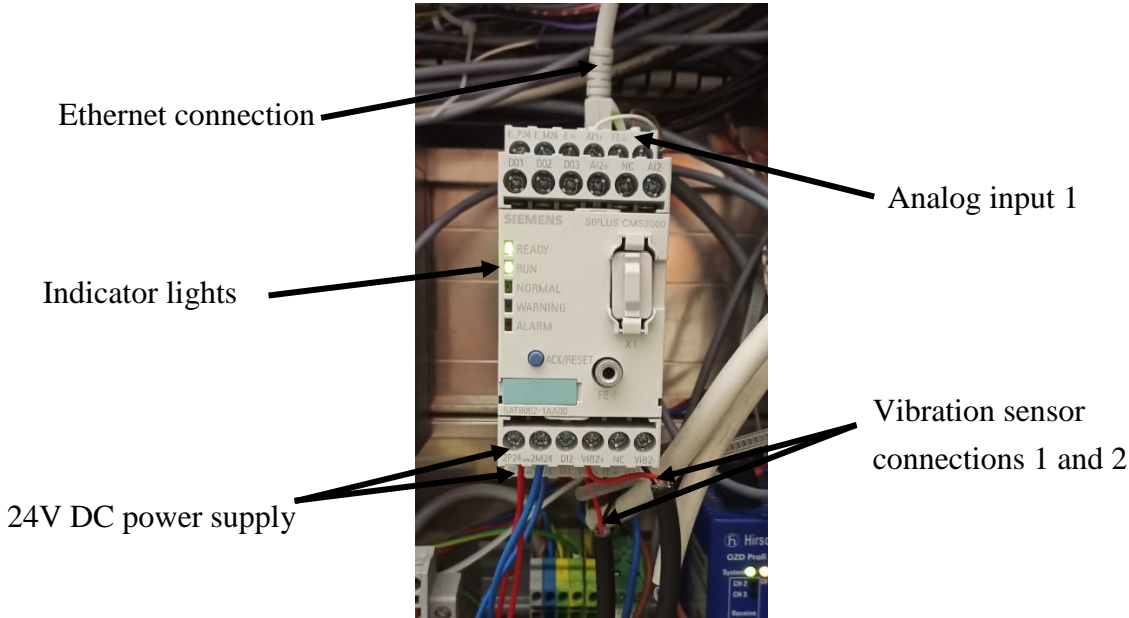


Figure 22: Siemens Siplus CMS2000 base unit. The module is powered from the 24 V DC supply and has IEPE sensor inputs, analog inputs, and digital inputs and outputs.

The web interface consists of a large number of segments that contain both module configuration settings and vibration data plots.

4.4 Analysis tools

Analyzing vibration data is only possible by using filters and algorithms that first process the information and then visualize it in a way we can understand. These so-called analysis tools exist in various degrees of complexity. The individual methods can be roughly divided into two categories: Time domain and frequency domain. [52]

4.4.1 Time domain analysis

The most commonly used assessment parameter for time analysis is the vibration velocity’s root mean square (vRMS) value (9).

$$v_{rms} = \sqrt{\frac{1}{T} \int_0^T v^2(t) dt} \tag{9}$$

Where T is the measurement duration, which must be greater than the largest period length of the measured data, and $v(t)$ is the vibration velocity as a function of time. A vRMS signal

reflects the energy content of the vibrations and thus provides an accurate picture on the effects of internal forces on the machine. This parameter can be used to analyze both the broadband and narrowband range. While a broadband spectrum covers the largest possible number of frequencies, the narrowband spectrum limits itself to essential (machine-typical) frequencies.

The vRMS of a broadband signal contains not one, but many machine-component-specific signals (Figure 23a). Therefore, it only provides information about the overall condition of the machine, and a frequency spectrum must be calculated for further analysis. However, it is possible to monitor individual parts of a machine by computing the vRMS for a narrow band. For example, if a shaft is rotating at 60 Hz, a 55-65 Hz narrowband analysis can provide information specific to the rotor (Figure 23b). While it is more precise and easier to use the frequency spectrum for analytics, this method is extremely helpful when setting up limit values. [54], [55]

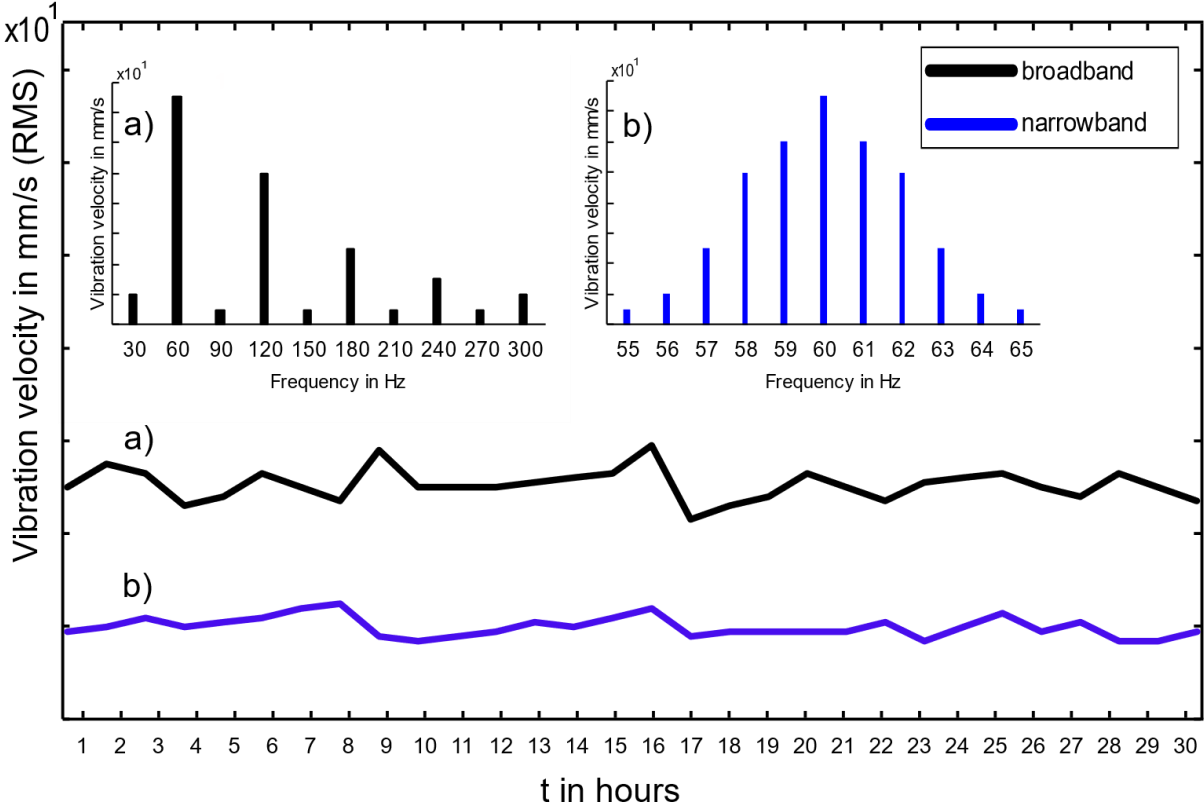


Figure 23: a) Simulated broadband frequency spectrum and vRMS (0 Hz - 300 Hz); b) Simulated narrowband frequency spectrum and vRMS (55 Hz - 60 Hz). The graphs in black present an overview of the machine in general, those in blue of a specific machine component (e.g. the rotor).

A second time-domain parameter frequently used with the CMS is the Diagnostics Characteristic Value (DKW), it is an excellent tool for high frequency monitoring. In a typical machine, high frequency components are usually bearings and gears. Since the centrifuge has no gears but two bearings, these are considered to be the main sources of such vibration. The DKW is the reciprocal value of the well-known parameter $K(t)$, and can be calculated using the following formula (10):

$$DKW(t) = \frac{a_{max}(t) \times a_{eff}(t)}{a_{max}(0) \times a_{eff}(0)} \quad (10)$$

Where $a_{max}(t)$ represents the maximum vibration acceleration at any given time, $a_{eff}(t)$ the RMS value, and $a_{max}(0) \times a_{eff}(0)$ the reference value. As the bearing condition deteriorates, the numerator increases in value relative to the denominator, so the DKW is expected to increase over time (Figure 24). However, since there are different levels of damage to a bearing, vibrations do not always increase as fast as shown in the figure below. Even a slight increase in the DKW could be a foreshadowing of a serious fault. Unfortunately, this parameter is only useful for monitoring the overall health of such components. For a deeper insight into bearing failures, an FFT calculation must be performed. [56]

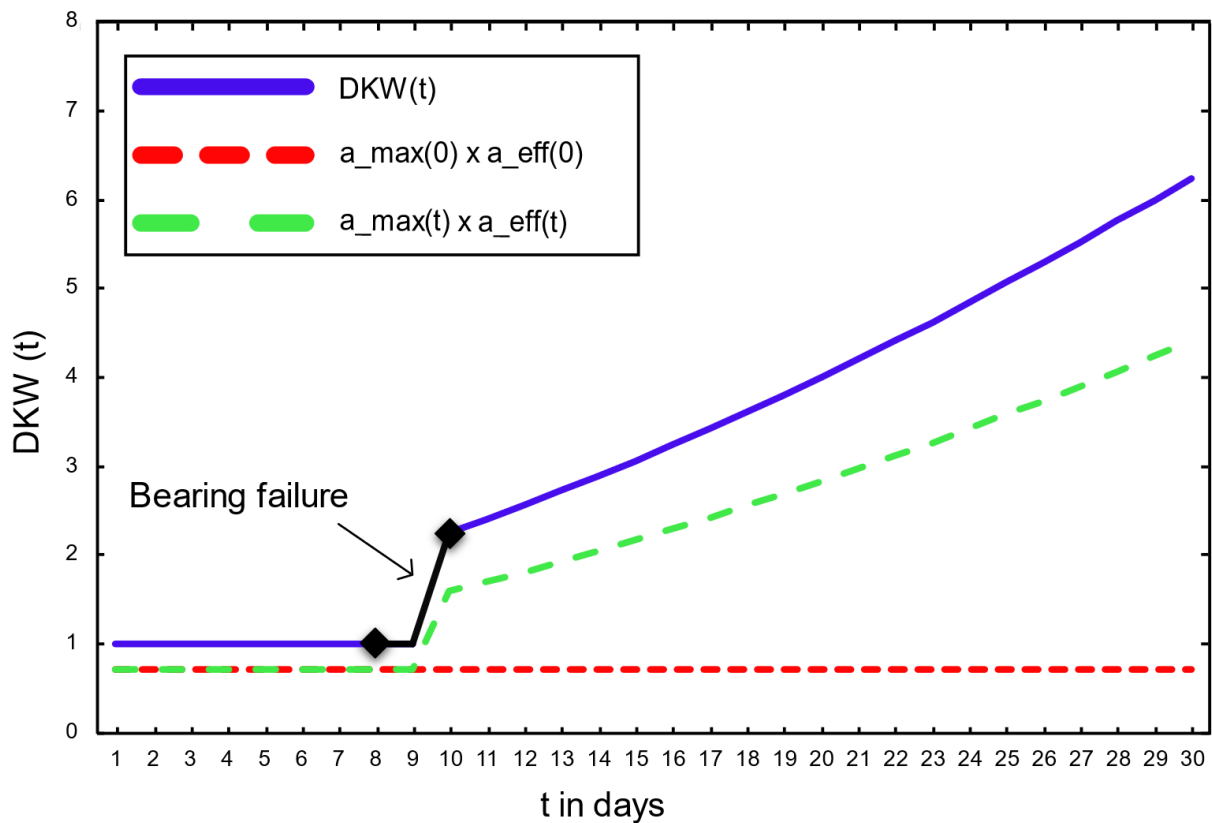


Figure 24: DKW trend of a failing bearing. Given in red is denominator, its value does not change over time, since these are the reference values for the DKW calculation. In green, the numerator can be seen increasing as soon as the bearing failure occurs. The DKW itself, the blue line, represents the change in difference between the denominator and the numerator.

4.4.2 Frequency domain analysis

An uncomplicated and quick method of deriving information about the nature of a vibration problem is to use the FFT to generate frequency spectra. Here, broadband (Figure 23a) or narrowband (Figure 23b) spectra can be computed as required. With the help of information from standards and publications, it is often possible to make an accurate statement about the cause of the increased vibrations based on peaks occurring within a frequency spectrum. In most cases, when measuring on a machine driven by a shaft, the highest vibrational level will

occur at the operating frequency, also known as the first harmonic (h_1). The h_1 vibrations, followed by their n -integer multiples (h_2, h_3, \dots, h_n), usually contain the most energy and are therefore easy to detect in a spectrum (Figure 25). Fortunately, most major machine faults can be detected by monitoring the harmonics. A typical sign of deterioration is an increase of the first three, in which case, according to standards such as DIN ISO 13373-3, the machine's shaft is likely to be misaligned. [57], [58]

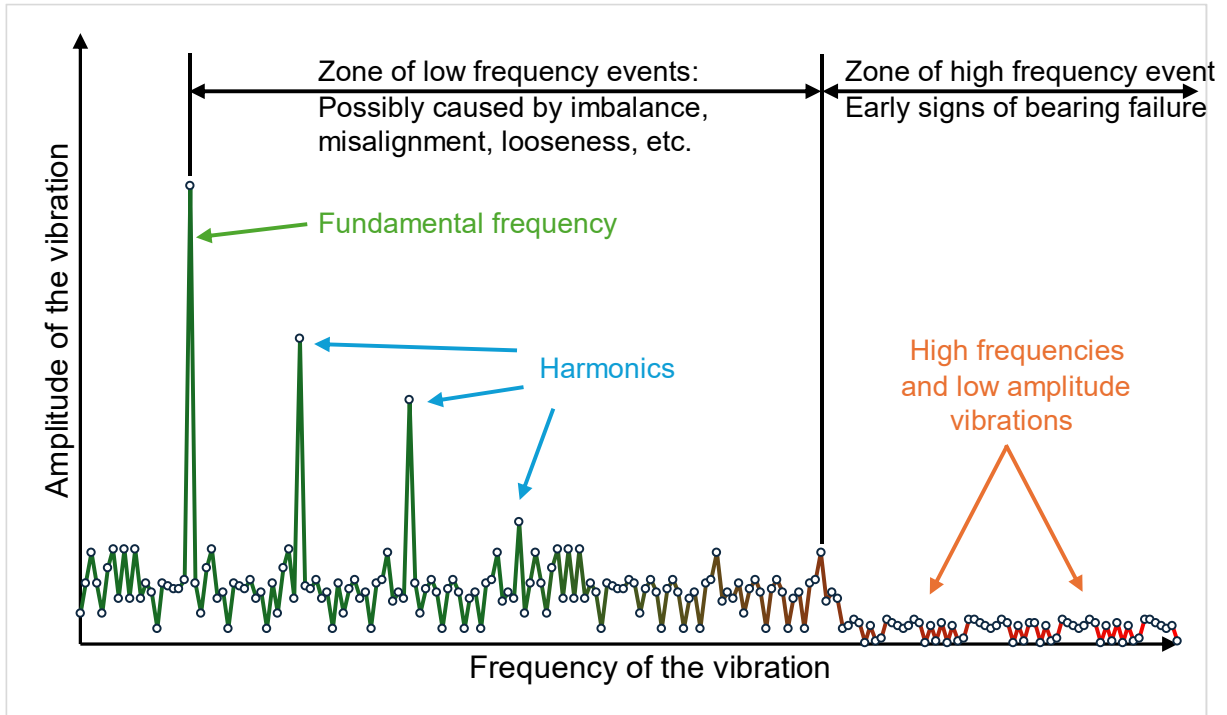


Figure 25: Simulated frequency spectrum of a machine vibration signal. [59]

Other faults, such as bearing wear, are not represented by harmonic peaks. These high-frequency signals contain significantly less energy than those from larger machine components, making them difficult to detect, as can be seen in Figure 25. In a frequency spectrum, especially when the measured unit is velocity, they are often undetectable and act as background noise. When dealing with bearings or a gear, vibration acceleration is usually the best unit to measure in, because it is more consistent and precise when dealing with high frequencies. What kind of spectrum one should use for analysis, depends heavily on how much information about these vibration sources exists. If not a lot of information is available, often a simple acceleration frequency spectrum is enough to monitor these parts. However, for systems where the exact rollover frequencies of the bearings can be calculated, a tool called envelope analysis has been developed for fault detection. There are multiple ways to generate such a spectrum, one of which is explained in [60]. It is important to find the best frequency range to analyze, ideally with a high amount of impulsive signals that often come from bearings. This range is then tuned for those low energy impulsive signals, while filtering out high energy signals coming from the shaft or other machine parts. [60]

5 Analyzing vibration measurements on the AUG centrifuge

5.1 Existing vibration data and deductions

Before further research and experimental data were collected for this thesis, the knowledge about vibration levels and the behavior of the AUG centrifuge consisted only of a relatively small amount of experimental data gathered from 2010 to 2022. It is known that there are several critical frequencies that must be avoided for a safe and stable operation. The most notable resonance regions are around 35 Hz, 70 Hz and 180 Hz (Figure 26). None of these areas conflict with any of the operational modes used at ASDEX Upgrade. The resonance that occurs around 35 Hz, as well as the exceptionally low vibration levels around 60 Hz, show why running the centrifuge at this frequency steadily and *continuously* is a good solution to avoid any build-up of vibration amplitude. The same argument can be made for the resonance area around 70 Hz. When starting the pellet injection mode (140 Hz), this range should be exceeded in a short time. The highest peak, shown in green around 180 Hz, limits the operating frequency of the centrifuge to speeds below this value. Since the amplitude here is about 5-6 times higher than that around 140 Hz, this area should be avoided by any means.

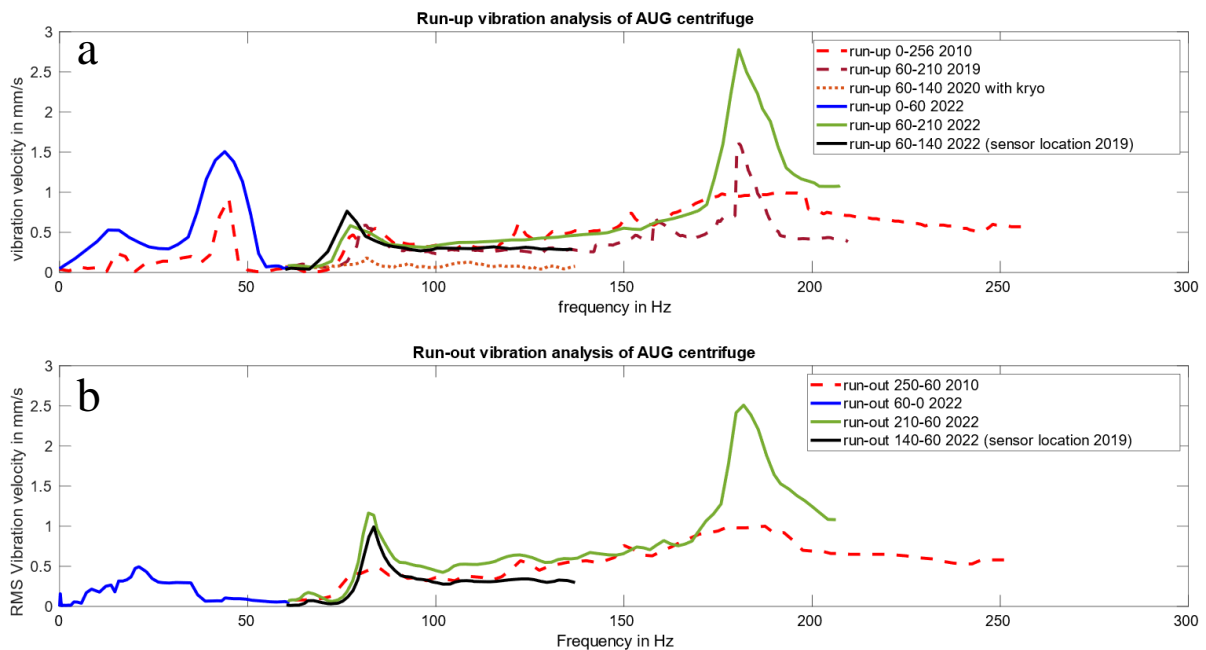


Figure 26: (a) Visualized vibration velocity data (vRMS) from (a) run-ups and (b) run-downs of the AUG centrifuge. The 2022 data is shown using a solid line. Measured amplitudes can change in size and location due to wear, but also different sensor locations and configurations of the pellet launching system. Different configurations can, for example, be with or without the cryostat on top of the centrifuge.

Apart from the vRMS data, little information was available. One example is the frequency spectra of different operational modes. These spectra provide information about the vibration levels of the system's harmonics. Almost every spectrum showed similar results, with the first harmonic displaying the highest amplitude compared to harmonics two through five. The only exception to this behavior is when the centrifuge's speed is 180 Hz (Figure 27). The unusually

high subharmonic peak ($0.5 \times$ rotor speed) could be an indicator of rotor instability, which would also explain the high v_{RMS} values when operating in this range. This theory is supported by the fact that the first critical speed of the rotor is also close to this value (≈ 191 Hz).

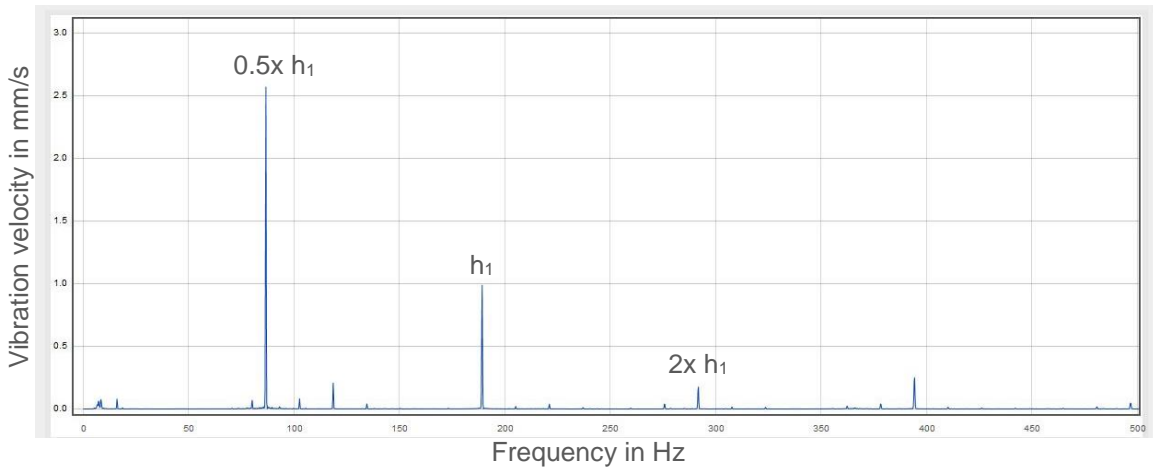


Figure 27: Vibration velocity spectrum at 180 Hz during start-up of the AUG centrifuge. The three most prominent peaks resemble the rotor speed h_1 and its (sub-)harmonics. During acceleration, the sub-harmonics were found to be present more often than during steady state operation. Since the magnitude of the peak was seen as supercritical, no stationary measurements were considered.

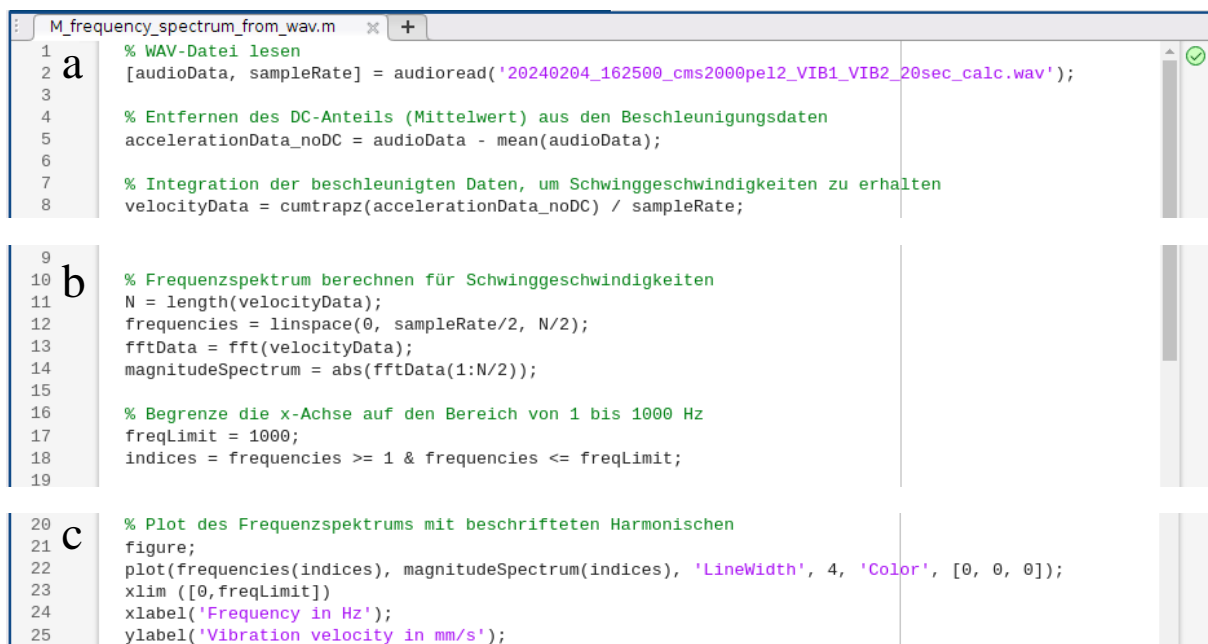
5.2 Software tools for vibration analysis

This vibration data can be accessed either through the web interface or *WinCC*, to which the *CMS2000* sends a cyclic ethernet telegram. While the web page allows to plot time and frequency domain data, it does not support modification or enhancement of it. To use more complex tools, or simply to plot the given data in different compositions, it must be downloaded and processed using different software. This works especially well with data transmitted via the ethernet telegram, which is unfortunately limited to RMS and DKW values. Otherwise, only so-called *fingerprints* and *raw data* signals can be stored. Although fingerprints contain frequency spectrum data, these files cannot be read by other software. The raw data is stored in audio files (.wav), which are accessible, but no information about the structure and content of this file is provided.

There are several methods to solve this problem, one of which is the *Siemens X-TOOLS* software. This allows the user to analyze the signals using various tools and algorithms. However, it is not bundled with *CMS2000* and must be purchased separately. Since it costs a considerable amount of money, it was decided to first try other methods that could already provide sufficient results.

Since it had been used for previous measurement campaigns, it seemed practical to write *MATLAB* code that would allow FFT analysis of the raw data. As mentioned earlier, the difficulty remains that it is unknown what values are contained and how they are stored. The code consists of three distinct parts (a-c), as shown in Figure 30. Part *a* reads the audio file and stores the data in double variables. The variable *audioData* consists of four columns, each

containing different values. To scale the information correctly, the DC offset is removed from all four signals [61], [62]. This is easily done by subtracting the mean from the original data. The final step in part *a* is to integrate the vibration acceleration to obtain velocity information, since the spectrum of this parameter is most often used for fault detection. Part *b* contains code that calculates various values necessary for plotting a spectrum, such as the frequencies and magnitude of the FFT data. This step also provides some insight into the structure of the raw data files. When rewritten into a new, separate variable, each of the four columns mentioned above can be used separately to compute the frequency spectrum. Since the spectra for columns one and two are nearly identical, and those for columns four and five provide no useful information, it is assumed that the latter do not contain acceleration-time signals. This is supported by the fact that when looking at the values stored in these variables, there is almost no variation, suggesting that a mean value may be present. Unfortunately, neither the vRMS nor the DKW correspond to these specific values, so the exact meaning remains unknown. Finally, step *c* consists of a simple plotting code for the computed data. Other methods, such as using pre-built *MATLAB* toolboxes, were tried, but all failed due to lack of structural information.



```

1  a  % WAV-Datei lesen
2     [audioData, sampleRate] = audioread('20240204_162500_cms2000pe12_VIB1_VIB2_20sec_calc.wav');
3
4     % Entfernen des DC-Anteils (Mittelwert) aus den Beschleunigungsdaten
5     accelerationData_noDC = audioData - mean(audioData);
6
7     % Integration der beschleunigten Daten, um Schwinggeschwindigkeiten zu erhalten
8     velocityData = cumtrapz(accelerationData_noDC) / sampleRate;
9
10  b  % Frequenzspektrum berechnen für Schwinggeschwindigkeiten
11     N = length(velocityData);
12     frequencies = linspace(0, sampleRate/2, N/2);
13     fftData = fft(velocityData);
14     magnitudeSpectrum = abs(fftData(1:N/2));
15
16     % Begrenze die x-Achse auf den Bereich von 1 bis 1000 Hz
17     freqLimit = 1000;
18     indices = frequencies >= 1 & frequencies <= freqLimit;
19
20  c  % Plot des Frequenzspektrums mit beschrifteten Harmonischen
21     figure;
22     plot(frequencies(indices), magnitudeSpectrum(indices), 'LineWidth', 4, 'Color', [0, 0, 0]);
23     xlim ([0, freqLimit])
24     xlabel('Frequency in Hz');
25     ylabel('Vibration velocity in mm/s');

```

Figure 28: *MATLAB* code for reading and analyzing raw data audio files, downloaded from the *Siemens CMS2000*. The code is divided into three sections, *a*, *b*, and *c*. Section *a* processes the raw data signal, section *b* calculates necessary parameters for a frequency domain analysis. At last, section *c* plots the variables in the correct order.

Similar code has been written vRMS and DKW analysis. These files can be downloaded from *WinCC* and their structure and contents are well known and documented. This makes it easy to write scripts that include storing speed, time and vibration information in different variables and plotting them in their intended composition.

5.3 Vibration velocity root mean square (vRMS)

As explained in section 4.4.1, the RMS of vibration velocity is an analysis tool in the time domain. When used on the centrifuge, it is the most important characteristic for the overall health of the machine. Analyzing this parameter during centrifuge run-up and -down is critical to finding favorable frequencies for low-vibration operation of the unit (e.g., 58 Hz). For the real-time monitoring system, however, most of the surveillance will take place during steady-state operation (58 Hz, 140 Hz).

Because two sensors are connected to the unit's housing, two different vRMS graphs (for each mode) can be plotted (Figure 29). Both sensors measure low vibration levels when the unit is set to 58 Hz. Here, the average vRMS for Vibration Sensor 1 (VIB1) is 0.2 mm/s, while Vibration Sensor 2 (VIB2) is lower at 0.08 mm/s. At 140 Hz, VIB1 measures an average vRMS of 0.43 mm/s and VIB2 0.52 mm/s. As expected, the magnitudes begin to increase as the speed increases. However, these are still stable and unproblematic values when compared to actual error ranges such as 180 Hz - 200 Hz with a vRMS well over 1 mm/s. The switch of which sensor measures the highest RMS (58 Hz – VIB1 and 140 Hz – VIB2) can be explained by the phase change of a vibration signal during a parameter change, in this case the centrifuge's frequency.

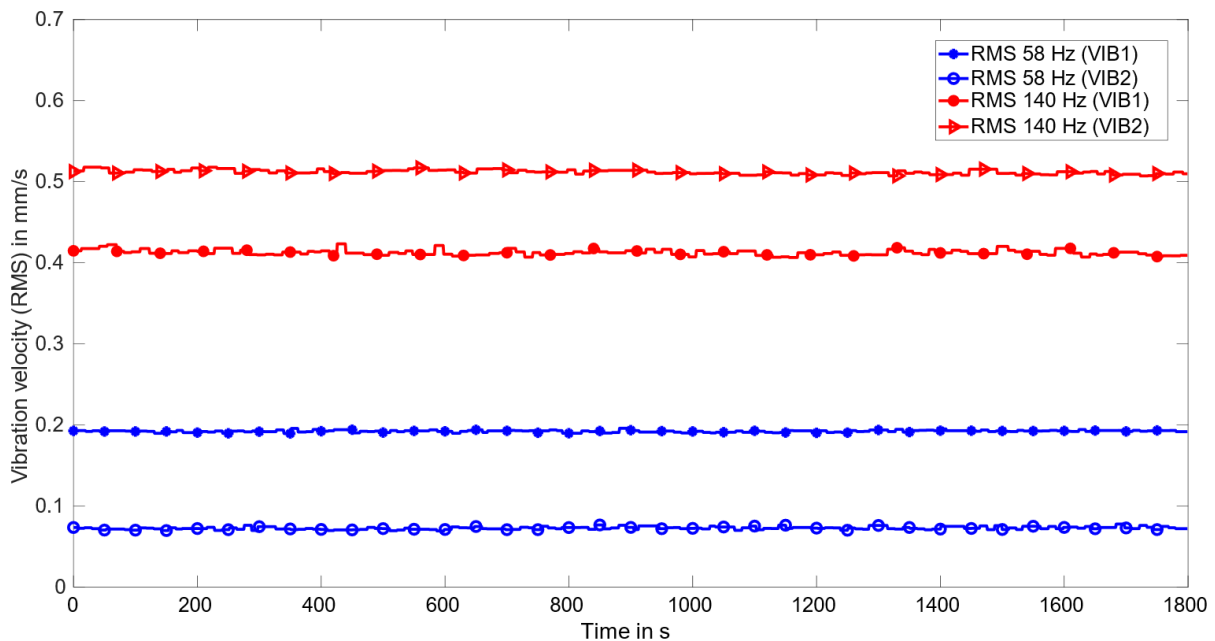


Figure 29: The graph compares vRMS values for 58 Hz and 140 Hz measured on the AUG centrifuge. The operational modes for pellet injection are referred to as 58 Hz and 140 Hz. Because the centrifuge's speed is regulated by resistors, this set value and the actual value can drift apart, as temperature fluctuates.

During measurements, it became apparent that the previously set steady state (60 Hz) was not at the optimal frequency. Although the newly selected state at 58 Hz is only a small change in speed, it has a significant effect on the average vRMS as well as better resistance to fluctuations due to speed drift, which will be further investigated in 6.1.1. The previous vRMS values for VIB1 and VIB2 were about twice as high as they are now. This improvement was found by

observing the vRMS during a run-up from 0 Hz to just over 80 Hz (Figure 30), where a local low for both sensors was detected at 58 Hz (*VIB1 & VIB2 steady area*). In addition, another low was measured for a bandwidth above 60 Hz. To determine what speed the centrifuge should be set to, the same test was repeated with a different sensor arrangement. Since only one low (58 Hz) was measured with this configuration, the small vibration levels for operation above 60 Hz are expected to be only due to a change in phase (*Misleading steady area*).

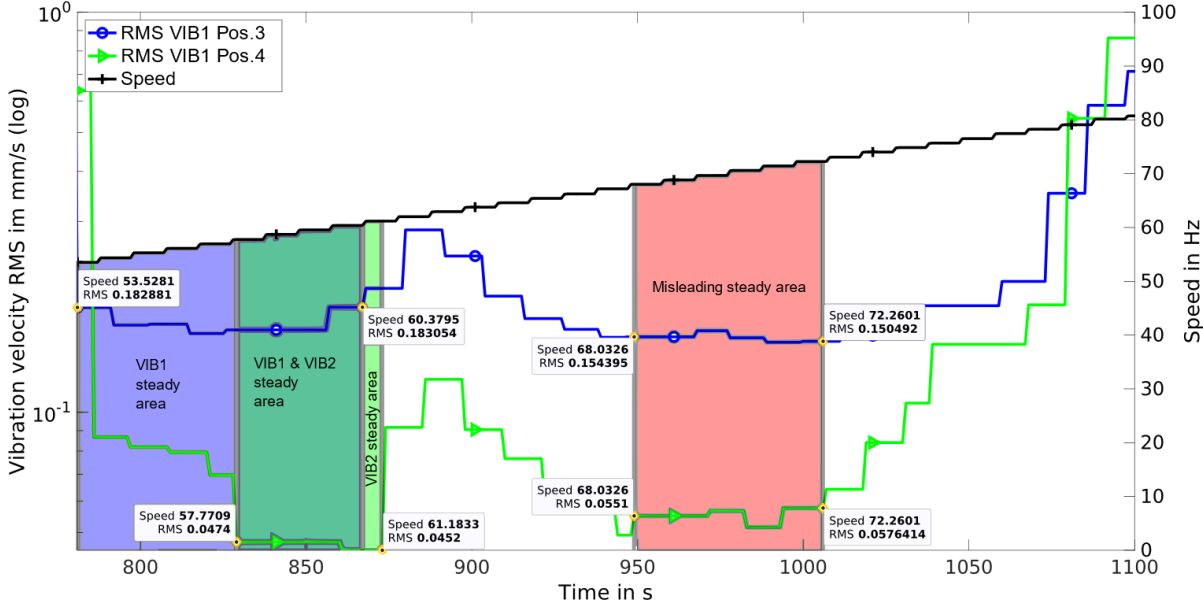


Figure 30: The graph shows the vRMS values of VIB1 and VIB2 as well as the rotational speed of the AUG centrifuge during a run-up. The vRMS is displayed on a logarithmic scale to highlight local lows and steady state areas. The colored areas resemble frequency ranges in which vibrations were stable for at least one of the sensors. It was also found that the vRMS values strongly depend on the magnitude of the acceleration of the centrifuge during the run-up. Vibration signals measured during full power acceleration from 0 Hz to 140 Hz give much higher amplitudes, especially in the resonance regions, compared to run-ups involving two steps from 0 Hz to 60 Hz and then to 140 Hz. This leads to the recommendation of a slower speed change and consequently lower vibration magnitudes when switching between operational modes is required.

5.4 Diagnostics Characteristic Value (DKW)

The bearing monitoring value, DKW, must be set for specific speeds. Depending on how fast the bearings rotate, different levels of vibration acceleration can be measured. These speed values need not to be pin-point specific, but rather set as ranges where there is no significant change in vibration behavior.

The first range of the centrifuge is around the newly set steady state frequency of 58 Hz. Here, the so-called *teaching values* form the DKW formula's denominator (10), as their average value is calculated. This is done in the *Run-Measuring-Mode* of the *CMS2000*. Over a period of approximately 2-3 hours, up to 1000 data points can be stored as teachings. The quality of the

teaching value's average, also called the reference value, improves as more data points are collected, especially in a very stable operating phase. A second frequency band, around 140 Hz, has been set up in the same way. Teaching values measured by VIB1 and VIB2 were 2.31 mm/s² & 2.63 mm/s² at 58 Hz, and 22.93 mm/s² & 36.04 mm/s² at 140 Hz. Once manually set as the official reference, the DKW for both ranges began to fluctuate around 1. This significant change in teaching values for 140 Hz, illustrates why looking solely at the vRMS of a system is often not enough to detect problematic machine behavior. While vibration velocity values do not appear to be critical, acceleration levels increase substantially. This knowledge was later used to evaluate the acceleration spectra for 58 Hz and 140 Hz (section 5.6).

Two more bands were attempted, one for 0 Hz - 58 Hz and the other for the 58 Hz - 140 Hz transient. However, this proved to be very difficult and ineffective due to the high variability of vibration acceleration during these phases (Figure 31). Therefore, no meaningful reference values could be calculated.

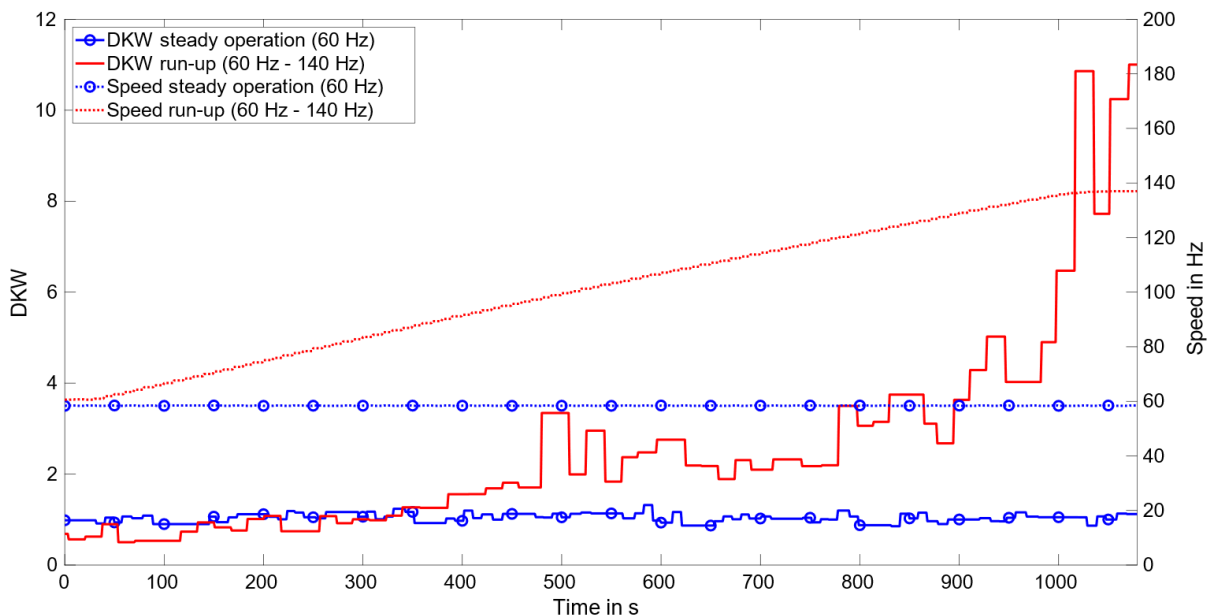


Figure 31: The graph shows a DKW and speed measurement during steady state operation at 58 Hz (blue) of the AUG centrifuge. In red, the DKW and speed progression during a run-up of the AUG centrifuge from 58 Hz to 140 Hz can be seen.

5.5 Frequency spectrum (velocity)

Looking at the more in-depth analysis tools, the velocity frequency spectrum was plotted for all relevant speeds (initially 60 Hz, later 58 Hz, and 140 Hz). While each state shows different levels of peak magnitudes (mm/s), they all share the same pattern. Although the first harmonic is very dominant, its n-times harmonics are difficult to find without knowing their exact frequencies (Figure 32). The rotational frequency's magnitude changes from 0.271 mm/s (VIB1, 58 Hz) to 0.585 mm/s (VIB1, 140 Hz) and from 0.086 mm/s (VIB2, 58 Hz) to 0.736 mm/s (VIB2, 140 Hz). Again, the same observations can be made as for the vRMS values, i.e., the vibration velocity increases as the centrifuge speed increases. In general, low harmonics

indicate that the machine is healthy, but this specific pattern is often seen when noticeable bearing play can be measured [54]. This suspicion is supported by the fact that earlier this year, as mentioned above, the *Pellet Team* measured some play in the system's bearings. Since neither the bearings nor the shaft are serviceable or replaceable, this must be accepted as the initial condition of the system.

In addition to the h_n peaks, several other stationary signals were found during testing. One is the line frequency. This particular frequency is commonly found in electrical systems that use alternating current. In the centrifuge's spectrum, it is at 100 Hz, which is twice the normal AC frequency in Europe. A change in magnitude is then most likely related to a motor fault, such as overheating or damaged rotor bars. However, the amplitudes measured on this unit have not (yet) changed over time and remained at low levels. For both operational modes, the vibration velocity was found to be < 0.1 mm/s. Since it is known that amplitudes up to 1 mm/s are still acceptable, it is not considered critical but needs to be monitored. [63]

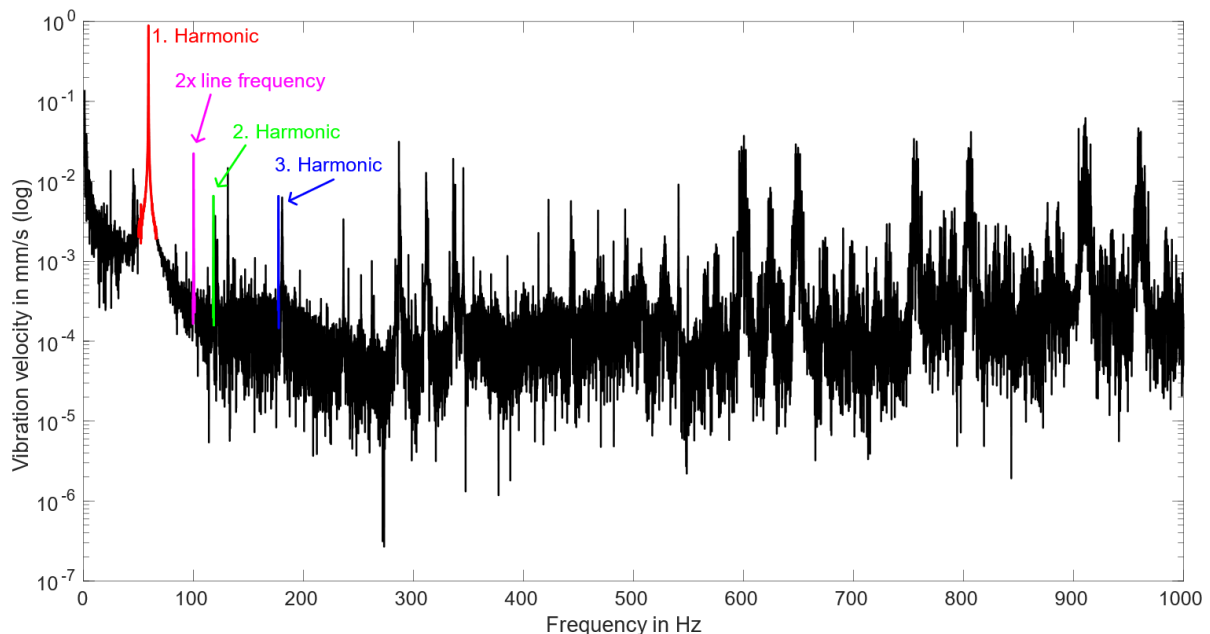


Figure 32: The graph shows a vibration velocity frequency spectrum at 58 Hz, measured by the sensor VIB2 on the AUG centrifuge. The y-axis is logarithmically scaled to emphasize the difference in amplitude between the rotational frequency and its second and third harmonics.

Furthermore, some sub-harmonic peaks were observed when the unit was accelerated to 140 Hz. As mentioned earlier, these vibration components are often indicators of shaft instability. However, these peaks mostly disappear or a significant decrease in amplitude can be observed when the centrifuge reaches its operating frequency. Finally, some noticeable peaks were found at relatively high frequencies for velocity-based frequency spectra. Since these vibrations occur together with sidebands and are found at frequencies (800 Hz - 900 Hz) much higher than the first harmonic (58 Hz - 140 Hz), they are expected to be related to bearing activity.

5.6 Frequency spectrum (acceleration)

A closer look into this bearing activity is possible by analyzing the vibration acceleration spectrum. According to [53], lower frequencies (0 - 3000 Hz) are suitable for analysis without further signal processing. Here, bearing faults can already be detected. Looking only at the spectra during 58 Hz operation, it may appear as if the very specific and clearly noticeable peaks that appear, represent bearing failures (Figure 33). However, this is often the case when the data is linearly scaled. Logarithmic scaling, which unfortunately is not possible within the *CMS2000* software, would be less misleading and less prone to errors. Because no solution could be found to get rid of errors that occur when plotting the raw acceleration data without integration (explained in section 5.2), another method had to be found. One way to compensate for this, is to simultaneously look at the acceleration time signal (raw data) and check for irregularities. Since the signals from both VIB1 and VIB2 appear to be stable, a smooth and therefore satisfactory bearing behavior is assumed for 58 Hz operation.

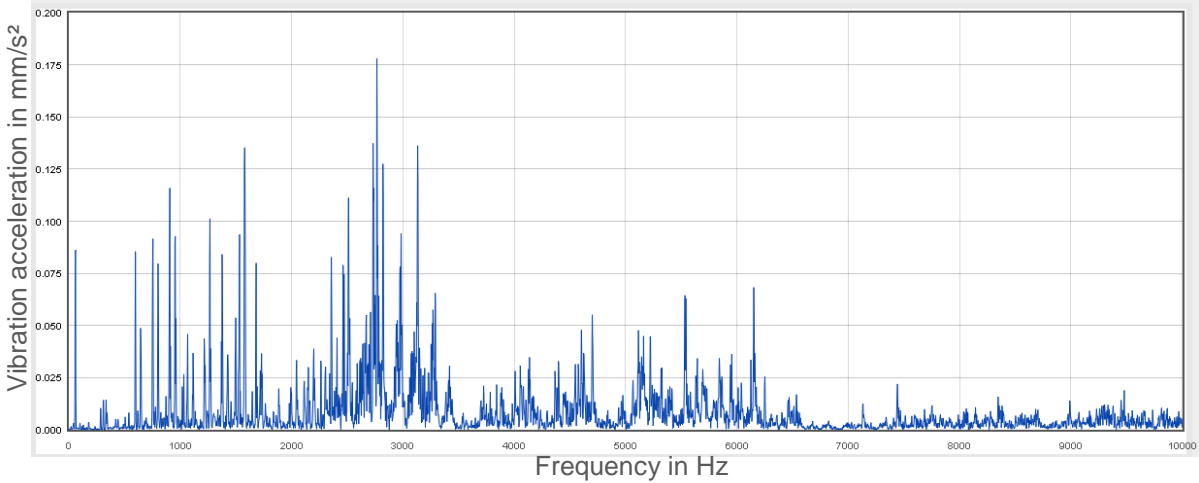


Figure 33: The graph, visualized by the *CMS2000* shows an acceleration frequency spectrum (VIB1), measured during 58 Hz operation on the AUG centrifuge.

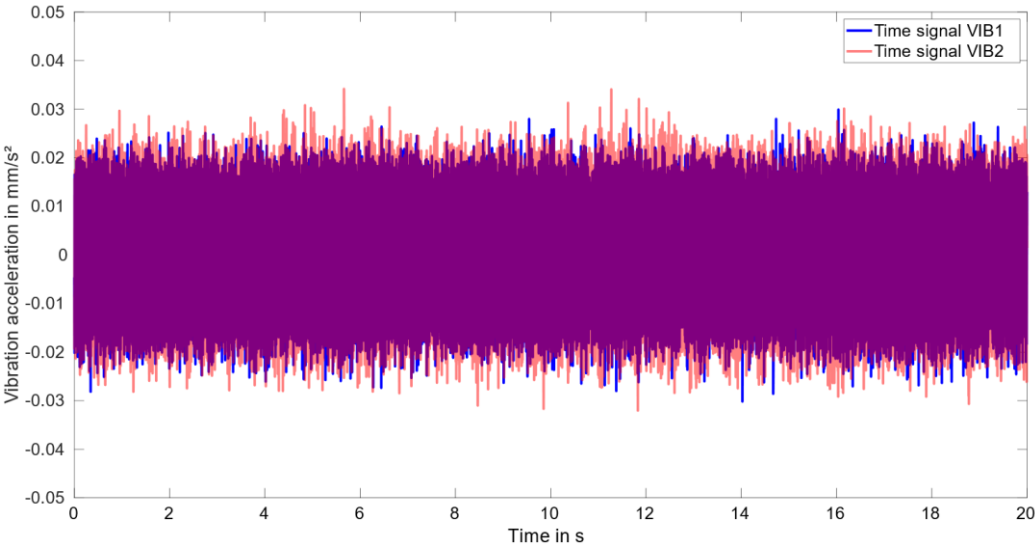


Figure 34: Time signal of the vibration acceleration, measured by VIB1 and VIB2 during 58 Hz operation of the AUG centrifuge.

Both the time and frequency signals for 140 Hz show irregularities. In particular, a peak near 2500 Hz is almost an order of magnitude higher than most of the peaks. To ensure that the signal is not misinterpreted, it is again useful to look at the time signal. Here, instead of single peaks as seen at 58 Hz, there are clusters of peaks throughout the signal. While there are clusters, no specific pattern (e.g., [58, p. 39]) can be detected. Depending on which part of a bearing contains a fault, the defect will take different shapes. The fact that no specific shape could be identified leads to the conclusion that a defect may be present at an early and not yet critical stage. Combining the knowledge that subharmonic peaks occur during a run-up to 140 Hz, and that the DKW at 140 Hz, as well as the acceleration time signal and frequency spectrum, all show either high values or irregularities, leads to the question of whether this mode of operation should be continued.

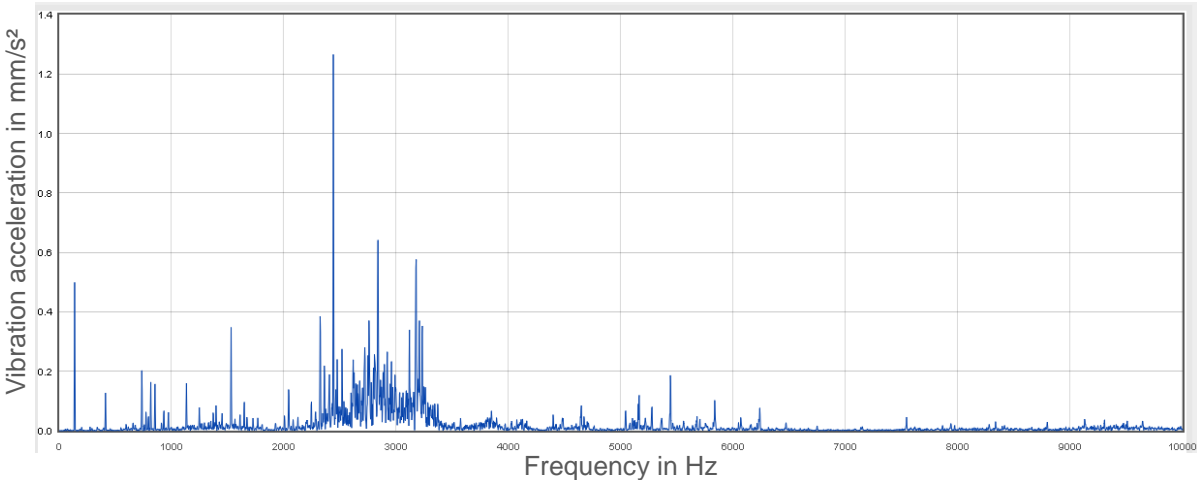


Figure 35: The graph, visualized by the *CMS2000* shows an acceleration frequency spectrum (VIB1), measured during 140 Hz operation on the AUG centrifuge.

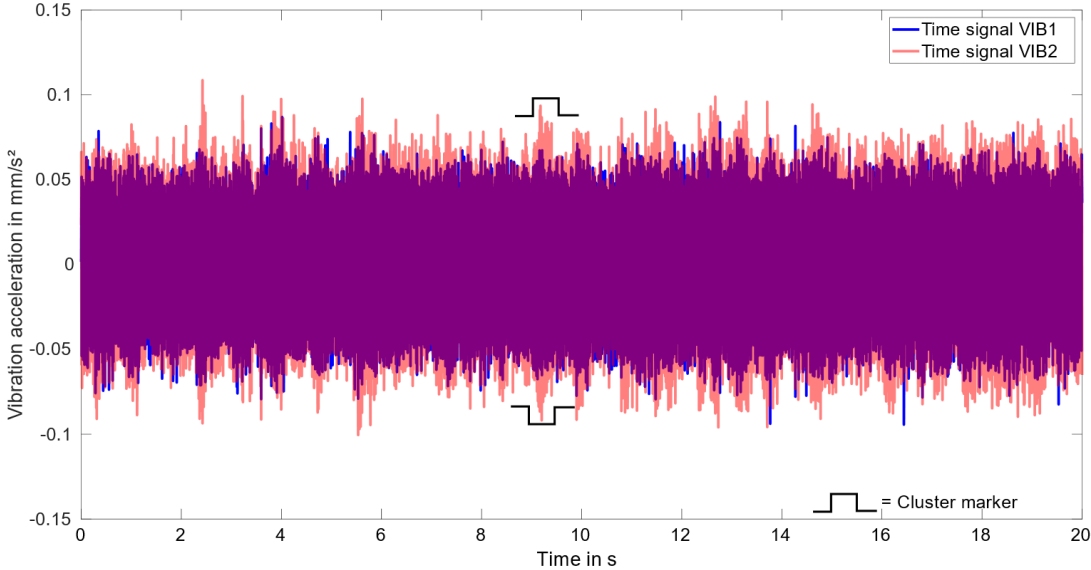


Figure 36: Time signal of the vibration acceleration, measured by VIB1 and VIB2 during 58 Hz operation of the AUG centrifuge.

Due to the low amplitudes and difficult to detect sidebands, the remaining frequency band (3000 – 10.000 Hz) is best analyzed by envelope analysis.

5.7 Envelope spectrum (acceleration)

Envelope analysis is usually an excellent way to monitor specific bearing (rollover) frequencies. If a peak at one of these frequencies appears, it becomes obvious which part (cage, inner or outer race, ball) has a defect. However, the exact dimensions or frequencies must be known. Unfortunately, there is no verified information on either of the centrifuge's bearings. The only orientation are the CAD bearings, which are designed to roughly fit the centrifuge model. One way to use this is to look at the spectrum and pinpoint specific peaks with high amplitudes. It is known that the order of peaks from low to high rollover frequencies corresponds to:

1. Fundamental Train (Cage) Frequency

$$FTF = \frac{f}{2} \left(1 - \frac{B_D}{P_D} \times \cos(\beta) \right) \quad (11)$$

2. Ball Pass Frequency Inner Race

$$BPF1 = \frac{N_B \times f}{2} \left(1 + \frac{B_D}{P_D} \times \cos(\beta) \right) \quad (12)$$

3. Ball Pass Frequency Outer Race

$$BPF0 = \frac{N_B \times f}{2} \left(1 - \frac{B_D}{P_D} \times \cos(\beta) \right) \quad (13)$$

4. Ball Spin Frequency

$$BSF = \frac{P_D \times f}{B_D} \left(1 - \left(\frac{B_D}{P_D} \right)^2 \times \cos^2(\beta) \right) \quad (14)$$

All variables, except f which represents the rotational frequency of the machine, for formulas (11-14) can be found in Table 1. Obvious amplitudes could be the starting point for an iterative process to find the correct bearing dimensions. Looking at the envelope spectrum during 58 Hz operation, several distinct peaks can be seen all throughout the bandwidth from 0 Hz to 1000 Hz (Figure 37).

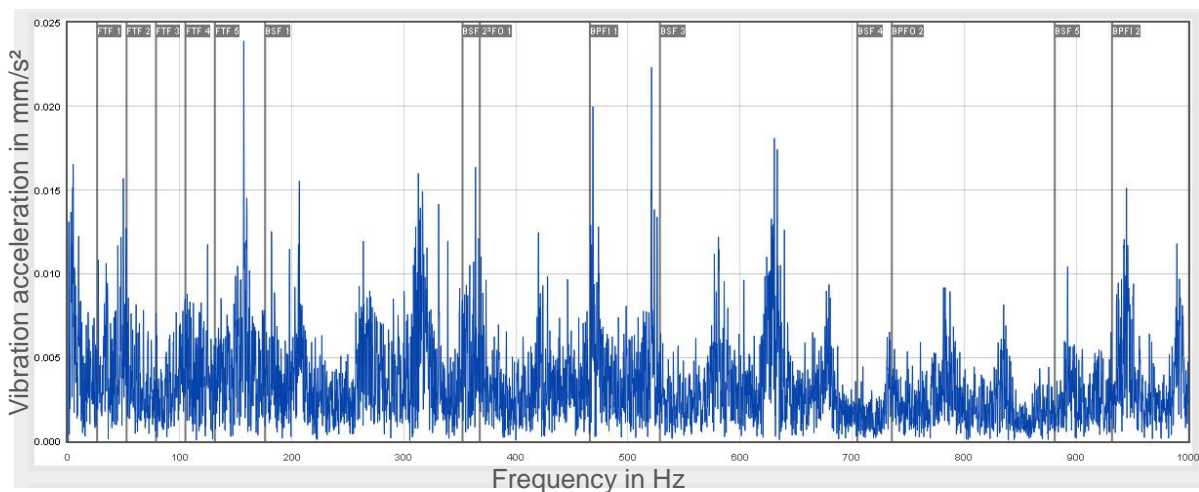


Figure 37: The graph, visualized by the *CMS2000* shows an envelope frequency spectrum (VIB1), measured during 58 Hz operation on the AUG centrifuge.

Unfortunately, only few of them were within the area of calculated rollover frequencies (and their harmonics) using formulas 11-14 with the given CAD dimensions and flagged by grey markers (Table 1, Figure 38). Furthermore, none of them did exactly match. To some extent, these peaks were again misleading, due to the linear scaling of the plot. Unfortunately, just as with the acceleration spectrum, errors occurring in *MATLAB* scripts for the envelope analysis could not be resolved, making it impossible to switch to a logarithmic scale. [60]

Table 1: AUG Centrifuge bearing dimensions according to the CAD model. Bearing 1 is the upper, Bearing 2 the lower one.

	Number of rolling elements (N_B)	Ball bearing diameter (B_D)	Bearing pitch diameter (P_D)	Bearing contact angle (β)
Bearing 1	14	9.5 mm	60 mm	45°
Bearing 2	14	9 mm	54 mm	45°

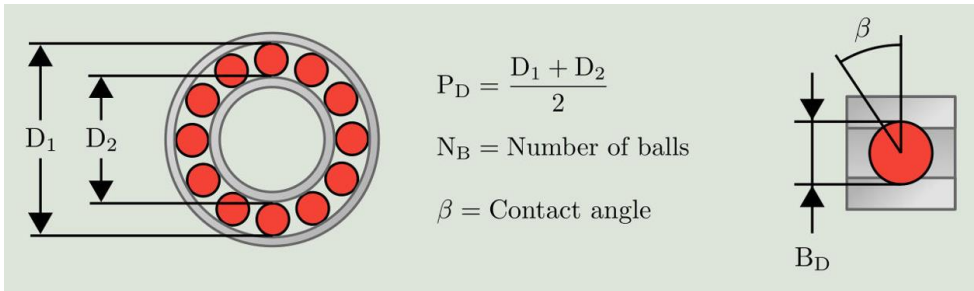


Figure 38: Dimensions of a bearing needed for rollover frequency calculations. [64]

Slight (theoretical) adjustments to one or more bearing parameters were picked and tested. However, changes are limited by known factors such as shaft diameter and the fact that, according to incomplete technical drawings, two shoulder ball bearings are installed. Taking this into account, all parameter adjustments had little effect on the rollover frequencies. The same method was tried for 140 Hz operation with the same results.

Looking for another way to find monitorable frequencies, empirical formulas (15-17) were used, replacing three of the more exact ones (11-13). [64]

$$BPFO = 0.4 \times N_B \times f \quad (15)$$

$$BPF1 = 0.6 \times N_B \times f \quad (16)$$

$$FTF = 0.4 \times f \quad (17)$$

Again, even when using a wide range of different values for N_B (10 - 18), no matches could be found for any of the rollover frequencies. In general, this can be seen as a positive, as no well-developed faults were so obvious, that they could be detected without knowing the exact frequencies. Unfortunately, it is not possible to monitor specific trends in the envelope spectrum, but rather only the entire bandwidth at once. This behavior relates to all relevant speeds and operational modes of the centrifuge.

6 Empirically deriving limit values

6.1 Elimination of disruptive effects

Limit values must be calculated from values measured under operating conditions without the presence of disruptive effects. If some or all of these effects are always present, they must be compensated for or taken into account when setting vibration velocity and acceleration limits. What exactly qualifies as a disruptive effect depends on the measurement task and chain. For the centrifuge, the task was to set very precise and meaningful limits, which meant that no other significant vibrations could be present during the measurements. In addition, parameters that influence the quality of the accelerometer transmission, such as those described in [8, pp. 89–94], had to be tested and removed or compensated.

6.1.1 Temperature

The most significant perturbation for the pellet launcher system is temperature fluctuation. This is because the speed control circuit of the centrifuge motor unit is based on a resistor to set its speed, and this parameter is temperature sensitive due to drift of the resistance value.

Whenever the speed of the centrifuge changes (e.g. during speed drifts), the vibration's phase does, too. As explained in section 3.1.1, a complete vibration signal contains both amplitude and phase information. The measured amplitude of a vibration signal depends on the vibration's phase and the sensor location.

This characteristic has already been used to select the ideal sensor location. However, an increase in speed does not always result in an increase in vibration velocity. For the first sensor setup (Pos. 1 & 2), the vRMS amplitude measured by VIB1 would increase while VIB2's would decrease as the speed increased from 61 to 62 Hz (Figure 39). Different sensor setups produced different results, such as both amplitudes rising or falling with the frequency of the centrifuge. Fortunately, the overall effect was drastically reduced (for all old and new sensor configurations) when the operating speed was changed from 60 Hz to 58 Hz. The reason for this, is a small resonance area close to 62 Hz, which even with an increase of 2 Hz - 3 Hz due to temperature change, is no longer a problem when running at 58 Hz. Prior to this, the measurement of teaching values, a process that takes several hours, was sometimes highly dependent on the rate and intensity of speed drifts due to temperature changes. In addition, the maximum vibration level decreased when the frequency was reduced to 58 Hz. Since this was done while the old measuring points were still in use, the graph in Figure 39 does not reflect the latest absolute vRMS values. However, the benefit remains the same.

Although the effect was reduced, it turned out to be temporary, as expected. From the first tests of this problem (January) to the end of this work (March), the outside temperature had changed significantly. This caused the previously set frequency of 58 Hz to often be well above this value, around 59 Hz to 60 Hz. Two ideas were developed and their benefits were compared to

the costs and effort involved. The first idea was to temper the switch cabinet (e.g. 32 °C) to ensure a constant resistance value and thus a constant centrifuge speed. This idea, although very precise, was quickly discarded due to the high effort involved. A simpler but less accurate solution is to use the four different resistors built into the motor controller. Each resistor can be set to a specific frequency. For example, the first resistor could represent 58 Hz for low temperatures, and the second resistor 58 Hz for high temperatures. This method is easy to implement and can be adjusted (or fine-tuned) at any time. Because the resistor responsible for the current setpoint was configured during low outdoor temperatures (~ 0°C -10°C), this method is set to be implemented when the temperatures rise even higher (e.g. in summer), so that the second resistor can represent 58 Hz during these periods. With the help of the PLC, depending on the true frequency of the centrifuge, an automatic process of switching between these two modes would be possible.

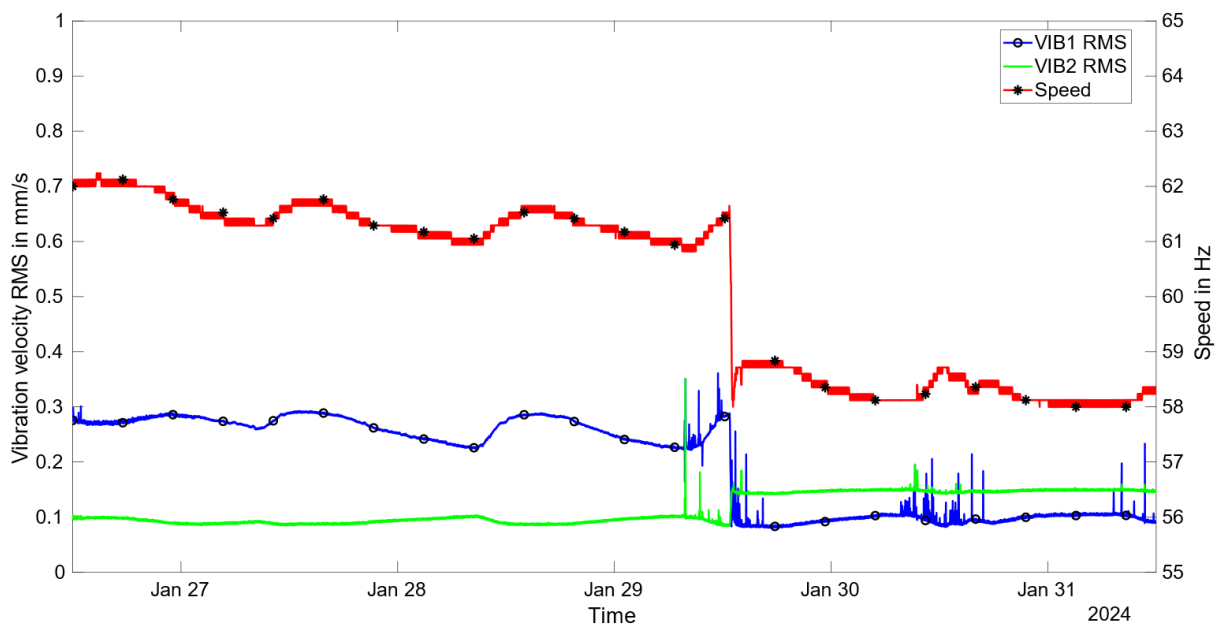


Figure 39: The graph shows the temporal evolution of the vRMS and the centrifuge's speed during the change from 60 Hz to 58 Hz as the new steady state frequency. The peaks starting on January 29th are not related to the machine, but only to construction work around it. Even though the RMS value of VIB2 increases with the change in speed, the overall vibration level at 58 Hz is preferred to that at 60 Hz.

6.1.2 Electromagnetic Fields

Another disturbance is electromagnetic fields, which are an unavoidable effect when dealing with fusion reactors or, more precisely, their plasma confinement. Since these cannot be compensated for and are present during every plasma discharge, limits are impossible to derive or use during this time. The sensitivity of piezoelectric accelerometers to magnetic fields is typically 0.1 - 2.5 (mm/s²)/T [8]. Unfortunately, the available documents do not give an exact value for the sensors used on the centrifuge. However, even 0.1 (mm/s²)/T would have a noticeable effect on the measurements, since the vibration amplitudes of the raw acceleration signals fluctuate around 0.02 - 0.03 mm/s² (at 58 Hz). With a magnetic flux density B of 50 mT,

measured at the centrifuge location during the plasma discharge, this would potentially change the magnitude of the signal by 0.005 mm/s² and thus invalidate the set limits by 16% - 25%. This could be (dis)proven by comparing the raw acceleration signal during the plasma discharge with a signal without the magnetic field present. However, since the new operational phase of ASDEX Upgrade will not start until summer 2024, this could not yet be tested.

In addition, the eddy currents in TMPs induced by magnetic fields create extra torque and friction in the system. Because this torque must be compensated to keep the pump, or in this case the centrifuge pellet launcher, at a constant frequency, the rotor current and therefore the internal forces increase. This changes the vibrational behavior of the system. A model shown in [65] addresses this problem with respect to the safe operation of TMPs in magnetic fields. Here, in tandem with higher motor currents, a significant temperature change of the rotor was observed with even lower magnetic flux density (< 25 mT) than at AUG. Rising temperatures change the material properties and therefore the damping of the system. However, for the same reason as above, the actual effect of such changes has not yet been tested. [65]

6.1.3 Triboelectric effects

Triboelectric effects occur when, for example, the sensor cable is subjected to mechanical stress or friction due to strong movement on a (metal) surface [8]. Since neither of these is expected during operation, a simple solution was found and implemented. Cable ties were used to secure the two cables to a nearby structure to minimize the contact area and to ensure that no person or object could strain the cables.

6.1.4 Stochastic vibrations

Stochastic vibrations, explained in detail in section 3.1.1, are often the result of external effects. Therefore, they do not resemble the vibrational behavior of the centrifuge and must be filtered or anticipated and compensated. According to [42], the vibrations always present around the machine should not exceed 25% of the vibrations generated by the system itself. As shown in Table 2, no limit was reached, resulting in a negligible effect of external systems.

Table 2: Comparison of vRMS values, measured on the AUG centrifuge by both sensors at 58 Hz and 0 Hz and the set limit for those. These values were measured on a Sunday to minimize external vibrations.

mm/s	vRMS (58 Hz)	vRMS limit (0 Hz) according to [42]	vRMS (0 Hz)
VIB1	0.2	0.05	0.01
VIB2	0.08	0.02	0.01

The effect of people working in the vicinity of the centrifuge was observed during several measurements, e.g. during the change from 60 Hz to 58 Hz as steady state operation (Figure 39). Since amplitudes of a factor of two can occur during such events, this must be

taken into account when implementing the shutdown scheme, e.g. by sending an alarm signal only if the RMS value is greater than the limit value for a certain period of time.

6.2 Calculating Warn- and Alarm-Limits

After taking all disturbances into account, limits for the vibration magnitudes can be calculated. For this system, two different limits were used. The so-called *Warn-Limit* (WL) represents a change in amplitude that is not yet considered critical for the short-term operation of the machine. Once the vibration reaches the set *Alarm-Limit* (AL), it should be stopped completely or slowed down to a non-critical frequency.

As described in section 4.2.2, there is no established standard for a system such as the AUG centrifuge pellet launcher. There are several different approaches to establishing vibration limits for other machines not covered by standards. For example, [66] uses a method of comparing the vibrations of intentionally damaged machines (or machine parts) with those of healthy ones. Obviously, this cannot be done for the centrifuge, since no comparable systems exist (or are available). Others, such as [67], set limits using statistical analysis. Here, a factor of either 2.66 for WLs or 3.267 for ALs was used for multiplication with the mean change in vibration during a given time period. This results in a different monitoring method that looks at the change in vibration rather than the absolute values. Since the *CMS2000* is not set up for such a monitoring solution, another way had to be found.

Not the limits themselves, but information on how they might be set in standards for other machines, combined with empirically derived vibration values, can also lead to customized ALs and WLs. Formula (18) given in [42] for setting limits describes a dynamic approach for calculation. Limits can be set depending on the driving frequency and machine specific parameters.

$$V_{Limit} = \bar{V}_{mean} \times Z_{bound} \times \left(\frac{f_z}{f_x}\right)^k \times \left(\frac{f_y}{f_w}\right)^m \quad (18)$$

Where V_{Limit} can be either a WL or AL and Z_{bound} is a function of frequency or other parameters such as pressure or temperature. The exponents k and m are to be chosen machine-specific and describe the influence of the rotational frequency on vibration magnitudes. The speed of the machine is represented as f , f_x is the lower and f_y the upper limit for a range in which the vibration behavior can be considered as steady. The various frequency parameters can be described as followed:

- $f_w = f_y$ for $f \leq f_y$
- $f_w = f$ for $f > f_y$
- $f_z = f$ for $f < f_x$
- $f_z = f_x$ for $f \geq f_x$

Using this formula for the centrifuge would be impractical for two reasons. First, it would be very complicated to determine k and m because of the large number of resonance regions and their different intensities. Second, even if a frequency range without such behavior could be found, setting up these parameters would require a considerable number of run-ups and downs of the centrifuge to find out exactly how speed affects vibration. Since one would have to accelerate and decelerate through multiple resonance areas, which increases the forces on machine parts, this should be avoided if possible.

Because the monitoring system is to be set up for steady state operation anyway, the first step to simplify, or rather tailor this formula to the AUG centrifuge, is removing the frequency factors completely. This leads to (18.1), with Z_{bound} being the only factor left to enable differentiating between WLS and ALS. As mentioned previously, this variable can be exchanged for a function of any system parameter. Since neither the frequency nor any other characteristic is set to change in a way that would significantly affect vibrations during operation, two constant factors had to be found.

$$V_L = \bar{V}_{mean} \times Z_{bound} \quad (18.1)$$

Looking at the complete set of standards (DIN ISO 20816 1-21), a simple and surprisingly accurate similarity was found between all limits for all machines. Meaning, that the Warn-Limits set up for any given machine is approx. 2-times the mean's value, whereas the Alarm-Limit works with a factor of about 3.2. Since these values (2.0, 3.2) were found to be true regardless of a machine's composition or task, they were also chosen for establishing the centrifuge's monitoring system.

In addition to this approach, a factor for fine-tuning these thresholds could be set up in the future if necessary. For example, a factor α could be used as an exponent for Z_{bound} (18.2).

$$V_L = \bar{V}_{mean} \times Z_{bound}^\alpha \quad (18.2)$$

$$\alpha(t) = 1 - \gamma(x) \times 0.2 \quad (19)$$

$$\gamma(x) = \begin{cases} -1 & x < 1 - r \\ 0 & \text{for } x = 1 \pm r \\ 1 & x > 1 + r \end{cases} \quad (20)$$

$$x = \frac{\bar{V}_{mean}(t_2)}{\bar{V}_{mean}(t_1)} \quad (21)$$

Where r represents a small value to account for meaningless fluctuations in the signal, and t is counted, for example, in months or years. $\bar{V}_{mean}(t_2)$ represents the latest set of measurements, $\bar{V}_{mean}(t_1)$ previous ones. The set factor of 0.2 is not derived from standards nor from any other

publication but is purely speculative for the centrifuge’s behavior. For obvious reasons, this process should be applied only a few times (1 or 2), especially when $x > 1 + r$.

6.2.1 Limit values for the vibration velocity’s RMS

To use (18.2), the average v_{RMS} must be determined. When working with the *CMS2000*, this is done simply by measuring its teaching values. It is the same process as for the DKW described in section 5.4, only this time they directly represent the mean value, not the denominator. Since two sensors and two different operational modes are used, four different values are measured. As with the DKW, a v_{RMS} teaching value for run-ups and downs is theoretically possible but would not be meaningful due to resonance areas with much higher amplitudes than those in regular ones. After measuring the mean v_{RMS} for all possible configurations, the WLS and ALs were calculated (Table 3) and implemented in the *CMS2000*.

Table 3: v_{RMS} teaching values and limits measured by VIB1&2 on the AUG centrifuge for 58 Hz and 140 Hz.

mm/s	v_{RMS} (58 Hz)	v_{RMS} (140 Hz)
Teaching values VIB1	0.200	0.430
Teaching values VIB2	0.080	0.520
Warn limit VIB1	0.400	0.860
Warn limit VIB2	0.160	1.040
Alarm limit VIB1	0.640	1.376
Alarm limit VIB2	0.256	1.664

6.2.2 Limit values for the DKW

As mentioned before, the DKW, by its nature, fluctuates around 1, and therefore does not directly represent the magnitude of a vibration. Since there is almost no information about the use of this parameter available, and it is not known how fast (or slow) it will increase, a Z_{bound} of 1.5 and 2 was chosen to calculate its limits. Once more long-term data is available, it can either be adjusted by using formula (19), or setting it to 2 and 3.2, like for the vibration velocity calculations. This time, because it was set up for each sensor and operational mode to be approx. 1, only one general limit for the DKW exist (Table 4).

Table 4: DKW teaching values and limits measured by VIB1&2 on the AUG centrifuge for 58 Hz and 140 Hz.

mm/s ²	DKW
Teaching values VIB1/VIB2	≈ 1
Warn limit VIB1/VIB2	1.5
Alarm limit VIB1/VIB2	2

6.2.3 Limit bands for the velocity's frequency spectrum

For frequency spectra, unfortunately, there is no teaching value system that could have been used to calculate WLs and ALs. Since a single spectrum sometimes requires more than one particular limit, so-called limit bands had to be created. The spectrum was divided into several sections in which the overall vibration level is similar. These sections were plotted in the time domain and a mean value was determined. Since all of the vibration amplitudes, except for the first harmonic, are small and do not differ much, only two bands were set up. The first one, for the frequency window v_1 , includes all frequencies of the spectrum from 0 Hz to 1000 Hz except for the first harmonic's $h_1 \pm 5$ Hz, and the second one, for window v_2 , includes only $h_1 \pm 5$ Hz. It is set to follow the centrifuge's frequency. This is done by using an analog input to send the actual speed information to the *CMS2000*. The small buffer for v_2 is necessary due to a buildup of the amplitude around the actual frequency, as can be seen in Figure 32. As with the v_{RMS} , (18.2) was used to calculate the WLs and ALs for each sensor and operational mode. For simplicity, Table 5 shows the results for VIB1 only. Unfortunately, it is unknown if the calculated values need to be adjusted after some time or not, and there are no exact teaching values that would allow the use of a formula such as (19). Therefore, the operator must determine whether and to what extent the limits should be modified. By examining the plotted spectra of the *CMS2000*, both the vibration amplitudes and limit bands can be observed. This visualization can aid in identifying the appropriate adjustment values.

Table 5: Actual vibration values in the vibration velocity spectrum and calculated WLs and ALs for VIB1 during 58 Hz and 140 Hz operation of the AUG centrifuge. Window v_1 represents every frequency in this spectrum (0 Hz -1000 Hz) except for v_2 , which is equal to h_1 , the centrifuge's rotational frequency.

mm/s	v_1 (58 Hz)	v_2 (58 Hz)	v_1 (140 Hz) mm/s	v_2 (140 Hz) mm/s
Actual values VIB1	0.025	0.220	0.050	0.500
Warn limit VIB1	0.050	0.440	0.100	1.00
Alarm limit VIB1	0.080	0.704	0.160	1.600

To be able to send fault specific messages, the first frequency window was subdivided into smaller windows *only* in the *CMS2000* configuration. While the limits remain the same, a different warning message can be sent for each sector. For example, if the second or third harmonic sector detects a violation, a customized message can be sent with that specific information and some hints as to what the problem might be. A more detailed table with each sector and sensor can be seen in *Appendix B, (B) Table 1* and *(B) Table 2*.

6.2.4 Limit bands for the acceleration's frequency spectrum

For the limits of the acceleration spectrum, the same process was repeated as for the velocity spectrum. Frequency sections consisting of similar vibration amplitudes were created and analyzed in the time domain. The mean value of each time plot was then used as \bar{V}_{mean} for

further calculations and the variable Z_{bound} was again set to 2. Again, two different types of sections were created, some dependent on the rotational frequency, some independent. One of each is shown in Table 6, while all seven sections, for both sensors, can be found in (B) Table 3 and (B) Table 4. Window a_1 represents that of the first harmonic, window a_2 the frequency range of 2000 Hz - 3500 Hz.

Table 6: Actual vibration values in the vibration acceleration spectrum and calculated WLs and ALs for VIB1 during 58 Hz and 140 Hz operation of the AUG centrifuge. Window a_1 represents the centrifuge's rotational frequency, a_2 the range of 2000 Hz - 3500 Hz.

mm/s ²	a_1 (58 Hz)	a_2 (58 Hz)	a_1 (140 Hz)	a_2 (140 Hz)
Actual values VIB1	0.085	0.200	0.440	1.500
Warn limit VIB1	0.170	0.400	0.880	3.000
Alarm limit VIB1	0.272	0.640	1.408	4.800

6.2.5 Limit bands for the envelope spectrum

As explained in section 5.7, there were no peaks for specific bearing parts and therefore no faults could be identified. Since the envelope spectrum is a tool for in-depth analysis rather than real-time monitoring, a limit was set for the entire bandwidth (0 Hz - 1000 Hz). Internally, for the envelope spectrum, the *CMS2000* does not allow the use of only one section, so a limit had to be added for each of the rotational speed dependent frequencies: FTF, BFPI, BPFO, BSF. Since these frequencies do not correspond to the actual bearing parts, they still received the same limit as the rest of the bandwidth e_1 (Table 7). Again, for simplicity, for VIB1 only, one limit dependent on the rotational frequency and one independent limit are shown here. The full set can be found in (B) Table 5 and (B) Table 6.

Table 7: Actual vibration values in the vibration envelope spectrum and calculated WLs and ALs for VIB1 during 58 Hz and 140 Hz operation of the AUG centrifuge. Window e_1 represents the entire bandwidth of the spectrum (0 Hz - 1000 Hz), except for the rollover frequencies such as FTF.

mm/s ²	e_1 (58 Hz)	FTF (58 Hz)	e_1 (140 Hz)	FTF (140 Hz)
Actual values VIB1	0.025	0.025	0.300	0.300
Warn limit VIB1	0.050	0.050	0.600	0.600
Alarm limit VIB1	0.080	0.080	0.960	0.960

6.2.6 Limit values for the centrifuge's speed

Another parameter for which limits can be set is the rotational frequency or speed of the centrifuge. Since previous run-ups have shown that critical vibrations appear at speeds above 160 Hz (Figure 26), this frequency was chosen as the upper limit. When the rotational frequency reaches this point, the motor current drops to zero and the centrifuge stops.

7 Shutdown scheme for the AUG centrifuge

7.1 Overview of the real-time vibration monitoring system

The complete vibration monitoring system is set up for real-time vibration monitoring. Therefore, it needs sensors for both vibration and speed monitoring, as well as components for data preparation and visualization (Figure 40). To allow for a safe shutdown scheme, which decelerates or turns off the centrifuge in case of an emergency, all components must be always in contact with each other. The measurement chain starts with two piezoelectric acceleration sensors for vibration measurements and a hall sensor for speed signals. It ends with an HMI, *WinCC*, representing the data prepared by a *CMS2000* and a PLC (*S7-300*).

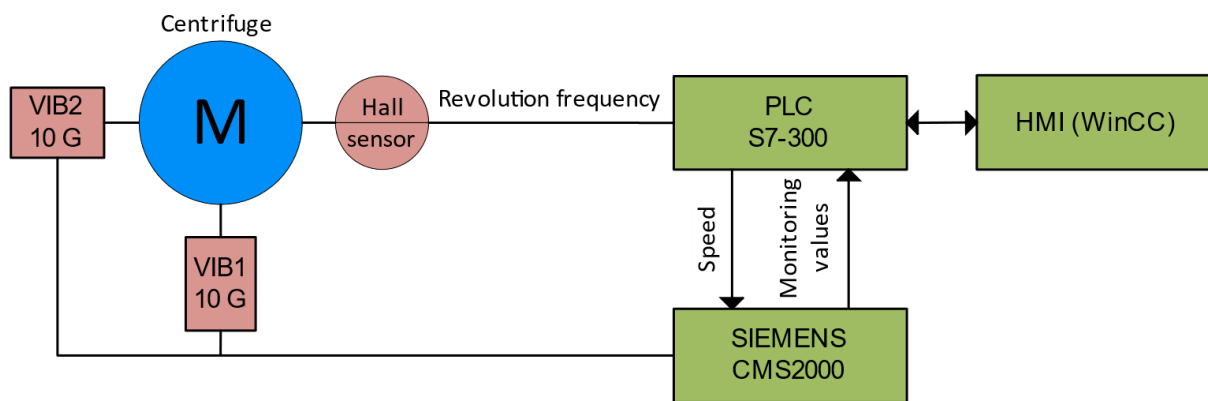


Figure 40: Schematic overview of the real-time vibration monitoring system for the AUG centrifuge.

While the CMS sends the vibration data to the PLC via Ethernet telegram, not all information necessary for a complete limit monitoring within the *S7-300* can be sent. Therefore, both the CMS and the PLC are used for limit violation detection. The PLC takes care of detecting and sending messages for critical *vRMS*, *DKW* and non-specific spectrum values. The CMS covers each specific section in all three spectra and is therefore inevitable for further fault analysis. Since a hall sensor is directly connected to the PLC, all speed limits can be handled internally.

The *Human Machine Interface* (HMI) is used to graphically display the current *RMS*, *DKW* and speed values for both sensors (Figure 41). In addition, indicator lights for each limited parameter were set up. The lights for *Messung* can either be green or red, the latter meaning that measurements are invalid. This can happen when there is no internet connection or data exchange between the CMS and PLC. The second row of lights, under *Messwert*, stays green as long as no limit has been breached. They turn yellow after a *WL*, or red after an *AL* was violated. The box in the bottom left corner of this dashboard is for manually setting up and later potentially changing the limit values. This is possible for the *vRMS* and *DKW* for each sensor and both operational modes, leading to 16 changeable values. Below that, the same can be done for a timer suppressing triggered warnings and alarms, further explained in section 7.2.1.

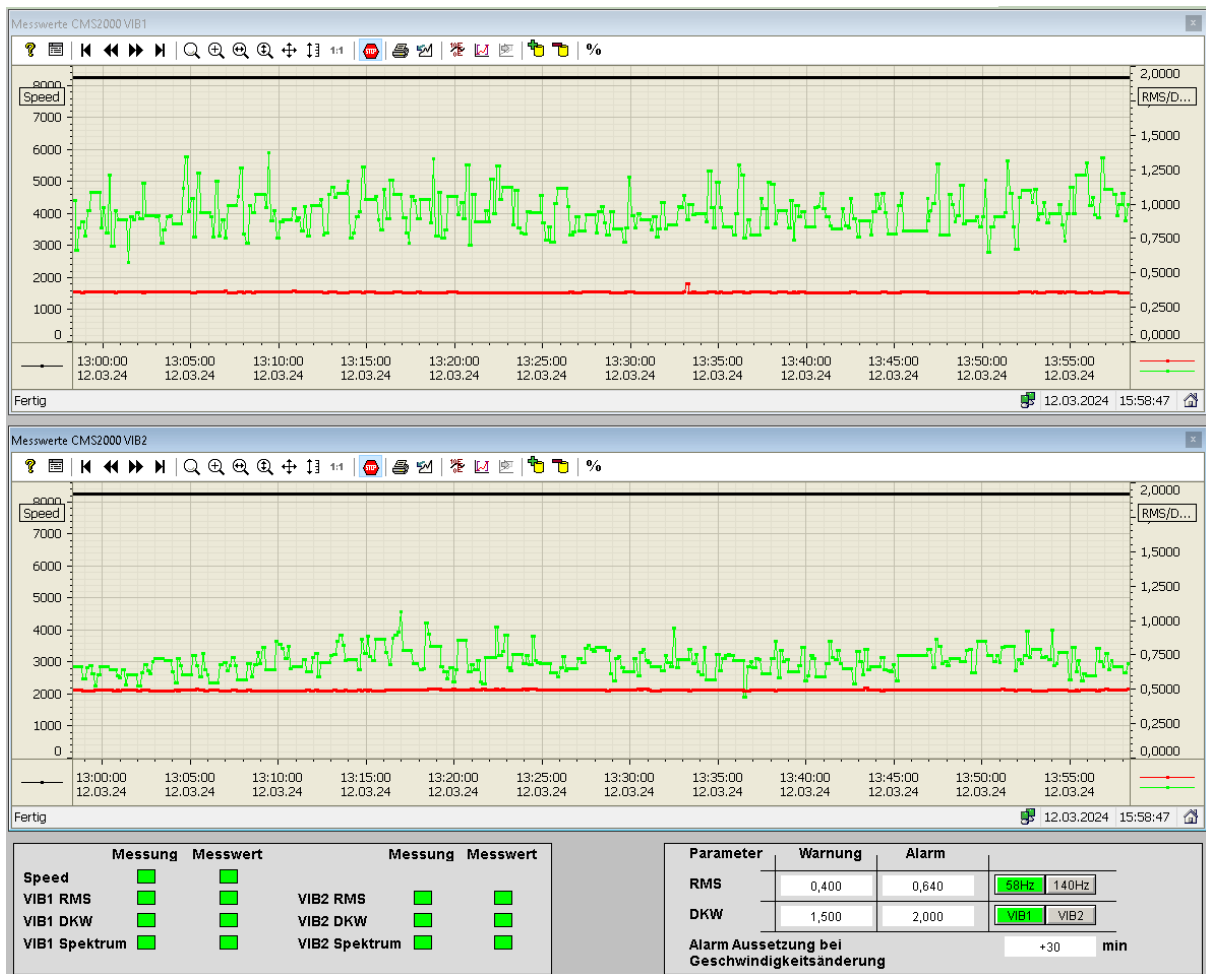


Figure 41: WinCC overview of the real-time vibration monitoring system.

7.2 System processes: Logic trees

It has been determined that exceeding the vibration or speed limits at any point, except during the plasma discharge phase, must result in one or more consequences. These consequences are notifications, shutdown (deceleration) of the system, or in some cases both. The way each scheme is set up is best explained by logic trees.

7.2.1 Speed monitoring

The first tree describes the process of monitoring the speed value and, in particular, what happens when the actual speed exceeds the set value (Figure 42). This can happen either because of an electrical fault or because of a planned change in operational mode. To distinguish between these two cases, the process includes a step that checks whether the operational mode has been changed. This can be done by looking at transition edges (negative or positive) of a set of four bits, where each represents an operational mode. If $Actual > Speed$ and a transition edge for one of the bits is present, a timer (e.g. 30 minutes) will be started and all alarms will be suppressed to allow the system to safely switch between frequencies. When the timer expires, monitoring will start over from zero. If *Setpoint changed* is false, an electrical fault is present.

The system then checks whether or not the centrifuge speed has reached the supercritical frequency of 160 Hz. If not, a warning will be triggered and an e-mail sent. One reason for this warning is the resistance-based speed control. After this violation, especially in 58 Hz operation, it can be decided whether this speed difference is due to a temperature change and then, as explained in 6.1.1, the potentiometer may either be changed manually or automatically so that *Actual* = *Set* again. As soon as the actual speed reaches the 160 Hz mark, an alarm message will be sent and the system will be shut down. To limit false alarms, an adjustable buffer 5 Hz has been set, meaning that the actual speed may exceed the set speed by this amount.

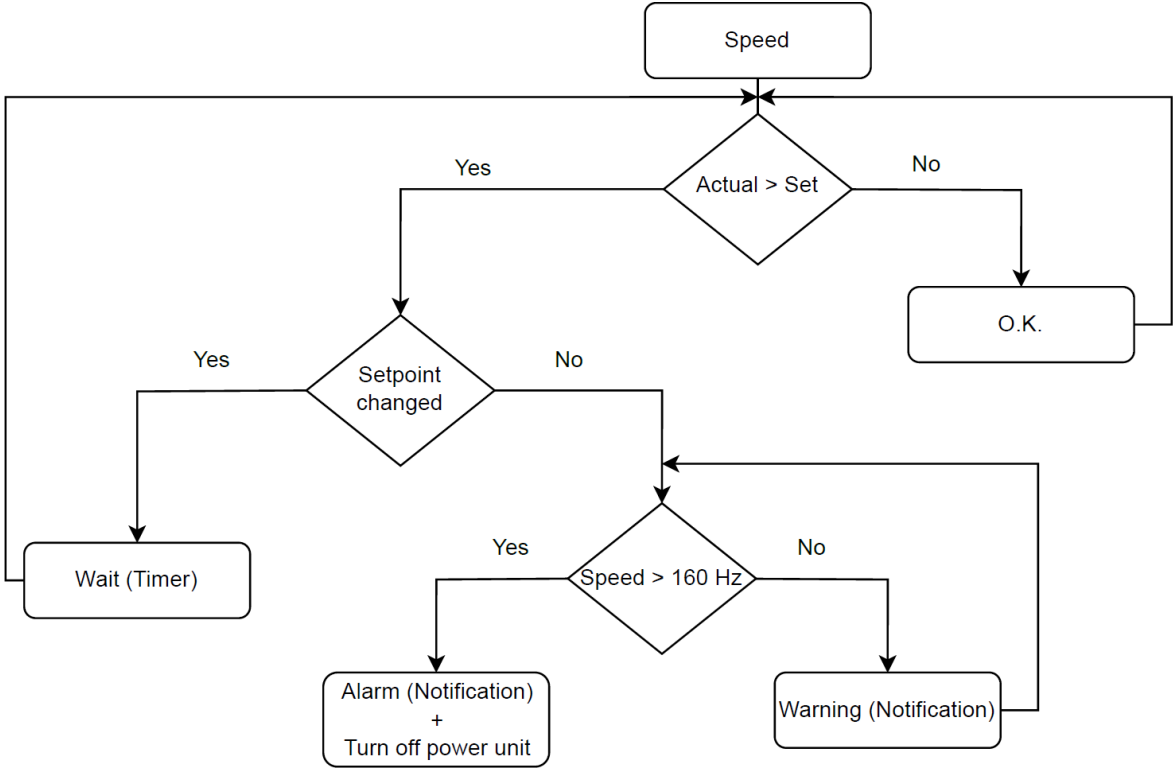


Figure 42: Logic tree for the PLC describing the monitoring process of the AUG centrifuge’s upper speed limit. The system differentiates between Warn-Limits and Alarm-Limits

7.2.2 Vibration monitoring

Monitoring the vibration limits is a straightforward process that involves handling all parameters, including vRMS, DKW, and three spectra statuses, in the same way. The system continuously checks for any vibration parameters that exceed their Warn-Limit. If this occurs, it immediately checks if the Alarm-Limit has also been breached. If not, a notification will be sent via e-mail and the system keeps monitoring the actual values. When both the Warn- and Alarm-Limits are exceeded, the PLC will check if the centrifuge is running at its lowest operational mode (58 Hz). If it is not, the system will be decelerated to its lowest mode instead of being shut down, while still sending out an alarm. This ensures that the system is guided to its safest frequency (58 Hz) and prevents premature shutdown. Because the frequency changes, the timer from speed monitoring suppresses alarms until the centrifuge reaches the desired mode. Upon reaching it, the monitoring process starts from the top. If a vibration parameter

exceeds its Alarm-limit while the centrifuge is running at 58 Hz, a message will be sent out and the power unit turned off. To prevent false alarms, the actual values must remain above the Warn- or Alarm-Limits for at least 30 minutes. Furthermore, for every detected limit breach, the CMS will record and save raw vibration data signals, that can be used for in-depth analysis.

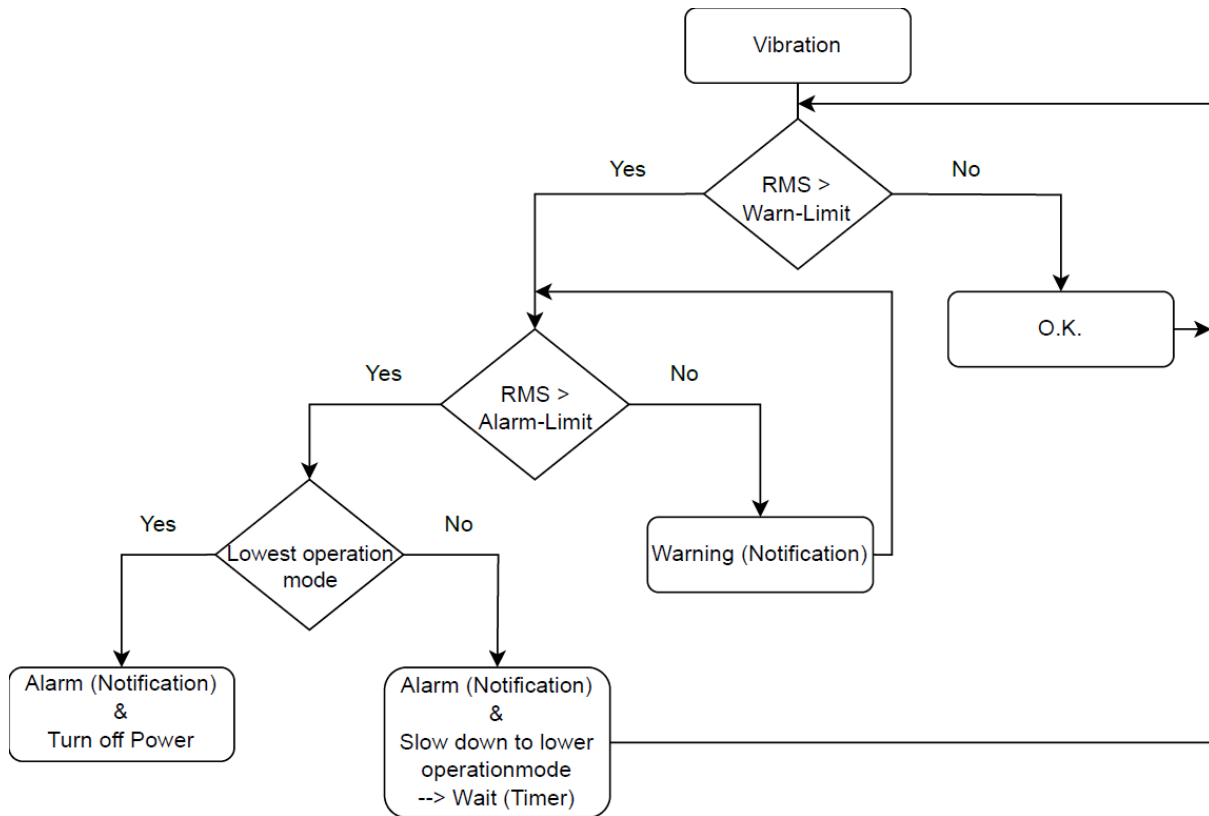


Figure 43: Logic tree for the PLC describing the monitoring process of the vibrations measured on the AUG centrifuge. Even though only vRMS is mentioned in this tree, the same applies to DKW and all spectra statuses. The system differentiates between Warn-Limits and Alarm-Limits.

7.2.3 Boundary condition monitoring

As explained in section 6.1.2, the shutdown scheme must not be active during plasma discharge. To guarantee this, time tokens already established at AUG can be utilized. The DV1 time token becomes active a few seconds before the discharge, and TS08 becomes active after the shot when electric currents in the Torus Hall are small and unproblematic. The monitoring system continuously checks the status of DV1 and suppresses alarms for speed and vibration limits if it is active. Upon verifying the activation of TS08, the process restarts from the beginning.

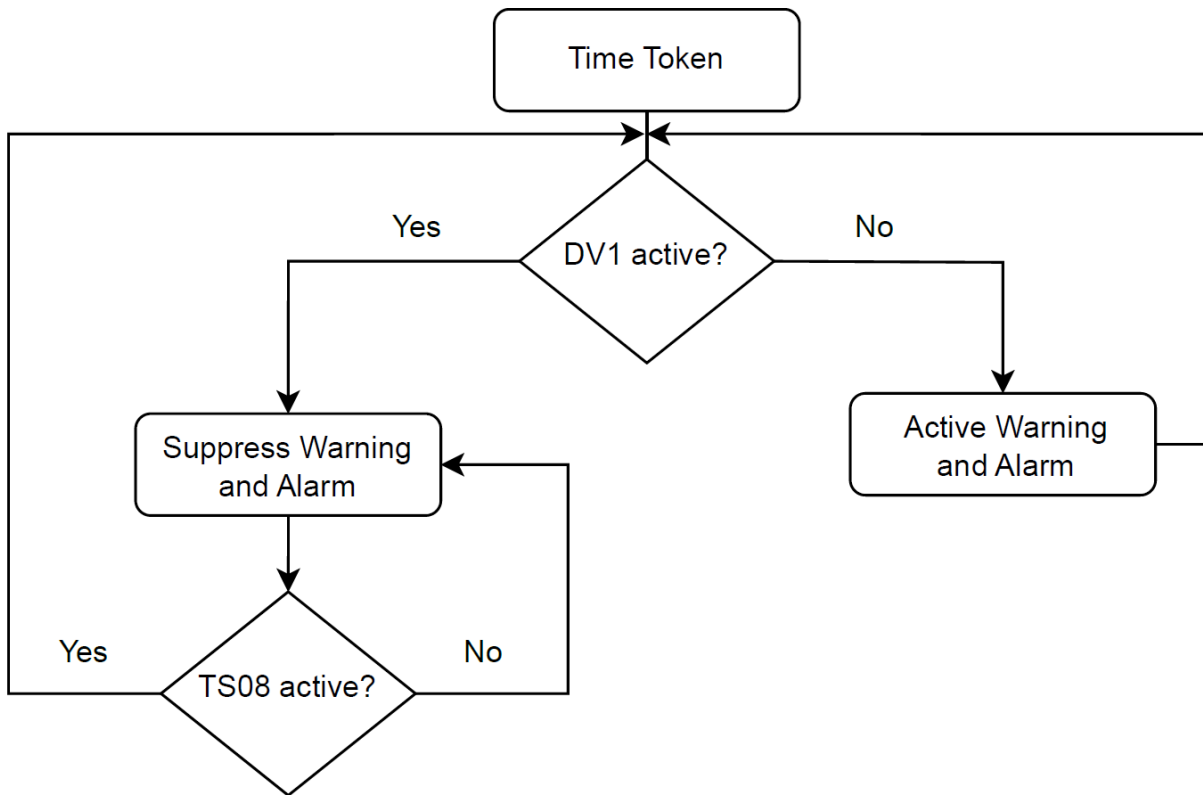


Figure 44: Logic tree for the PLC describing the monitoring process of plasma discharges. The time token DV1 means *Diagnostics preparation 1* and TS08 *End of discharge*. DV1 starts before, TS08 after the plasma discharge. As long as one of them, or both are active, all alarms and signals will be suppressed.

8 Summary

Over the last 30 years, the ASDEX Upgrade centrifuge pellet launcher has proven to be a baseline model for future particle flux and ELM control at JT-60SA, ITER, and DEMO [68]. To ensure reliable operation of this system for as long as possible, a real-time vibration monitoring system was implemented. Once the reason was identified, the next step was to determine how to proceed.

An FEM tool, *Ansys*, was used to analyze if the vibrations measured on the machine's housing provided enough information about the rotor's health. Since the accordingly derived first critical speed was well above any of the operational modes in use, a rigid rotor behavior was assumed, and housing vibrations were found to be sufficient. The first step in establishing a measurement chain was to select a sensor suitable for this specific task. After comparing the dynamic ranges and availability of different sensor types, it was determined that piezoelectric accelerometers were the best option. Two of these sensors were placed near the lower bearing, which is a vibration source of the centrifuge. This allowed for overall vibration measurements and diagnostics for at least one of the bearings. A module for processing the raw vibration signals was already in place prior to the start of this thesis. The *Siemens CMS2000* can convert vibration acceleration data into velocity and plot both units in the time and frequency domain.

The time domain used for long-term monitoring consists of two parameters. The RMS of the vibration velocity and the DKW for the vibration acceleration. Measurements of the vRMS are used to monitor the overall health of the machine, it is the main indicator of how long a machine can still operate. The DKW is mainly used to monitor the bearings of this system and will increase when a fault occurs or wear progresses. Frequency domain analysis is most commonly performed to analyze a failure that has already occurred. Various standards and publications provide information on what happens in this domain after certain machine parts have aged or been damaged. Due to its unique composition and application, there are no reference machines and it is not known whether the measured vibrations represent a good or bad condition. With only a limited amount of historical vibration data available, the current condition had to be used as a baseline. In order to know when this condition changes in a way that affects the safety of the machine, vibrations had to be derived empirically and an approach was developed using standards to calculate appropriate limits.

This approach involves dividing the limits into two categories. Multiplying the mean values of the vibration signals by a factor of 2 results in Warn-Limits, and a factor of 3.2 results in Alarm-Limits. This was done for the vRMS, DKW and different frequency windows of all three different spectra. While measuring the mean values, potential disruptive effects such as temperature change became apparent. Finding operating states (58 Hz) where these effects are limited and defining boundary conditions for when the system should be active and when it should be inactive (plasma discharge) helped to eliminate or at least minimize them.

The calculated vibration limits were implemented in a real monitoring system using the *CMS2000*, a PLC (*S7-300*) and an HMI called *WinCC*. By setting up logic trees, specific conditions and variables control whether a limit has been exceeded and what consequences need to follow. Implementing this for vibration data showed that the same should be done for the speed of the centrifuge. Since the magnitude of the vibration is strongly dependent on the rotational frequency, safety measures were taken to prevent electrical faults from leading to supercritical speeds and thus vibrations.

In conclusion, a state-of-the-art vibration monitoring system has been implemented on a fusion technology machine. In comparison with other systems at AUG, it includes a rather wide range of different parameters and what-ifs for limit violations. Although this adds complexity, it also makes the monitoring and analysis of the measured vibration more detailed and thorough. Smaller faults can be detected at an early stage, which for this system is critical for safe operation. The continuous real-time aspect of this setup plays an inevitable role in a reliable shutdown scheme. This also sets a baseline for future pellet launcher centrifuges or other fusion relevant machines where a monitoring system could be of great benefit from the start.

9 Literature

1. HANNAH RITCHIE, PABLO ROSADO, et al. Energy Production and Consumption [online]. *Our World in Data*, 2024. Available under: <https://ourworldindata.org/energy-production-consumption>
2. Welsby, D., Price, J., et al. Unextractable fossil fuels in a 1.5 °C world [online]. *Nature*, 2021, **597**(7875), 230-234. ISSN 1476-4687. Available under: doi:10.1038/s41586-021-03821-8
3. *Sun: Facts - NASA Science* [online]. 9 Januar 2024 [Last access: 2024.01.09]. Available under: <https://science.nasa.gov/sun/facts/>
4. ITER. *Advantages of fusion* [online]. 13 März 2024 [Last access: 2024.03.13]. Available under: <https://www.iter.org/sci/Fusion>
5. Barbarino, M. A brief history of nuclear fusion. *Nature Physics*, 2020, **16**(9), 890-893. ISSN 1745-2481.
6. Lalanne, C. *Sinusoidal Vibration: Mechanical Vibration and Shock Analysis*: Wiley, 2009. ISBN 978-1-84821-122-3 978-0-470-61190-6.
7. Soedel, W. *Vibrations of shells and plates*. 3rd ed. New York: Marcel Dekker, 2004. Mechanical Engineering. Volume 177. ISBN 9780429216275.
8. Kolerus, J., Wassermann, J., et al. *Zustandsüberwachung von Maschinen: Lehr- und Arbeitsbuch - Studienausgabe*. 7. Auflage. Stuttgart, Deutschland: utb GmbH, 2017. ISBN 978-3-8385-5181-4.
9. *Nachhaltige Ökonomie* [online] [Last access: 2023.11.15]. Available under: <https://www.tatsachen-ueber-deutschland.de/de/nachhaltigkeit-und-umwelt/nachhaltige-oekonomie>
10. Lang, P.T., Andelfinger, C., et al. The new centrifuge high-speed pellet injector for ASDEX Upgrade.
11. Das Fusionskraftwerk [Last access: 2023.11.09]. Available under: <https://www.ipp.mpg.de/9809/kraftwerk>
12. *Startseite - Max-Planck-Gesellschaft* [online]. 19 Dezember 2023 [Last access: 2023.12.19]. Available under: <https://www.mpg.de/de>
13. *Forschung* [online]. 19 Dezember 2023 [Last access: 2023.12.19]. Available under: <https://www.ipp.mpg.de/7308/forschung>
14. *Status of research* [online]. 19 Dezember 2023 [Last access: 2023.12.19]. Available under: <https://www.ipp.mpg.de/16427/stand>
15. *Startseite - Max-Planck-Institut für Plasmaphysik* [online]. 19 Dezember 2023 [Last access: 2023.12.19]. Available under: <https://www.ipp.mpg.de/>
16. Lang, P.T., Nakano, T., et al. A Flexible Pellet Injection System for the Tokamak JT-60SA: The Final Conceptual Design [online]. *Fusion Science and Technology*, 2019, **75**(3), 178-196. ISSN 1536-1055 [Last access: 2023.11.17]. Available under: doi:10.1080/15361055.2018.1471960

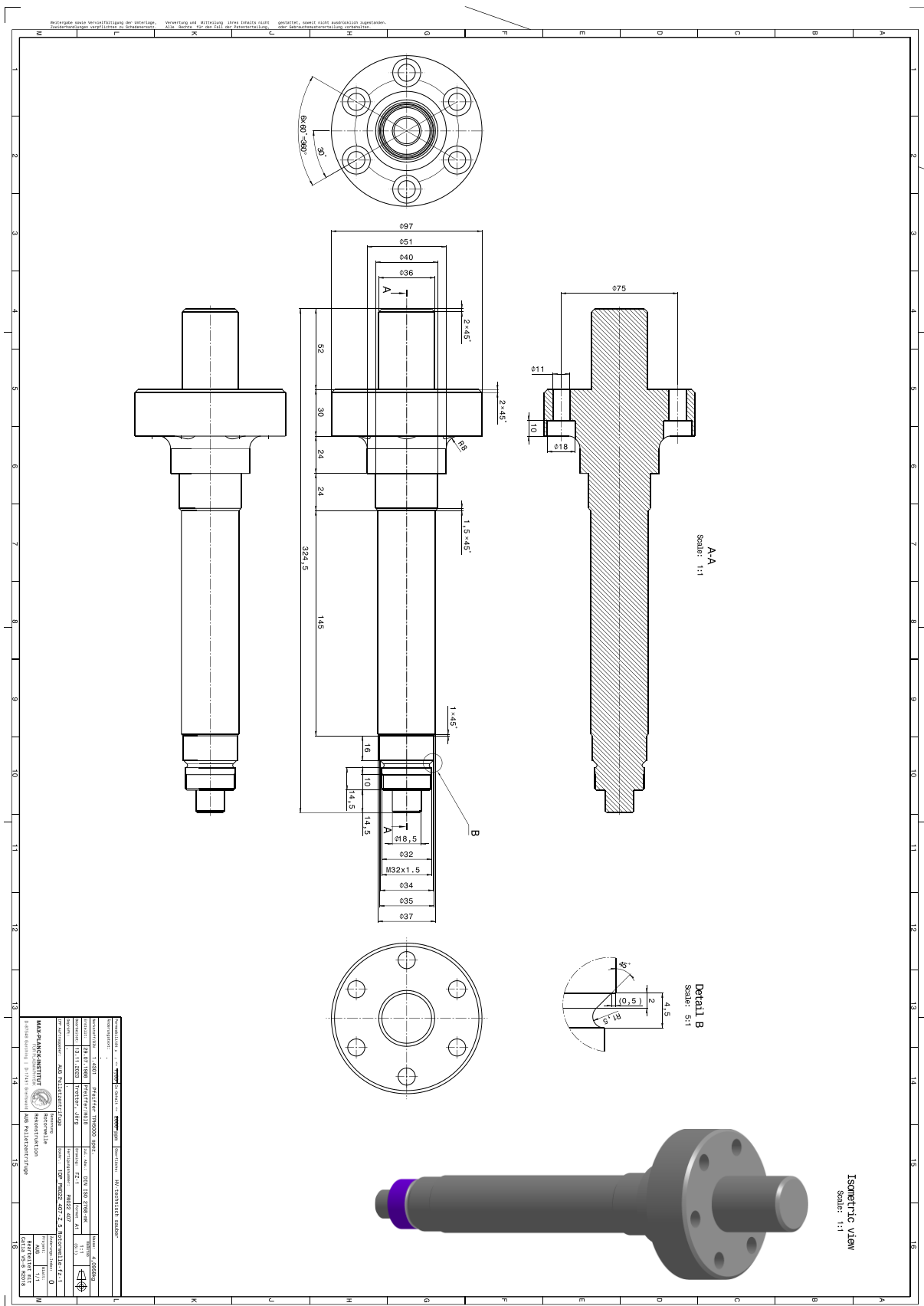
17. *Positionspapier Fusionsforschung* [online], 2023. Available under: https://www.bmbf.de/SharedDocs/Publikationen/de/bmbf/7/775804_Positionspapier_Fusionsforschung.html
18. *Bundesregierung stärkt Fusionsforschung | Bundesregierung* [online]. 19 Dezember 2023 [Last access: 2023.12.19]. Available under: <https://www.bundesregierung.de/bregde/themen/forschung/foerderprogramm-fusionsforschung-2198072>
19. *Tokamak-Szenario-Entwicklung* [online] [Last access: 2023.11.17]. Available under: <https://www.ipp.mpg.de/ippcms/de/for/bereiche/e1>
20. Andelfinger, C., Buchelt, E., et al. A new centrifuge pellet injector for fusion experiments [online]. *Review of Scientific Instruments*, 1993, **64**(4), 983-989. ISSN 0034-6748 [Last access: 2023.11.17]. Available under: doi:10.1063/1.1144101
21. Lang, P.T., Blanken, T.C., et al. Feedback controlled, reactor relevant, high-density, high-confinement scenarios at ASDEX Upgrade [online]. *Nucl. Fusion*, 2018, **58**(3), 36001. ISSN 0029-5515 [Last access: 2023.11.17]. Available under: doi:10.1088/1741-4326/aaa339
22. Lang, P.T., Cierpka, P., et al. A system for cryogenic hydrogen pellet high speed inboard launch into a fusion device via guiding tube transfer [online]. *Review of Scientific Instruments*, 2003, **74**(9), 3974-3983. ISSN 0034-6748 [Last access: 2023.11.17]. Available under: doi:10.1063/1.1602940
23. Lang, P.T., Frigione, D., et al. ELM pacing and trigger investigations at JET with the new ITER-like wall [online]. *Nucl. Fusion*, 2013, **53**(7), 73010. ISSN 0029-5515 [Last access: 2023.11.17]. Available under: doi:10.1088/0029-5515/53/7/073010
24. ASDEX UPGRADE, NI TEAMS, et al. High-Efficiency Plasma Refuelling by Pellet Injection from the Magnetic High-Field Side into ASDEX Upgrade [online]. *Phys. Rev. Lett.*, 1997, **79**(8), 1487-1490 [Last access: 2023.11.17]. Available under: doi:10.1103/PhysRevLett.79.1487
25. Plöckl, B., Lang, P.T., et al. Comparison of different pellet injection systems for ELM pacing [online]. *Fusion Engineering and Design*, 2011, **86**(6), 1022-1025. ISSN 0920-3796 [Last access: 2023.11.17]. Available under: doi:10.1016/j.fusengdes.2011.02.007
26. Kuttner, T., Rohnen, A., et al. *Praxis der Schwingungsmessung: Messtechnik und Schwingungsanalyse mit MATLAB®*. Wiesbaden: Springer Fachmedien Wiesbaden, 2019. ISBN 978-3-658-25047-8 978-3-658-25048-5.
27. DIN 1311-1:2000-02, Schwingungen und schwingungsfähige Systeme - Teil Grundbegriffe, Einteilung.
28. Kuttner, T., Rohnen, A., et al. *Praxis der Schwingungsmessung: Messtechnik und Schwingungsanalyse mit MATLAB®*. 2., überarb. u. erw. Aufl. 2019 Edition. Wiesbaden: Springer Vieweg, 2020. ISBN 978-3-658-25047-8.
29. Haas, R. Tutorial Hammermessung, 2014. Available under: https://www.th-koeln.de/mam/downloads/deutsch/hochschule/fakultaeten/fahrzeugtechnik_und_produkton/tutorial_hammermessung.pdf

30. Prechtl, M. *Mathematische Dynamik: Modelle und analytische Methoden der Kinematik und Kinetik*. 3. Auflage. Berlin, Germany: Springer Spektrum, 2021. Masterclass. ISBN 978-3-662-62106-6.
31. Franke, D. *Ausricht- und Kupplungsfehler an Maschinensätzen: Erfassung, Diagnose und Auswirkungen von Fehlansrichtungen in Wellensträngen*: Springer Berlin Heidelberg, 2020. ISBN 978-3-662-61026-8.
32. TIMOTHÉE GERBER, NADINE MARTIN, et al. Identification of harmonics and sidebands in a finite set of spectral components. In: , 2013.
33. Vibration Analysis: Understanding Sidebands [online]. *Fluid Life*, 6. Dezember 2021 [Last access: 2024.01.31]. Available under: <https://www.fluidlife.com/blog-understanding-sidebands/>
34. Gaul, L. The influence of damping on waves and vibrations [online]. *Mechanical Systems and Signal Processing*, 1999, **13**(1), 1-30. ISSN 0888-3270 [Last access: 2023.11.26]. Available under: doi:10.1006/mssp.1997.0185
35. Heine, B. *Werkstoffwahl für technische Anwendungen: Grundlagen und Beispiele*: Carl Hanser Verlag GmbH Co KG, 2015.
36. Antes, H. Fundamente unter Dynamischen Lasteinwirkungen. In: J. LEHN, H. NEUNZERT und H. WACKER, Hg. *Anwendungen der Methode der Randelemente in der Elastodynamik und der Fluidodynamik*. Wiesbaden: Vieweg+Teubner Verlag, 1988, S. 85-114. ISBN 978-3-519-02626-6 978-3-322-91212-1.
37. Brunton, S.L., Kutz, J.N., et al. *Data-driven science and engineering. Machine learning, dynamical systems, and control*. Cambridge: Cambridge University Press, 2019. ISBN 9781108422093.
38. Forland, C. Why phase information is important for diagnosing machinery problems [online], 1999. Available under: http://turbolab.hanyang.ac.kr/9_Why%20phase%20information%20is%20important%20for%20diagnosing%20machinery%20problems.pdf
39. Cooley, J.W., Tukey, J.W., et al. An algorithm for the machine calculation of complex Fourier series [online]. *Mathematics of Computation*, 1965, **19**(90), 297-301. ISSN 0025-5718. Available under: doi:10.1090/s0025-5718-1965-0178586-1
40. Sinha, J.K. *Vibration analysis, instruments, and signal processing*. Boca Raton: Taylor & Francis, 2015. ISBN 9781482231458.
41. DIN ISO 13373-1:2002-07, Zustandsüberwachung und -diagnostik von Maschinen - Schwingungs-Zustandsüberwachung - Teil Allgemeine Anleitungen (ISO_13373-1:2002).
42. DIN ISO 20816-1:2017-03, Mechanische Schwingungen - Messung und Bewertung der Schwingungen von Maschinen - Teil Allgemeine Anleitungen (ISO_20816-1:2016).
43. DIN ISO 5348:2022-05, Mechanische Schwingungen und Stöße - Mechanische Ankopplung von Beschleunigungsaufnehmern (ISO_5348:2021).

44. DIN ISO 10816 Beiblatt 1:2013-12, Mechanische Schwingungen - Bewertung der Schwingungen von Maschinen durch Messungen an nicht-rotierenden Teilen - Beiblatt Methodisches Vorgehen bei der Auswahl von Normen zu Maschinenschwingungen einschließlich der Wellenschwingungen (ISO/TR_19201:2013).
45. Haas, R. *Tutorial Hammermessung* [online], 2014. Available under: <https://dokumen.tips/documents/tutorial-hammermessung-th-koeln-45-messen-mit-der-vordefinierten-grafik-14.html?page=3>
46. Gjelstrup, S. *What is Modal Analysis: The Ultimate Guide* [online], 2023. 31 August 2023 [Last access: 2024.01.25]. Available under: <https://dewesoft.com/blog/what-is-modal-analysis>
47. DIN ISO 20816-5:2018-12, Mechanische Schwingungen - Messung und Bewertung der Schwingungen von Maschinen - Teil Maschinensätze in Wasserkraft- und Pumpspeichieranlagen (ISO_20816-5:2018).
48. DIN ISO 10816-7:2009-08, Mechanische Schwingungen - Bewertung der Schwingungen von Maschinen durch Messungen an nicht-rotierenden Teilen - Teil Kreiselpumpen für den industriellen Einsatz (einschließlich Messung der Wellenschwingungen) (ISO_10816-7:2009).
49. DIN ISO 20816-3. *Mechanische Schwingungen – Messung und Bewertung der Schwingungen von Maschinen – Teil 3: Industriemaschinen mit einer Leistung über 15kW und Betriebsdrehzahlen zwischen 120 min⁻¹ und 30000 min⁻¹ (ISO 20816-3:2022).*
50. *Piezelektrischen Beschleunigungssensoren Brüel & Kjær* [online] [Last access: 2023.11.03]. Available under: <https://www.bksv.com/de>
51. *Produktdetails - SiePortal - Siemens DE* [online]. 19 Dezember 2023 [Last access: 2023.12.19]. Available under: <https://mall.industry.siemens.com/mall/de/de/Catalog/Product/6AT8008-2AA02-0AA0>
52. DIN ISO 13373-2:2016-11, Zustandsüberwachung und -diagnostik von Maschinen_ - Schwingungs-Zustandsüberwachung_ - Teil_2: Verarbeitung, Analyse und Darstellung von Schwingungsmesswerten (ISO_13373-2:2016).
53. *Condition Monitoring Systeme SIPLUS CMS2000* [online], 2016 [Last access: 2023.12.14]. Available under: https://support.industry.siemens.com/cs/attachments/56902401/Compact_Operating_Instructions_SIPLUS_CMS2000_Basic_Unit.pdf?download=true
54. VDI 3839-1. *Hinweise zur Messung und Interpretation der Schwingungen von Maschinen - Allgemeine Grundlagen.*
55. Mühl, T. *Einführung in die elektrische Messtechnik. Grundlagen, Messverfahren, Geräte ; mit 12 Tabellen und 54 Beispielen sowie 15 Aufgaben mit Lösungen.* 3., neu bearb. Aufl. Wiesbaden: Vieweg + Teubner, 2008. Studium. ISBN 9783835101890.

56. SIPLUS CMS2000 Manual [online], 2016. Available under:
https://support.industry.siemens.com/cs/attachments/56901901/Operating_Instructions_SIPLUS_CMS2000_en-US.pdf
57. DIN ISO 13373-3:2015-12, Zustandsüberwachung und -diagnostik von Maschinen_- Schwingungs-Zustandsüberwachung_- Teil_3: Anleitungen zur Schwingungsdiagnose (ISO_13373-3:2015).
58. VDI 3839-2. *Hinweise zur Messung und Interpretation der Schwingungen von Maschinen - Schwingungsbilder für Anregungen aus Unwuchten, Montagefehlern, Lagerungsstörungen und Schäden an rotierenden Bauteilen.*
59. Technologies, I. Zudaks Solutions - Zudak Solutions [online]. *Zudak Solutions*, 30. November 2021 [Last access: 2024.02.10]. Available under: <https://www.zs-reliability.com/>
60. Bechhoefer, E. *A quick introduction to bearing envelope analysis*, 2016.
61. *What Is DC Offset?* - *Audiophiles* [online], 2023. 6 Februar 2024 [Last access: 2024.02.06]. Available under: <https://audiophiles.co/what-is-dc-offset/>
62. *Subtract offset or trend from time-domain signals contained in iddata objects - MATLAB detrend - MathWorks Deutschland* [online]. 6 Februar 2024 [Last access: 2024.02.06]. Available under: <https://de.mathworks.com/help/ident/ref/iddata.detrend.html>
63. Mais, J. *Spectrum analysis* [online]. *The key features of analyzing spectra*, 2002. Available under:
https://cdn.skfmediahub.skf.com/api/public/0901d196802186cb/pdf_preview_medium/0901d196802186cb_pdf_preview_medium.pdf
64. Fernandez, A. *Rolling element bearing components and failing frequencies* [online], 2017. 20 Oktober 2023 [Last access: 2024.02.20]. Available under: <https://power-mi.com/content/rolling-element-bearing-components-and-failing-frequencies>
65. Wolf, J., Bornschein, B., et al. Investigation of turbo-molecular pumps in strong magnetic fields [online]. *Vacuum*, 2011, **86**(4), 361-369. ISSN 0042-207X. Available under: doi:10.1016/j.vacuum.2011.07.063
66. *Standardization of absolute vibration level and damage factors for machinery health monitoring*, 2002.
67. Budik, T., Jankovych, R., et al. Operational limits in vibration diagnostics [online]. *Advanced Mechatronics Solutions*, 2016, **393**, 13-18. ISSN 2194-5365. Available under: doi:10.1007/978-3-319-23923-1_2
68. Ploeckl, B., Day, C., et al. The enhanced pellet centrifuge launcher at ASDEX Upgrade: Advanced operation and application as technology test facility for ITER and DEMO [online]. *Fusion Engineering and Design*, 2015, **96-97**, 155-158. ISSN 0920-3796. Available under: doi:10.1016/j.fusengdes.2015.01.006

A Appendix A: Finite Element Method



(A) Figure 1: Technical drawing of the centrifuge pellet launcher's shaft, including mass and dimensions.

a

TABELLE 5
Modell (A4) > Geometrie > Bauteile

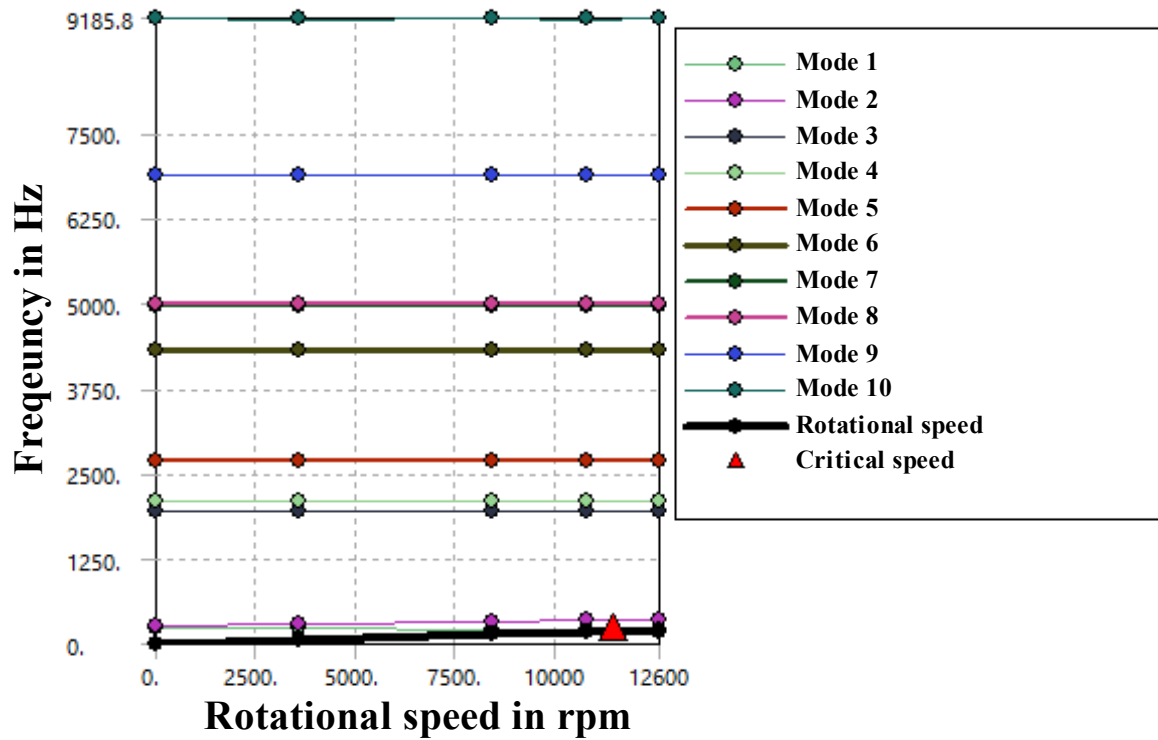
Objektname	1DP_PM022_407-Z_5_Rotorwelle- FreeParts\Hauptkörper
Zustand	Vernetzt
Grafikeigenschaften	
Sichtbar	Ja
Leuchten	0
Glanz	1
Transparenz	1
Spiegelung	1
Definition	
Unterdrückt	Nein
ID (Beta)	20
Steifigkeitsverhalten	Flexibel
Koordinatensystem	Standardkoordinatensystem
Referenztemperatur	Nach Umgebung
Bedeutung	Keine
Material	
Zuordnung	Baustahl
Nichtlineare Effekte	Ja
Berücksichtigung der thermischen Dehnungen	Ja
Rahmen	
Länge X	97. mm
Länge Y	97. mm
Länge Z	323.5 mm
Eigenschaften	
Volumen	5.1258e+005 mm ³
Masse	4.0237e-003 t
Schwerpunkt X	-1.9033e-003 mm
Schwerpunkt Y	5.1624e-004 mm
Schwerpunkt Z	-138.02 mm
Trägheitsmoment Ip1	27.683 t·mm ²
Trägheitsmoment Ip2	27.682 t·mm ²
Trägheitsmoment Ip3	2.1901 t·mm ²
Statistik	
Knoten	7401
Elemente	3993
Netzqualität	Keine

b

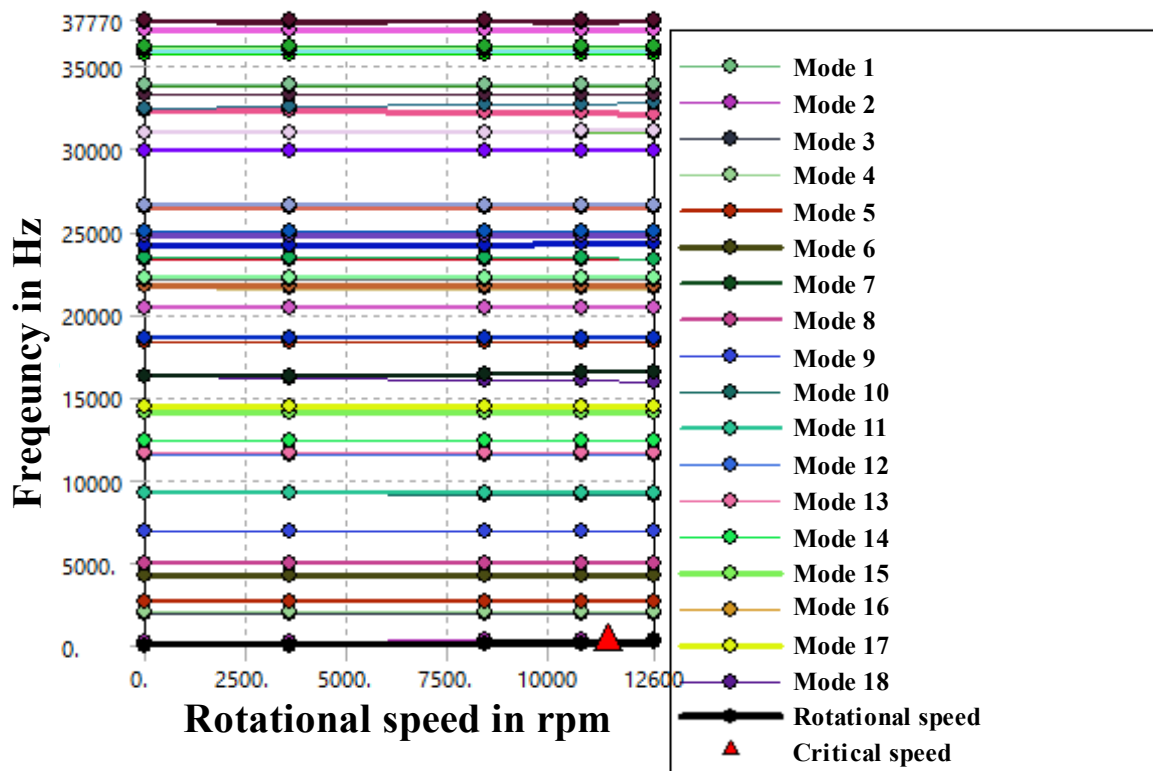
TABELLE 6
Modell (A4) > Geometrie > Massen

Objektname	Punktmasse
Zustand	Vollständig definiert
Zuweisung	
Zuweisungsmethode	Geometrieauswahl
Angewendet durch	Externe Zuordnung
Geometrie	5 Flächen
Koordinatensystem	Globales Koordinatensystem
X-Koordinate	-2.5e-002 mm
Y-Koordinate	-1.7e-002 mm
Z-Koordinate	-17.69 mm
Position	Definiert
Definition	
Masse	2.2199e-002 t
Massenträgheitsmoment X	295. t·mm ²
Massenträgheitsmoment Y	447. t·mm ²
Massenträgheitsmoment Z	455. t·mm ²
Unterdrückt	Nein
Verhalten	Verformbar
Pinball-Bereich	Alle

(A) Figure 2: (a) Properties of the centrifuge pellet launcher's shaft (e.g. mass and material); (b) Properties of the point mass used in the critical speed analysis (e.g. mass)



(A) Figure 3: Campbell diagram of a simulation with six speed-steps and 20 modes. A mode displays the critical speed's frequency. Both the x- and y-axis represent possible values for the shafts speed, only in different units.



(A) Figure 4: Campbell diagram of a simulation with six speed-steps and 50 modes. A mode displays the critical speed's frequency. Both the x- and y-axis represent possible values for the shafts speed, only in different units. Only the first 18 modes are listed in this legend.

B Appendix B: Limit value tables

(B) Table 1: *CMS2000* velocity spectrum limit band sections and their WL and AL values at 58 Hz.

58 Hz	2x line frequency (100 Hz)	Sub-harmonic	1x harmonic	2x harmonic	3x harmonic	4x harmonic	5x harmonic	unusual behavior (remaining frequencies)
Actual values VIB1	0.025	0.025	0.220	0.025	0.025	0.025	0.025	0.025
Actual values VIB2	0.025	0.025	0.085	0.025	0.025	0.025	0.025	0.025
Warn limit VIB1	0.050	0.050	0.440	0.050	0.050	0.050	0.050	0.050
Warn limit VIB2	0.050	0.050	0.170	0.050	0.050	0.050	0.050	0.050
Alarm limit VIB1	0.080	0.080	0.704	0.080	0.080	0.080	0.080	0.080
Alarm limit VIB2	0.080	0.080	0.272	0.080	0.080	0.080	0.080	0.080

(B) Table 2: *CMS2000* velocity spectrum limit band sections and their WL and AL values at 140 Hz.

140 Hz	2x line frequency (100 Hz)	Sub-harmonic	1x harmonic	2x harmonic	3x harmonic	4x harmonic	5x harmonic	unusual behavior (remaining frequencies)
Actual values VIB1	0.050	0.050	0.500	0.050	0.050	0.050	0.050	0.050
Actual values VIB2	0.050	0.050	0.700	0.050	0.050	0.050	0.050	0.050
Warn limit VIB1	0.100	0.100	1.000	0.100	0.100	0.100	0.100	0.100
Warn limit VIB2	0.100	0.100	1.400	0.100	0.100	0.100	0.100	0.100
Alarm limit VIB1	0.160	0.160	1.600	0.160	0.160	0.160	0.160	0.160
Alarm limit VIB2	0.160	0.160	2.240	0.160	0.160	0.160	0.160	0.160

(B) Table 3: *CMS2000* acceleration spectrum limit band sections and their WL and AL values at 58 Hz.

58 Hz	0 Hz – 2000 Hz	2000 Hz – 3500 Hz	3500 Hz – 6000 Hz	6500 Hz – 10000 Hz	1x harmonic
Actual values VIB1	0.200	0.200	0.090	0.025	0.085
Actual values VIB2	0.225	0.300	0.110	0.040	0.034
Warn limit VIB1	0.400	0.400	0.180	0.050	0.170
Warn limit VIB2	0.450	0.600	0.220	0.080	0.068
Alarm limit VIB1	0.640	0.640	0.288	0.08	0.272
Alarm limit VIB2	0.720	0.960	0.352	0.128	0.109

(B) Table 4: *CMS2000* acceleration spectrum limit band sections and their WL and AL values at 140 Hz.

140 Hz	0 Hz – 2000 Hz	2000 Hz – 3500 Hz	3500 Hz – 6000 Hz	6500 Hz – 10000 Hz	1x harmonic
Actual values VIB1	0.350	1.500	0.180	0.060	0.440
Actual values VIB2	0.400	1.000	0.220	0.100	0.600
Warn limit VIB1	0.700	3.000	0.360	0.120	0.880
Warn limit VIB2	0.800	2.000	0.440	0.200	1.200
Alarm limit VIB1	1.120	4.800	0.576	0.192	1.408
Alarm limit VIB2	1.280	3.200	0.704	0.320	1.920

(B) Table 5: *CMS2000* envelope spectrum limit band sections and their WL and AL values at 58 Hz.

58 Hz	1x BPFO	1x BPFI	1x FTF	1x BSF	unusual behavior (remaining frequencies)
Actual values VIB1	0.025	0.025	0.025	0.025	0.025
Actual values VIB2	0.032	0.032	0.032	0.032	0.032
Warn limit VIB1	0.050	0.050	0.050	0.050	0.050
Warn limit VIB2	0.064	0.064	0.064	0.064	0.064
Alarm limit VIB1	0.080	0.080	0.080	0.080	0.080
Alarm limit VIB2	0.102	0.102	0.102	0.102	0.102

(B) Table 6: CMS2000 envelope spectrum limit band sections and their WL and AL values at 140 Hz.

140 Hz	1x BPFO	1x BPFI	1x FTF	1x BSF	unusual behavior (remaining frequencies)
Actual values VIB1	0.300	0.300	0.300	0.300	0.300
Actual values VIB2	0.200	0.200	0.200	0.200	0.200
Warn limit VIB1	0.600	0.600	0.600	0.600	0.600
Warn limit VIB2	0.400	0.400	0.400	0.400	0.400
Alarm limit VIB1	0.960	0.960	0.960	0.960	0.960
Alarm limit VIB2	0.640	0.640	0.640	0.640	0.640